

# Advanced Model Updating Strategies for Structural Dynamic Systems

Von der Fakultät für Bauingenieurwesen und Geodäsie  
der Gottfried Wilhelm Leibniz Universität Hannover  
zur Erlangung des Grades

DOKTOR-INGENIEUR

- Dr.-Ing. -

genehmigte Dissertation  
von

**Karsten Schröder, M. Sc.**

geboren am 13.12.1986 in Minden

2018

Referent: Prof. Dr.-Ing. habil. Raimund Rolfes

Korreferent: Prof. Keith Worden, University of Sheffield

Tag der Promotion: 29.06.2018



"IT DOESN'T MATTER HOW BEAUTIFUL YOUR THEORY IS. IT DOESN'T MATTER HOW SMART YOU ARE. IF IT DOESN'T AGREE WITH EXPERIMENT, IT'S WRONG."

*Richard P. Feynman, 1918 - 1988*



# Abstract

In conjunction with increasing computational power, numerical models gained importance in virtually all engineering sciences during the last decades. Sophisticated modeling approaches are employed to simulate the physical behavior of the investigated structures for many practical problems. However, many of these models do not match with data measured in real-world structures to a certain degree. These inaccuracies are often caused by parameters needed for sophisticated modeling being imprecise, determined using engineering judgment or even completely unknown. Structural systems are a particular case with many unknown parameters due to varying environmental conditions, approximated loads and imprecise knowledge of boundary conditions.

This thesis aims to modify parameterized numerical models of structural systems automatically to increase conformity between simulation results and measured data. This process is known as model updating from the relevant literature. The deviation between numerical results and measured data is minimized using optimization methods via modifications of parameters of the numerical model.

A further aim is to apply the same methodology to damage localization. If a model building a good representation of measurement data is found using a first model updating step, the methodology is applied again after a damage event to localize these damages. This technique is useful in structural systems, where assemblies may be inaccessible, and ongoing visual inspections are likely to be costly.

Different metrics formulated in both frequency and time domain are investigated for their application in model updating within this text. A new scheme for the automated adjustment of numerical models is presented, enabling a comprehensive view of methods and techniques needed to perform iterative model updating. The aim is to minimize the outcome of these metrics, which results in nonlinear optimization problems providing several local minima. A new two-step algorithm employing state-of-the-art optimization methods is introduced to minimize the metrics, constituting a possible implementation of the scheme. The two steps consist of the global optimization method Simulated Quenching and the local Sequential Quadratic Programming. The need for a global algorithm is demonstrated using the concept of convexity and practical examples. Both methods can handle constraints to keep parameters within a specific user-defined range. Since the al-

gorithm is a random procedure, it is started multiple times. A method to employ the objective function value to distinguish correct from wrong solutions is demonstrated.

The distinctive metrics and their performance for updating different structures are investigated using a study on a simulated wind turbine in operation, a model of a three-story frame, a real scaled 34m wind turbine rotor blade and a scaled prestressed concrete tower. Although the examples focus quite heavily on assemblies from wind turbines, all concepts and methods introduced in this thesis are designed to be applied to general structural systems. A transfer of the methods to other physical processes is conceivable, although these applications may require different sensor settings.

The classical approach to deviation quantification between model and measurement, using eigenfrequencies and mode shapes, performs good for most examples, but it has the drawbacks that the consideration of nonlinearities in the numerical model is not straightforward and it is not as sensitive to structural changes such as damage. Transient analyses are needed to account for nonlinearities, yielding time series that can be compared directly to measured data. Advantages and disadvantages of metrics for various structures are discussed in detail.

Keywords: Model Updating, Structural Health Monitoring, Damage Localization, Global Optimization, Local Optimization

# Zusammenfassung

Durch die gestiegene Leistung moderner Rechensysteme hat die Bedeutung numerischer Modelle in nahezu allen Ingenieurwissenschaften in den vergangenen Jahrzehnten an Bedeutung gewonnen. Immer detailliertere numerische Modelle verlangen jedoch auch nach mehr und genaueren Eingangsgrößen. Diese sind häufig nur ungenau bekannt, durch Erfahrungswerte belegt oder gar gänzlich unbekannt. Die fehlende Kenntnis der Parameter ist eine mögliche Ursache für die häufig auftretenden Diskrepanzen zwischen Simulationsergebnissen und an realen Strukturen aufgezeichneten Messdaten. Ingenieurbauwerke stellen eines der klassischen Beispiele mit vielen Unbekannten dar, verursacht durch variierende Umgebungsbedingungen, approximierten Lasten oder unbekanntes Lagerungsbedingungen. Übergeordnetes Ziel dieser Arbeit ist es, die Abweichungen zwischen Simulationsergebnissen und Messdaten durch die automatisierte Änderung von Parametern des Simulationsmodells zu verringern. Diese Methodik ist in der einschlägigen Literatur als *Model Updating* bekannt. Die Abweichungen zwischen Modell und Messung werden mit Hilfe von Optimierungsmethoden durch Variation von Modellparametern minimiert.

Ein weiteres Ziel ist es, die gleiche Methodik auf das Problem der Schadenslokalisierung anzuwenden. Wenn ein Modell, welches die Messdaten mit ausreichender Genauigkeit widerspiegelt, gefunden wurde, kann die gleiche Vorgehensweise nach einem Schaden erneut angewendet werden, um diesen zu lokalisieren. Dies ist insbesondere bei Ingenieurbauwerken von hohem Interesse, bei denen fortlaufende visuelle Inspektionen hohe Betriebskosten verursachen. Häufig sind strukturelle Bauteile zudem nur sehr schlecht oder gar nicht zugänglich und können nur durch globale Verfahren inspiziert werden.

Die Quantifizierung der Abweichung zwischen Simulationsergebnissen und Messdaten ist essentiell für ein erfolgreiches Model Updating. Hierfür werden in diesem Text verschiedene Metriken im Zeit- und Frequenzbereich hinsichtlich ihres Einsatzes für Model Updating vorgestellt und anhand mehrerer Beispiele untersucht. Ein neues Schema wird eingeführt, welches alle wesentlichen Methoden, die für Model Updating benötigt werden, gruppiert und in ein Ablaufschema integriert. Ein neuer Zweischrittalgorithmus wird eingeführt um die Metriken zu minimieren. Dieser stellt eine mögliche Realisierung des Schemas dar und besteht aus einer

Kombination der globalen Optimierungsmethode Simulated Quenching und dem lokalen sequentiellen quadratischen Programmieren. Indizien für den Bedarf eines globalen Optimierungsalgorithmus werden vorgestellt. Beide Optimierungsmethoden beinhalten die Möglichkeit, Nebenbedingungen zu berücksichtigen. Diese werden benötigt, um die Parameter innerhalb eines bestimmten Bereiches zu restringieren. Es wird gezeigt, wie der Zielfunktionswert für eine Unterscheidung von falschen und korrekten Lösungen genutzt werden kann.

Die verschiedenen Metriken und ihre Möglichkeit zum Einsatz in der Anpassung von Modellen wird mit Hilfe verschiedener Strukturen untersucht. Diese beinhalten eine (numerische) Windenergieanlage im Betrieb, ein Modell eines Dreigeschossrahmens, ein 34m langes Rotorblatt einer Windenergieanlage und einen skalierten vorgespannten Turm aus Beton. Obwohl die hier vorgestellten Anwendungsfälle Strukturen aus dem Bereich Windenergie in den Vordergrund stellen, sind alle vorgestellten Konzepte und Methoden auf allgemeine strukturdynamische Systeme übertragbar. Auch die Übertragung auf andere physikalische Prozesse ist denkbar. Der klassische Ansatz zum Vergleich von Modellergebnissen und Messdaten, Eigenfrequenzen und Eigenvektoren, liefert gute Ergebnisse für die meisten Strukturen. Dieser Ansatz hat jedoch den Nachteil, dass Nichtlinearitäten im Modell nicht ohne Weiteres berücksichtigt werden können. Transiente Analysen sind erforderlich, um diese numerisch eingehend zu untersuchen. Die so erzeugten Zeitreihen können direkt mit Messdaten verglichen werden. Vor- und Nachteile verschiedener Metriken für verschiedene Anwendungsszenarien werden detailliert betrachtet.

Schlagworte: Model Updating, Structural Health Monitoring, Schadenslokalisation, Globale Optimierung, Lokale Optimierung



# Vorwort

Diese Dissertation ist während meiner Tätigkeit als wissenschaftlicher Mitarbeiter am Institut für Statik und Dynamik der Leibniz Universität Hannover entstanden. Die Problematik von Abweichungen zwischen gemessenen und errechneten physikalischen Größen begleitet mich seit Beginn meines Master-Studiums wiederkehrend. Herr Professor Raimund Rolfes gab mir im Rahmen dreier Forschungsvorhaben die Möglichkeit, mich in diesem spannenden Gebiet zu engagieren. Für seine konstruktiven Anregungen, die stets offene Atmosphäre und die gesamte Betreuung bedanke ich mich herzlich. Ferner gilt mein Dank Herrn Professor Keith Worden für die unkomplizierte Übernahme des Korreferates. Herrn Professor Michael Beer und Herrn Professor Udo Nackenhorst danke ich herzlich für den Prüfungsvorsitz und den Prüfungsbeisitz.

Für die Aufnahme im Rahmen eines Forschungsaufenthalts am National Renewable Energy Laboratory in Boulder, Colorado danke ich stellvertretend Jason Jonkman, Rick Damiani und Fabian Wendt, die mit ihren Anregungen zu dieser Arbeit beigetragen haben. Die Zeit in Colorado ist eine äußerst wertvolle Erfahrung für mich, an die ich mich gern zurückerinnere.

Zu großem Dank bin ich dem gesamten Kollegium des ISD verpflichtet. Allen voran muss hier zweifelsohne Cristian Gebhardt erwähnt werden. Ohne seine Anregungen, seine positive Einstellung und seine Beharrlichkeit wäre diese Arbeit wahrscheinlich nie entstanden. Für ihre Unterstützung in technischen Fragestellungen bedanke ich mich herzlich bei Michael Treiber und Christian Claußen. Den Kollegen Benjamin Reil, Jan Goretzka, Moritz Fricke, Moritz Häckell, Alexander Meurer, Roozbeh Nabavi, Timo Rogge, Sven Scheffler, Sina Hühne und Dorian Pache danke ich für 'konstruktive Gespräche' bei vielen Anlässen. Saskia Grove und Marianne Junge danke ich für ihre hervorragende Arbeit als wissenschaftliche Hilfskräfte. Ein Ehrenplatz gebührt Stavroula Tsiapoki, die durch viele Diskussionen und Anregungen Wertvolles zur Arbeit beigetragen hat.

Zu guter Letzt gilt mein Dank meinen Eltern und meinem Bruder, die stets ein offenes Ohr für mich hatten und haben. Eine herausragende Rolle hat meine Frau Janine gespielt, die immer und mit vollem Einsatz hinter mir steht.



# Contents

<b>List of Figures</b>	<b>xiii</b>
<b>List of Tables</b>	<b>xvii</b>
<b>Nomenclature</b>	<b>xxi</b>
<b>1. Introduction</b>	<b>1</b>
1.1. Motivation . . . . .	1
1.2. State of the art . . . . .	3
1.2.1. Model updating fundamentals . . . . .	4
1.2.2. Structural health monitoring . . . . .	12
1.3. Goals and objectives . . . . .	17
1.4. Structure of the thesis . . . . .	19
<b>2. Theoretical Background</b>	<b>21</b>
2.1. Basics of computational structural dynamics . . . . .	21
2.1.1. Numerical representation of dynamic systems . . . . .	21
2.1.2. Data pre- and post-processing . . . . .	24
2.2. Metrics for comparison of numerical models and measured data . . . . .	26
2.2.1. Error metrics in modal domain . . . . .	27
2.2.2. Error metrics in frequency domain . . . . .	28
2.2.3. Error metrics in time domain . . . . .	30
2.3. Optimization algorithms for model updating . . . . .	31
2.3.1. Simulated Annealing and Simulated Quenching . . . . .	32
2.3.2. Sequential Quadratic Programming . . . . .	33
2.3.3. Adaptive combination of Simulated Quenching and Sequential Quadratic Programming . . . . .	42
<b>3. Effective Application of Model Updating</b>	<b>45</b>
3.1. General considerations on model updating . . . . .	45
3.1.1. Comprehensive workflow for model updating . . . . .	46
3.1.2. On the globality of the optimization problem . . . . .	47
3.1.3. On the choice of error metrics for model updating . . . . .	49

# Contents

3.2. Plausibility test of damage localization using a simulated cantilever beam . . . . .	50
3.3. Application to a simulated real scale offshore wind turbine . . . . .	59
3.4. Conclusion . . . . .	70
<b>4. Concept Validation for Parameter Identification</b>	<b>73</b>
4.1. Model Updating at a three-story building structure . . . . .	73
4.1.1. Experimental set up of the frame structure . . . . .	73
4.1.2. Numerical model of the three-story frame . . . . .	76
4.1.3. Updating the numerical model of the frame structure . . . . .	80
4.2. Ice accretion at a full-scale rotor blade . . . . .	88
4.2.1. Experimental set up of the rotor blade test . . . . .	89
4.2.2. Numerical model of the blade . . . . .	91
4.2.3. Model updating for ice detection and quantification . . . . .	96
4.3. Conclusion . . . . .	100
<b>5. Concept Validation for Damage Localization</b>	<b>103</b>
5.1. Damage localization at a scaled tripile model . . . . .	103
5.1.1. Experimental set up and numerical modeling of the tripile . . . . .	104
5.1.2. Damage localization at the tripile . . . . .	106
5.2. Damage localization at a full scale rotor blade . . . . .	114
5.2.1. Damage localization at the rotor blade using artificial data . . . . .	115
5.2.2. Damage localization at the rotor blade using experimental data . . . . .	117
5.3. Damage localization at a scaled prestressed concrete tower . . . . .	121
5.3.1. Experimental set up and numerical modeling of the tower . . . . .	121
5.3.2. Damage localization at the tower . . . . .	127
5.4. Conclusion . . . . .	132
<b>6. Summary, Conclusion and Outlook</b>	<b>135</b>
6.1. Summary . . . . .	135
6.2. Conclusion . . . . .	136
6.3. Outlook . . . . .	138
<b>A. Calculation of stiffness reductions in circular cross sections</b>	<b>141</b>
A.1. Straight elimination of cross sectional area . . . . .	141
A.2. Angular elimination of cross sectional area . . . . .	143
<b>Bibliography</b>	<b>145</b>

# List of Figures

1.1. Parameter uncertainties in structural models by the example of an offshore wind turbine . . . . .	2
1.2. Three-tier damage detection framework . . . . .	15
1.3. Three columns of model-based structural health monitoring . . . . .	16
2.1. Flow Chart of the Simulated Quenching algorithm . . . . .	34
2.2. Comparison of linear and exponential cooling schemes . . . . .	35
2.3. Adaptive reduction of the parameter set for damage localization . . . . .	44
3.1. Workflow for iterative deterministic model updating . . . . .	46
3.2. Convex and non-convex sets . . . . .	48
3.3. Non-convex shape of $\rho^\omega$ used as objective function at simple harmonic oscillator system . . . . .	49
3.4. Simulated cantilever beam . . . . .	52
3.5. Comparison of time series computed using beam and shell representations of cantilever beam . . . . .	53
3.6. Comparison of normalized power spectral density computed using beam and shell representations of cantilever beam . . . . .	54
3.7. Objective function values of a single Simulated Quenching run . . . . .	56
3.8. Objective function values of a single Sequential Quadratic Programming run . . . . .	56
3.9. Influence of damage location on measured signal at the tubular beam structure . . . . .	59
3.10. Element numbering of the simulated monopile model . . . . .	61
3.11. Final objective function values after running ten Simulated Quenching runs and Sequential Quadratic Programming adaptively, using $\rho^{\omega+\phi}$ as objective function . . . . .	65
3.12. Overview on geometric properties of the NREL 5MW wind turbine . . . . .	66
3.13. Comparison of the monopiles damaged and undamaged tower top acceleration time series in wind direction . . . . .	66

# List of Figures

3.14. Final objective function values after running eight Simulated Quenching runs and Sequential Quadratic Programming adaptively using $\rho^{l^2}$ at the monopile model . . . . .	69
4.1. Experimental set up of the three-story building structure . . . . .	74
4.2. Example force time series applied to baseline condition . . . . .	76
4.3. Comparison of measured and simulated baseline condition acceleration at the top floor as a response to the force . . . . .	77
4.4. Averaged power spectral density of the uppermost accelerometer of the frame structure in baseline condition . . . . .	77
4.5. Numerical model of the three-story frame . . . . .	78
4.6. Comparison of measured and simulated mode shapes of the frame structure and according modal assurance criterion values . . . . .	79
4.7. Final objective function values after running the model updating algorithm using $\rho^s$ for state 3 . . . . .	84
4.8. Overview on the success of different metrics for model updating at the frame structure . . . . .	87
4.9. Heavy icing at a wind turbine rotor blade . . . . .	89
4.10. Nomenclature at a cross-section of a wind turbine rotor blade . . . . .	89
4.11. Rotor blade installed in test rig . . . . .	90
4.12. Sensor positions on rotor blade . . . . .	90
4.13. Ice accretion steps and installation of additional masses for simulation of ice accretion . . . . .	91
4.14. Discretization of the model according to blade construction plans . . . . .	93
4.15. Time series of sensor P6 (flapwise) after impulse load at 33m at the blade . . . . .	94
4.16. Power spectral density of sensor P6 in flapwise direction after impulse load at 33m at the blade . . . . .	94
4.17. Parameterization of blade the model according to blade construction plans and discretization . . . . .	96
4.18. Overview of the vector parameter $\psi$ for all four ice steps using $\rho^{\omega+\phi}$ . . . . .	99
4.19. Comparison of added masses during experiment and average additional mass determined using model updating . . . . .	99
4.20. Combination of transmissibility functions starting from measurement point five . . . . .	100
5.1. Overview of sensor locations and saw cut induced to the investigated tripile model . . . . .	105

5.2.	Element numbering of the investigated tripile structure and illustration of two eigenmodes . . . . .	107
5.3.	Final objective function values after running ten Simulated Quenching runs and Sequential Quadratic Programming adaptively using modal properties as objective function at the tripile model . . . . .	109
5.4.	Acceleration time series, measured by the uppermost accelerometer at the undamaged tripile model under impulse load . . . . .	110
5.5.	Overview on success of damage localization using different metrics at the tripile structure for different cut depths . . . . .	114
5.6.	Parameterization of the blade model according to blade construction plans and discretization for damage localization . . . . .	115
5.7.	Final objective function values after running eight Simulated Quenching runs and Sequential Quadratic Programming adaptively using modal properties as objective function at the blade model with an artificial stiffness reduction of 0.5% . . . . .	116
5.8.	Overview on stiffness parameter 4 for all investigated damage states at the rotor blade . . . . .	118
5.9.	Vector parameter $\psi$ applied to results of damage localization at the blade using $\rho^{\omega+\phi}$ . . . . .	119
5.10.	Vector parameter $\psi$ applied to results of damage localization at the blade using $\rho^\tau$ . . . . .	120
5.11.	Overview on the experimental prestressed concrete tower structure	122
5.12.	Damage degree 1 applied to the experimental structure . . . . .	123
5.13.	Acceleration time series of a test conducted at the tower . . . . .	125
5.14.	First eigenfrequencies of configurations 5 and 6 identified from the impulse tests . . . . .	126
5.15.	First eigenfrequencies of all tests conducted for configuration 1 . . . . .	126
A.1.	Geometrical properties of circle cross section damaged with a straight cut . . . . .	142
A.2.	Geometrical properties of circle cross section in case of a angular elimination of area . . . . .	143





# List of Tables

3.1. Advantages and disadvantages of different analysis types for comparison of measurement data and numerical models in structural dynamics . . . . .	51
3.2. Comparison of eigenfrequencies of the shell model for different damage severities . . . . .	53
3.3. Minimal objective function values and corresponding stiffness parameters from ten Simulated Quenching runs using $\rho^s$ at the cantilever model with $\Delta\alpha = 10^\circ$ . . . . .	55
3.4. Minimal objective function values and corresponding stiffness parameters from ten Sequential Quadratic Programming runs using $\rho^s$ at the cantilever model with $\Delta\alpha = 10^\circ$ , starting with the results from Table 3.3 . . . . .	57
3.5. Averaged stiffness parameters of the damaged area after model updating for different damage severities . . . . .	59
3.6. Geometric properties of the OC3 monopile model . . . . .	61
3.7. Comparison of damaged and undamaged eigenfrequencies at the monopile model . . . . .	61
3.8. Minimal objective function values and corresponding stiffness parameters from ten Simulated Quenching runs using $\rho^{\omega+\phi}$ at the monopile model. . . . .	62
3.9. Resulting minimal objective function values and corresponding stiffness parameters from ten Sequential Quadratic Programming runs, using $\rho^{\omega+\phi}$ at the monopile model, starting adaptively with the results from Table 3.8 . . . . .	63
3.10. Resulting minimal objective function values and corresponding stiffness parameters from eight Simulated Quenching runs using $\rho^{l_2}$ at the monopile model . . . . .	67
3.11. Resulting minimal objective function values and corresponding stiffness parameters from eight Sequential Quadratic Programming runs using $\rho^{l_2}$ at the monopile model, starting adaptively with the results from Table 3.10 . . . . .	68

# List of Tables

4.1. Overview on structural states investigated in the three-story frame by Los Alamos National Laboratories . . . . .	75
4.2. Masses of components used for building the frame structure . . . . .	78
4.3. Comparison of measured and simulated eigenfrequencies of the three-story frame . . . . .	79
4.4. Normalized minimal objective function values and according parameters for ten Simulated Quenching runs, using $\rho^{\omega+\phi}$ to identify parameters of baseline condition . . . . .	82
4.5. Normalized minimal objective function values and according parameters for ten Simulated Quenching runs, using $\rho^{\omega+\phi}$ to identify parameters of state 3 . . . . .	83
4.6. Normalized minimal objective function values and according parameters for ten Simulated Quenching and subsequent Sequential Quadratic Programming runs, using $\rho^s$ to identify baseline condition	85
4.7. Normalized minimal objective function values and according parameters for ten Simulated Quenching and subsequent Sequential Quadratic Programming runs, using $\rho^s$ to identify state 3 . . . . .	86
4.8. Normalized minimal objective function values and according parameters for Simulated Quenching and subsequent Sequential Quadratic Programming, using $\rho^{l2}$ to identify baseline condition . . . . .	87
4.9. Positions of geophones and accelerometers on rotor blade . . . . .	90
4.10. Normalized geometry properties of the blade and the according numerical model . . . . .	92
4.11. Comparison of rotor blade eigenfrequencies and mode shapes identified from measurement data and simulation model . . . . .	94
4.12. Parameters after updating the numerical model to measured properties, using $\rho^{\omega+\phi}$ as objective function . . . . .	96
4.13. Results of ten runs, using Simulated Quenching and Sequential Quadratic Programming adaptively, employing $\rho^{\omega+\phi}$ as objective function for investigation of ice step 1. Objective function values are normalized to the initial values. . . . .	97
5.1. Overview on investigated damage steps . . . . .	106
5.2. Comparison of undamaged and damaged eigenfrequencies of the tripile model . . . . .	106
5.3. Resulting minimal objective function values and corresponding stiffness parameters from ten Simulated Quenching runs using $\rho^{\omega+\phi}$ at the tripile model for damage step 7 . . . . .	108

5.4.	Resulting minimal objective function values and corresponding stiffness parameters from Sequential Quadratic Programming runs using $\rho^{\omega+\phi}$ at the tripile model for damage step 7, starting adaptively with the results from Table 5.3 . . . . .	108
5.5.	Resulting minimal objective function values and corresponding stiffness parameters from eight Simulated Quenching runs using $\rho^{l_2}$ at the tripile model for damage step 7, including only transient decay . . . . .	111
5.6.	Resulting minimal objective function values and corresponding stiffness parameters from Sequential Quadratic Programming runs using $\rho^{l_2}$ at the tripile model for damage step 7, including only the transient decay and starting adaptively with the results from Table 5.5 . . . . .	111
5.7.	Resulting minimal objective function values and corresponding stiffness parameters from eight Simulated Quenching runs using $\rho^{l_2}$ at the tripile model for damage step 7, including transient procedure . . . . .	112
5.8.	Resulting minimal objective function values and corresponding stiffness parameters from Sequential Quadratic Programming runs using $\rho^{l_2}$ at the tripile model for damage step 7, including transient procedure and starting adaptively with the results from Table 5.7 . . . . .	112
5.9.	Resulting minimal objective function values and corresponding stiffness parameters from Simulated Quenching and adaptive Sequential Quadratic Programming runs using $\rho^s$ at the tripile model for damage step 7 . . . . .	113
5.10.	Final results after running Simulated Quenching and adaptive Sequential Quadratic Programming to solve problem (5.1) using $\rho^{\omega+\phi}$ as objective function, stiffness reduction 0.5% . . . . .	116
5.12.	Results of Simulated Quenching and adaptive Sequential Quadratic Programming using $\rho^{\omega+\phi}$ to locate damage in the rotor blade . . . . .	119
5.13.	Results of Simulated Quenching and adaptive Sequential Quadratic Programming using $\rho^{\tau}$ to locate damage in the rotor blade . . . . .	120
5.14.	Mass distribution of the tower . . . . .	122
5.15.	Damage degrees applied to the experimental structure . . . . .	124
5.16.	Configurations investigated at the experimental structure . . . . .	124
5.18.	Locations of elements of simulation model and their density . . . . .	127
5.17.	Material properties of the concrete in the simulation model . . . . .	127
5.19.	Results of Simulated Quenching and Sequential Quadratic Programming using $\rho^{l_2}$ to locate clamping failure in the tower . . . . .	129
5.20.	Results of Simulated Quenching and Sequential Quadratic Programming using $\rho^{\mu}$ to locate clamping failure in the tower . . . . .	129

List of Tables

5.21. Results of Simulated Quenching and adaptive Sequential Quadratic Programming using  $\rho^{l^2}$  to locate altered clamping conditions damage in the tower . . . . . 131

5.22. Results of Simulated Quenching and adaptive Sequential Quadratic Programming using  $\rho^\mu$  to locate altered clamping conditions damage in the tower . . . . . 131

# Nomenclature

---

Symbol	Description
$\mathbf{A}$	Matrix containing all linear constraint vectors or system matrix in state space representation
$\mathbf{a}$	Linear constraint vector
$\mathbf{B}$	Input matrix in state space representation
$\mathbf{C}$	Damping matrix or output matrix in state space representation
$c_i$	$i$ -th constraint
$c_1, c_2$	Stiffness and mass proportional Rayleigh damping coefficient
$D$	Number of data points within a signal
$\mathbf{f}$	Vector of forces acting on a structure
$\mathbf{H}$	Transfer function
$H$	Number of considered eigenmodes
$\mathbf{K}$	Stiffness matrix
$K$	Number of considered nodes, e.g. number of sensors/channels
$k$	Iteration counter
$\mathbf{M}$	Mass matrix
$N$	Number of points in time series
$n$	number of model or optimization parameters
$P$	Number of degrees of freedom
$\mathbf{p}_k$	Step towards the solution of optimization problems at iteration $k$
$\mathbf{Q}$	Matrix containing the quadratic terms in a quadratic optimization problem
$s_{xx}$	Power Spectral Density
$\mathbf{u}$	Vector of displacements
$\dot{\mathbf{u}}$	Vector of velocities
$\ddot{\mathbf{u}}$	Vector of accelerations
$\mathbf{v}$	Vector containing any time series, e.g. an acceleration signal
$\mathbf{v}_f$	filtered time series

---

Symbol	Description
$\zeta_i$	Damping ratio of $i$ -th eigenmode
$\boldsymbol{\theta}$	Vector of model parameters
$\boldsymbol{\theta}_k$	Vector of parameters at iteration step $k$
$\boldsymbol{\lambda}$	Vector of Lagrange multipliers
$\rho$	Objective function, metric for comparison of model and measurement
$\rho^\omega$	Metric based on eigenfrequencies
$\rho^\phi$	Metric based on eigenvectors
$\rho^{\omega+\phi}$	Metric based on both eigenfrequencies and mode shapes
$\rho^{l_2}$	Metric based on time series
$\rho^\mu$	Metric based on Mahalanobis distance
$\rho^s$	Metric based on power spectral densities
$\rho^\tau$	Metric based on transmissibility functions
$\sigma$	Standard deviation
$\Phi$	Matrix containing all eigenmodes column-wise
$\phi_i$	$i$ -th eigenvector
$\phi_1$	$l_1$ merit function
$\psi_i$	Normalized measure for the mean deviation of a vector from 1.0: $\psi_i = \frac{ \mathcal{M}_{p_i} - 1 }{\max(\psi)}$
$\boldsymbol{\omega}$	Vector containing all eigenfrequencies
$\omega_i$	$i$ -th eigenfrequency
$\mathbb{I}$	Identity matrix
$\mathcal{F}(\bullet)$	Fourier Transform operator
$\mathcal{L}(\bullet, \bullet)$	Lagrangian operator: $\mathcal{L}(x, y) = \rho(x) - yc(x)$
$\mathcal{L}_\theta(\bullet, \bullet)$	Derivative of Lagrangian with respect to $\boldsymbol{\theta}$
$\mathcal{L}_{\theta\theta}^2(\bullet, \bullet)$	Hessian of Lagrangian with respect to $\boldsymbol{\theta}$
$\bar{\bullet}$	Complex conjugate
$\bullet^{-1}$	Inverse
$\bullet^*$	Optimum
$\ \bullet\ $	$l_2$ -norm: $\ \bullet\  = \sqrt{\sum_i \bullet_i^2}$
$ \bullet $	Absolute value
$\nabla\bullet$	Nabla operator: $\nabla\bullet = \left[ \frac{\partial\bullet}{\partial x_1} \dots \frac{\partial\bullet}{\partial x_n} \right]^T$
$\mathcal{M}\bullet$	Expectation value of signal or vector $\bullet$ (=arithmetic mean)
$\bullet \star \bullet$	Cross correlation of two signals
$D(\bullet, \bullet)$	Directional derivative

Symbol	Description
$\bullet_c$	Continuous representation
$\bullet_d$	Discrete representation
$\bullet_k$	k-th iteration
$\bullet_m$	Measured signal or quantity
$\bullet_s$	Simulated signal or quantity
$\mathcal{A}$	Active set
$\mathcal{E}$	Set of equality constraints
$\mathcal{I}$	Set of inequality constraints
$\mathcal{W}$	Working set
$\mathcal{Y}$	Set of eigenvectors considered for model to measurement comparison
$\mathcal{Z}$	Set of time series considered for model to measurement comparison





# 1. Introduction

## 1.1. Motivation

Numerical models are key technologies in many engineering applications. They assist the executive engineers in design decisions and comprise more accurate representations of physical systems than calculations by hand can do. The better representations aid designers especially in complex systems, resulting in better designs and advanced product development. Furthermore, these models allow a deeper understanding of the underlying physics and cost savings during development processes through virtual prototyping.

However, numerical models usually return results that differ from those measured in real structures. Considering these discrepancies as errors caused by uncertainties in both measurement and simulation allows a classification. According to [85], uncertainties in computer models can be categorized into six classes: *Parameter uncertainty* is the first category, regarded as one of the most important uncertainties [55]. It encloses uncertain inputs to the computer code, such as unknown parameters of the model. Examples of parameter uncertainties in structural dynamics are given in Figure 1.1. *Model inadequacy* contains the inability of models to reflect the real physical behavior, even if all input parameters are known, caused by lack of knowledge of the underlying physics of the investigated problem. *Residual variability* describes the variability of processes that may be inherently unpredictable and stochastic and therefore hard to predict. *Parametric variability* is present, if parameters cannot be expressed deterministically, adding additional uncertainty to the model. The *observation error* includes all errors obtained during observations or measurements of an investigated structure. Also, all errors caused by interpretation and post-processing of measurement data are included. The last class is *code uncertainty*, containing all possible errors concerning implementations of computer code used to solve numerical models.

The improvement of a numerical model using incomplete and possibly imprecise measurement data is the central goal in model updating [55]. It is a technique focusing on parameter uncertainty and parametric variability, leaving all remaining uncertainties untouched. Hence, the executive engineers are responsible for taking

# 1. Introduction

care of these uncertainties. Code uncertainties can be regarded as relatively small, especially if commercial tools with a broad user community are used. Residual variabilities are hard to predict. Their handling is cumbersome, especially regarding iterative environments such as model updating. Thus, these uncertainties are omitted within this context. When comparing measurement data and results from numerical models, the measurements are assumed to be 'the truth' [102], reducing the observation error to zero. This results in the need for highest attention during the realization and execution of measurement campaigns or experiments. Furthermore, post-processing of the measurement data must be done attentively in order not to produce wrong measurement results. Model inadequacy is another uncertainty being heavily influenced by the engineers. If a model is not able to mirror the physical behavior of the investigated system or if wrong initial parameters are chosen, no model updating algorithm can estimate parameters that fit the responses of the model to measured data.

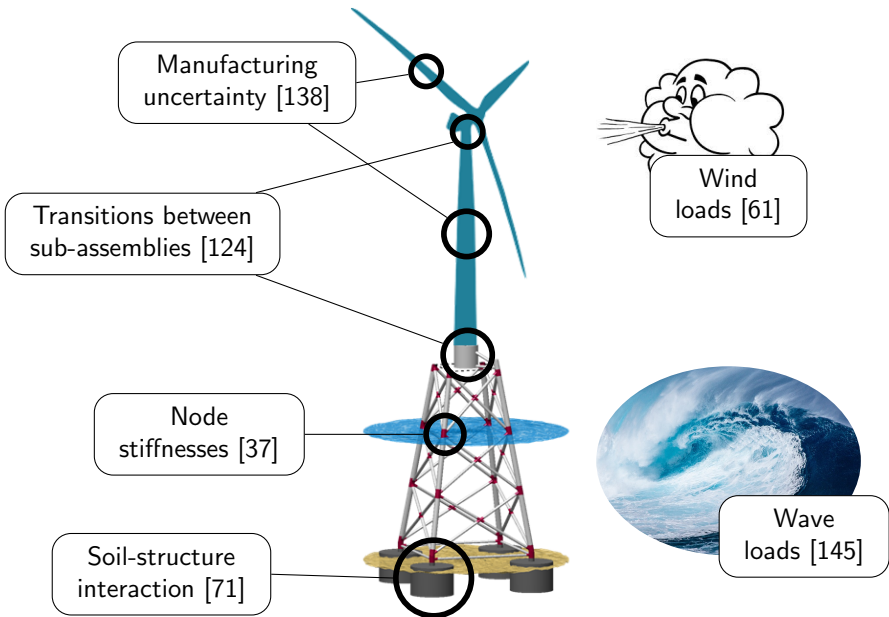


Figure 1.1.: Parameter uncertainties in structural models by the example of an offshore wind turbine

Because of its potential to reduce the important parametric uncertainties, model updating is of high interest in numerical modeling. Due to their size and complexity, structural systems immanently contain many unknowns that cannot be determined directly. Accurate models of these large structures are important to correctly estimate the fatigue behavior of sensitive infrastructure such as bridges, skyscrapers or offshore structures, among others.

If a model displaying a good representation of the measured data is identified using model updating techniques, the same methodology can be applied throughout the lifespan of this structure in monitoring systems that examine the structural state. Operation and maintenance of these big systems cause severe costs for the operators throughout the service life of these constructions. Visual inspections of the structures are time-consuming, costly and sometimes dangerous for the service staff. Monitoring systems can replace the human supervision by automated online systems using different sensors placed among the structure. Furthermore, due to real-time monitoring instead of fixed maintenance intervals, damages are supposed to be identified at an early stage, reducing repair costs. Model updating can deliver an important input to such a monitoring system to localize damages within the investigated structures.

The following sections give an overview on both the general and the structural health monitoring application of model updating and introduce state of the art ideas and technologies in a literature review.

## 1.2. State of the art

Originating from the application in space structures in the early and mid 1980s [13], model updating techniques are being investigated during the last decades [119,120]. Beginning in the early 1990s, the methods were increasingly applied to other structural systems such as civil engineering [160] and aerospace structures [112]. Available methods can be categorized by direct and indirect methods, the former being evolved before the latter due to lacking computational power in that period [118]. Direct methods try to solve the model updating problem using an analytical approach, e.g., solving an equation system with the system matrices incorporated directly in the formulation. The first application of a direct method is described in [12]. Direct methods are missing flexibility, having the disadvantage that the underlying models cannot be parameterized [55]. Every entity of a model is variable instead, and there is no control over the magnitude of the entities. A simultaneous updating of mass and stiffness matrices is not possible using these approaches. Furthermore, positive definiteness of matrices is not guaranteed, and interpretation of results may be impossible since the numerical models must be reduced to the

## 1. Introduction

dimension of measured systems. This leads to possible unphysical solutions during the updating process. Increasing computational power allowed the application of iterative methods for model updating, resolving some of the major drawbacks of direct methods.

### 1.2.1. Model updating fundamentals

There are two different branches of model updating known in the literature. These are known as deterministic and probabilistic model updating. In deterministic model updating, a minimization problem is solved using advanced optimization methods, whereas probabilistic model updating is mostly based on Bayesian probability formulations<sup>1</sup>. This section explains both branches and the basic ideas. This fundamental classification is followed by the ingredients needed for deterministic model updating: the processing of measurement data, methods to compare measurement and simulation data and the optimization algorithms needed to minimize the objective function formulated using a certain comparison metric [53]. The section is closed by an overview of applications to different structural systems.

#### Deterministic model updating

Increasing computational power allows implementing iterative methods, resolving the missing flexibility of direct methods. These iterative methods are classified by the data basis being employed for the application [55], modal, frequency and time domain data, with modal data being the 'classical' approach to model updating. Modal properties inherit the advantage that their computation is typically done without loads acting on the structure. Therefore, this often complex estimation usually simulated by complex numerical tools can be omitted. Besides, damping plays a minor role in low damped systems and may be neglected if only modal properties are considered [111]. The sensitivity of all modal parameters to structural changes is proven in [101].

Because measured data and results from numerical models are compared in model updating, the measured data must be preprocessed accordingly. The extraction of modal properties using operational modal analysis methods is a particular active research area with ongoing research efforts [23]. Results of modal analyses are commonly ordered by the magnitude of their eigenvalues. A distinct allocation of measured and simulated eigenmodes is achieved using the modal assurance criterion [3]. The modal assurance criterion provides information on the orthogo-

---

<sup>1</sup>In the end, this also results in the need to solve an optimization problem

nality of eigenvectors. A value of 1 indicates linear dependency, whereas a value of 0 indicates independence of vectors. Because uncertainties are present in every measurement, a value  $> 0.8$  is accepted as a good correlation of two considered eigenvectors [95]. It may be used as an indicator of damages [149]. In model updating, the modal assurance criterion is often employed to correlate eigenmodes from measurement and simulation. In addition to the assignment of eigenmodes, eigenvectors may be differently scaled and out of phase. This is resolved using the modal scale factor [39], leaving orthogonality properties unaffected.

Due to space and cost limitations, eigenvectors identified from measured data have a lower dimension than eigenvectors from numerical models since only a certain number of sensors can be placed on the structure. The easiest way to deal with this is to define nodes of the numerical model at the same location of sensors installed on the structure and reduce the simulated eigenvectors to these nodes. In addition to this rather simple approach, two ways to modify the vectors are known [10]. Firstly, an expansion of the measured eigenvectors to the dimension of the simulation model and secondly, a reduction of the simulated eigenvectors to the dimension of the measured vectors. For the expansion of identified eigenvectors both vector space enhancement methods and minimization methods that use system matrices are known from the literature. The latter are classified to be more robust, but numerically more costly in [8]. Several methods for the reduction of simulated eigenvectors are known. [11] concludes that the system equivalent reduction expansion process is suitable in model updating applications because modal properties are nearly unbiased with this procedure [83].

After preprocessing of measurement data and model expansion or reduction is done, an objective function is formulated. This objective function is a metric, quantifying the deviation between numerical model and measured data [122]. It may be formulated using modal quantities such as eigenfrequencies or mode shapes, frequency domain or time domain data. The associated numerical model is parameterized, an important step with high influence on the results of the optimization that needs engineering judgment [55]. Any algorithm will only be able to estimate correct parameters if the correct parameters are selected to be treated as variable by the optimization algorithm [56]. In case a constrained optimization algorithm is chosen, constraints may be defined that ensure the parameters or combinations of them to stay within the defined bounds [92].

# 1. Introduction

## Probabilistic model updating

Another approach to parameter identification in numerical models is to use probabilistic methods that do not return deterministic values for the parameters but statistic parameters. These Bayesian approaches [16], which are based on Bayes' theorem [14], modify probability density functions of model parameters considering both the information contained in the data and uncertainties resulting from inaccurate measurements and model predictions [154] (which can also be identified as modeling error) instead of updating the parameters directly. In addition to all information needed for deterministic model updating, these methods require probability distributions for the parameters that may be hard to estimate [100] or described by simplified statistical models that do not represent the real probabilities of parameters. The probability density function is received from measurement results and depicts the probability of the model parameters without referring to any observed information than the measured data, which may be influenced by various effects. This is problematic because one correct prior<sup>2</sup> probability density function does not exist, and the decision on it is subjective. However, the prior probability density function influences the results significantly, because the optimum parameters are determined using these statistical meta-models. Furthermore, these functions are conventionally assumed to be uncorrelated zero-mean Gaussian distributions, having the advantage of improved computational times but being inaccurate in most application examples [155]. The estimation of the parameters can be based on the least-squares approach [33], where the estimator is developed using posterior probability density functions. The parameters with the least variance are assumed to inherit the highest probability [111]. Again, the estimated and the measured parameters are assumed to be independent. In [51] the least-squares approach is expanded with particular weighting matrices and no assumption of independence to the minimum variance approach, which is a more realistic approach accounting for cross-correlation. The posterior probability density function is the product of the prior probability density function and the likelihood function [33], which is identical to the prior probability function for a fixed observed data set [155]. Other common estimator techniques are the Monte Carlo algorithm [106] and its further developments, e.g. Markov Chain Monte Carlo [4] and Transitional Markov Chain Monte Carlo [116], the Laplace method of asymptotic approximation [16], the Kalman filter [7], the Gibbs sampler [17] and the Kriging predictor [87].

Probabilistic model updating is applied to a broad spectrum of structures, in-

---

<sup>2</sup>The term prior is used in Bayesian statistics and expresses the beliefs of a user before evidence is taken into account.

cluding bridges [17] and multi-story structures [30], but applications to real-scale structures are rarely seen in the literature. In [113] it is concluded, that both deterministic and probabilistic approaches perform well for parameter identification. Both methods strongly depend on engineering judgment, while the probabilistic approach needs even more input to estimate the probability distribution. This statement is confirmed by [133]. Therefore, the approaches and methods discussed within this thesis address the deterministic approach of model updating.

## Feature extraction from measurement data

Preprocessing of measurement data is essential for model updating. In this thesis, preprocessing includes all steps needed to adapt measured data to be able to evaluate the metrics chosen for comparison of measured and simulated data. Special methods are employed if the metric is formulated in the modal domain. The response of a dynamic system that can be described by its modal properties is a result of the excitation and its mechanical properties [60]. The excitation is often complex and unknown in civil engineering structures [144, 166], resulting in the need for output-only methods that do not require the system input to extract features from measurement data.

Modal properties are regarded as the 'classical approach' to model updating. The methods used for extraction of modal parameters are classified in frequency and time domain methods. Due to the high number of methods in this area [98, 121], only the basic ideas are introduced here. The most basic approach is to transfer a measured signal to the frequency domain using Fourier transform and visually pick the characteristic peaks of the frequency signal. This method is referred to as basic frequency domain method or 'peak-picking' [40]. Peaks in the frequency signal can be interpreted as eigenfrequencies of the structure. The main disadvantage of the method is the user dependency caused by the manual picking of peaks. A method closely related to the peak-picking method is the frequency domain decomposition. This method uses the singular value decomposition to construct a series of single degree of freedom systems, each correlating with an eigenmode of the structure [24]. In addition to the eigenfrequencies, mode shapes are additional results of this method. Damping is estimated using the enhanced frequency domain decomposition [75].

Autoregressive models are time domain methods for the extraction of modal properties. Originating from financial mathematics [21], these methods were later applied to structural dynamics [22, 139]. Vector autoregressive models allow processing all measured time series at the same time [66]. Stochastic Subspace Identification is another class of time domain methods [129]. It is based on the state-space

## 1. Introduction

formulation of a fictitious system [69] being constructed using eigensystem realization algorithm to be able to reproduce the measured responses [82]. White noise is applied to this system to excite all eigenmodes of the system simultaneously. The eigenmodes of the structure are obtained via modal transformation of the system equations, often containing many more modes than the real structure has. Hence, powerful methods are needed to distinguish real eigenmodes from mathematical ones [68]. If model updating is performed based on data in frequency or time domain, the signals are processed using standard methods known from system identification and structural dynamics.

### Comparison of measurement data and numerical model

After data cleansing and preprocessing are implemented, the data extracted from measurements and results from numerical models are compared to quantify the deviation between measurement and model [123]. Eigenfrequencies are the most basic property to compare measurement data and numerical model [55], having the advantage that both the simulation as well as their identification from measurement data is quite easy. On the other hand, eigenfrequencies are not very sensitive to changes in the structural dynamics [42]. Hence, many authors try to incorporate the eigenvectors to model updating. There are numerous techniques to compare eigenvectors. The basic ones are a comparison of the vectors using the modal assurance criterion [3], curvatures of eigenvectors [130], modal strain energies [97] and direct comparison approaches [146]. Eigenfrequencies are employed to update numerical models in [66], whereas [77] uses eigenvectors. A hybrid implementation is investigated in [111]. Because eigenfrequencies can often be measured more precisely, they are usually weighted higher in objective functions [96]. [130] uses the curvatures of eigenvectors to update numerical models, whereas [101] investigates damping terms for model updating.

Quite recently, authors started to use frequency response functions as a basis for model-to-measurement comparison [59, 152, 156]. Others use the poles identified from transmissibility functions for model updating [158] or other, more general approaches formulated in frequency domain [92]. However, the use of modal properties for model updating purposes is still an area of active research [127, 159]. The comparison of model and measurement in the time domain is not used very often. Usually these data are compared employing the  $l_2$ -norm [58, 76, 146]. A direct comparison of time series enables to include nonlinearities and contains all physical effects such as damping. However, the approach has the major drawback that more sophisticated modeling approaches that include all physical effects that influence the dynamic behavior is necessary. Additional modeling of loads is



necessary in particular. This modeling is often non-trivial in structural systems.

## Optimization algorithms

Sophisticated optimization algorithms are needed to minimize the objective function being formulated using the metrics mentioned in the previous section. Optimization problems are hard to solve if they provide the attributes [9]

- high number of dimensions
- many local minima
- strongly nonlinear
- low smoothness levels
- noise
- discreteness of optimization parameters.

Problems arising in model updating applications inherit all points except discreteness [52]. Obviously, the shape of the objective function is directly influenced by the choice of metrics. Especially the smoothness level, which is fundamental for many optimization methods, may be raised by skilled choices of comparison metrics. A global optimization algorithm is needed to account for the fact that the arising problems provide many local minima. Global optimization algorithms are classified into deterministic and heuristic algorithms. Deterministic algorithms are suited better for problems having a low number of dimensions [169]. Therefore, heuristic methods are favored when it comes to bigger problems. Many of these methods are inspired by processes arising in nature and can be applied to many different problems. Thus, these algorithms are often referred to as *metaheuristics* [6]. The most famous metaheuristics imitate the behavior of a swarm of birds, namely the Particle Swarm Optimization algorithm [84], or the evolutionary process of a population, namely Genetic Algorithms [107]. Both are applied in model updating [20, 74]. especially Genetic Algorithms are used in various model updating approaches, for both general model updating [131] and damage detection [73, 104, 136].

Simulated Annealing is another metaheuristic algorithm, based on the Metropolis algorithm that uses Boltzmann-statistics to simulate a thermodynamic system, resulting in a Markov-Chain-Monte-Carlo procedure [114]. Simulated Annealing implements the soft annealing of metals known from metallurgy. The crystal structure of metals is dissolved if they are heated above a certain temperature, enabling the removal of defects in the material. Residual stresses in the material can be circumvented by soft annealing of the metal, allowing the particles to arrange in the

## 1. Introduction

crystal lattice in a state of minimal energy. Simulated Annealing tries to imitate this manner. At a certain temperature, particles can be either in the crystal lattice or the liquid phase. The probability of being in one of the phases is dependent on the Boltzmann-probability which is controlled by the temperature.

Transferred to optimization, this means that better solutions are always accepted whereas worse solutions are accepted depending on the Boltzmann-probability. Solutions are generated randomly, and the associated objective function value is interpreted as their energy. The slowly decreased surrounding temperature is represented by a decreasing probability to accept worse solutions. On the one hand, this allows leaving local minima, on the other hand approaching towards an optimum is secured in the final phase. The algorithm was applied to many different problems, especially in the chip-industry for an optimal arrangement of chip components [141] and the solution of the famous *traveling-salesman-problem* [38].

The method has some specific advantages compared to other metaheuristics. It is relatively easy to implement and is transferable to many optimization problems with small effort [86]. The consideration of arbitrary constraints is easy (see Section 2.3.1). It can be proven that Simulated Annealing always converges towards the global solution<sup>3</sup> [64, 140]. Furthermore, Simulated Annealing is suitable for parallelization [175]. The authors of [86] conclude that solutions can be approximated relatively fast with Simulated Annealing, whereas high effort is needed to converge towards the exact global optimum.

Simulated Quenching is an enhancement of Simulated Annealing attempting to reach a faster Annealing time leading to lower computational times [164]. The main disadvantage of this enhanced method is lower security to converge towards the global optimum. Thus, Simulated Quenching can be seen as a compromise between reliability of finding the correct solution and computational efficiency. Quantum Annealing is another enhancement of Simulated Annealing, characterized by allowing *quantum jumps* known from quantum dynamics between local optima [46], avoiding to take the long way over a local maximum to reach the next minimum. These methods are regarded to be applicable to quantum computers.

The slow convergence of metaheuristic procedures towards an optimum can be circumvented by aborting the algorithm at a certain point and starting a local optimization algorithm instead. Most metaheuristics require input values that define how long an algorithm is running before being started. These values must be chosen depending on the problem. The local algorithm is then started after the termination of the metaheuristic. This local algorithm must be nonlinear and able to handle constraints to prevent the parameters from being outside feasible

---

<sup>3</sup>An infinite starting temperature is needed to guarantee to find the global optimum for arbitrary objective functions, which would cause infinite computing times.

regions.

Optimization methods that use derivatives are known to converge a lot faster [48]. Several local optimization algorithms have been employed for model updating since the early research initiatives in this area, often without a previous global optimizer and even more often unconstrained. In [110], an optimal gradient method is used for model updating, whereas Newton-Raphson algorithms are used in [72] and [66]. Quadratic Programming is employed for model updating in [78]. A least squares approach is investigated in [152], enhanced to nonlinear least squares in [159] and newton least squares in [127]. In [162], [161] and [9] local minimization methods are coupled in order to approximate a global optimum.

Newton-methods are the biggest class of algorithms using information of both the first and second derivatives. If the Hessian of the objective function cannot be determined analytically, this matrix can be approximated using finite differences. This numerically expensive evaluation is often circumvented using an approximated Hessian, resulting in the subclass of Quasi-Newton methods. The BFGS-method is a well documented and approved method to approximate the Hessian iteratively<sup>4</sup>. Sequential Quadratic Programming methods are regarded as the most successful and effective Quasi-Newton class of methods for the solution of local, constrained, nonlinear optimization problems [18]. These methods approximate a complex optimization problem by a series of quadratic programming problems and solve the problem iteratively. There are many variants, the most renowned implementations are given in [62] and [126]. Sequential Quadratic Programming methods are characterized by specifically high stability even for badly scaled problems with little computing time. They need fewer evaluations of the objective function than most other Quasi-Newton methods [48], which is of high interest in model updating where every evaluation of the objective function includes a solution of the finite element model. Sequential Quadratic Programming is used for model updating in [79] and [146].

## Model updating in structural systems

Besides space, aircraft and mechanical engineering structures, civil engineering structures are one of the classical fields of application for model updating techniques [36]. Multi-story buildings provide an example widely used for model updating. These frame structures can often be modeled by simple spring-mass-damper systems. Therefore, frame structures have become one of the most studied exam-

---

<sup>4</sup>BFGS is named after its inventors R. Broyden [26], C. G. Fletcher [47], D. Goldfarb [63], and F. Shanno [153], who developed and published the method nearly simultaneously in 1970.

## 1. Introduction

ples for the investigation of dynamic structural systems. Model updating to such a frame structure is applied in [25], where, besides other examples, a one-story frame is successfully updated using sensitivity methods. The authors of [2] investigate the application of regularization methods for model updating using a frame structure, whereas modal properties are used to update a reinforced concrete frame in [41]. In [94], a numerical model of a seven-story frame is investigated and updated using measurements from an experimental structure. Models of more general buildings are updated in [49] and [50], including a historic tower and a university building. Bridges are another classical application for model updating in structural systems with a lot of active research. The authors of [162] investigate model updating for a highway bridge using several, coupled local minimization runs to account for the problem having several minima. In [44], a short-span railway bridge is updated using train-load induced displacement measurements employing the Nelder-Mead Simplex method for updating, whereas the Gauss-Newton method is used to update a model of a  $47m$  long three-span steel-bridge excited by a shaker in [59]. A Bayesian framework is employed in [115] including a series of linear optimization problems to update a numerical model of a truss-bridge with  $118m$  spans. A  $59.5m$  long cable-stayed pedestrian bridge is updated based on modal properties in [151], employing particle swarm optimization in combination with a sequential niche technique [15] for optimization.

A relatively new field for model updating is wind energy, which gains importance due to the increasing need for renewable energies. A model of a wind turbine is updated in [74], aiming at service life estimation of the wind turbine. The authors use modal properties and genetic algorithms to update the model. A section of a wind turbine blade is updated in [99] based on modal properties using response surfaces, whereas model updating for horizontal axis wind turbines using a probability framework is investigated in [165]. Simulated Annealing is applied to a numerical model of a wind turbine in [148], whereas Simulated Quenching is used in [147].

### 1.2.2. Structural health monitoring

Monitoring systems for structures are subdivided in *condition monitoring* and *structural health monitoring* systems. Condition monitoring is regarded as a specialized area of structural health monitoring focusing on electrical systems and (rotating) machinery such as gears and bearings, whereas structural health monitoring addresses the investigation of a structure through parameters indicative of the state of the structure [5], focusing on the load bearing assemblies. Both condition monitoring and structural health monitoring may be applied to different

assemblies of the same structure<sup>5</sup> [67]. The following section gives an overview of structural health monitoring, the basic concepts and the application of model updating for structural health monitoring in civil structures.

## Fundamentals of structural health monitoring

Structural Health Monitoring systems consist out of two components: sensing equipment and algorithms for analysis and interpretation of measurement data [31]. The number, sort, and positions of sensors are affected by the available measurement equipment as well as the algorithms. According to Rytter [142], the different approaches for data analysis can be grouped into four levels:

Level I: Damage detection

Level II: Damage localization

Level III: Damage quantification

Level IV: Prediction of the remaining service life

The first level, damage detection comprises methods aimed to detect whether damage is present in a structure or not. Damage localization moves on to the next level, giving information on the location of damages, which is of high interest in big structures with areas that may not be checked visually. The following level tries to estimate the severity of the damage. Based on this information, level IV aims to predict the influence of the damage on the serviceability of the structure, often especially regarding fatigue behavior. A higher level leads to higher complexity of the underlying analysis. Also, each level should be managed before the next level is concerned [171]. Some authors introduce an additional level 'damage type' between II and III [57, 171]. Others propose a fifth level for active, self-healing structures [28]. The underlying principle is an active structure that reacts on damages using piezo-elements to avoid expansion. This stage is restricted to small construction elements such as screws and boltings [132].

The 'fundamental axioms of structural health monitoring' introduced by Worden et al. [172] provide general principles that are well accepted among the structural health monitoring society. These are

Axiom 1: All materials have inherent flaws or defects.

Axiom 2: The assessment of damage requires a comparison between two system states.

---

<sup>5</sup>E.g., consider a wind turbine. Here, condition monitoring is employed to monitor the gearbox, the bearings and the electrical system which are usually installed in the nacelle, whereas structural health monitoring focuses on the rotor blades and the support structure below the nacelle.

## 1. Introduction

Axiom 3: Identifying the existence and location of damage can be done in an unsupervised learning mode, but identifying the type of damage present and the damage severity can only be done in a supervised learning mode.

Axiom 4a: Sensors cannot measure damage. Feature extraction through signal processing and statistical classification is necessary to convert sensor data into damage information.

Axiom 4b: Without intelligent feature extraction, the more sensitive a measurement is to damage, the more sensitive it is to changing operational and environmental conditions.

Axiom 5: The length- and time-scales associated with damage initiation and evolution dictate the required properties of the structural health monitoring sensing system.

Axiom 6: There is a trade-off between the sensitivity to damage of an algorithm and its noise rejection capability.

Axiom 7: The size of damage that can be detected from changes in system dynamics is inversely proportional to the frequency range of excitation.

Besides the vibration-based methods contemplated here, there is a big number of different methods for structural health monitoring of civil structures [31]. Vibration-based methods provide the essential advantage that the sensors used to measure vibration data are well established, leading to highly reliable sensors to measure structural dynamics. The reliability of sensors is of high importance, especially for long-term structural health monitoring systems (see Axiom 5). Furthermore, the dynamic behavior of a structure may be measured with a relatively low number of sensors which is important due to the size of structural systems. It is well accepted that any damage causes a local stiffness decrease and an increase of the damping [1, 65, 128]. If big enough, any local decrease of stiffness influences the dynamic global response of a structure. Hence, monitoring the 'dynamic fingerprint' of a structure has the advantage, that sensors must not necessarily be close to the damage location [57], but a comparison of undamaged and damaged system state is needed (see Axiom 2). Axioms 4a and b aim at the core of this thesis: algorithms are needed to interpret measured data because sensors cannot measure damage directly. In this thesis, a good initial guess (a numerical model representing the structure) is adjusted to represent measured data. This process can be interpreted as the 'learning phase', whereas damage localization using model updating, as intended here, is the testing phase. The algorithms presented in this thesis provide a method to convert sensor data to damage information. Because

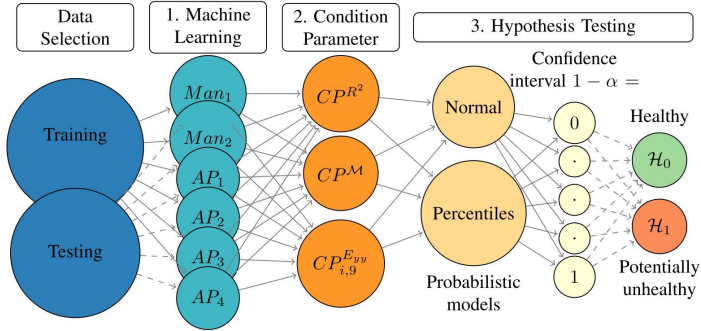


Figure 1.2.: Three-tier damage detection framework: After the training phase, incoming test data is analyzed using a combination of machine learning, condition parameter, and hypothesis testing methods to estimate the current state of the structure [70].

damage localization is level II monitoring, level I must be accomplished first. Recently, a three-tier structural health monitoring scheme for wind turbines was proposed in [70], facing level I structural health monitoring. The scheme uses both environmental and operational conditions and vibration based measurement data. A practical implementation is given in [69]. This framework (see Figure 1.2) is designated to implement and compare arbitrary combinations of methods for each of the three tiers. Every reference-based structural health monitoring system includes a comparison of initial and new data sets, resulting in an initial training phase of the procedure. Data selection is included as a first informal step, affecting the overall performance of the structural health monitoring system. To assess the damage state of a structure, data normalization and clustering of data sets to groups with similar environmental and operational conditions by machine learning represents the first tier. Subsequently, the extraction of condition parameters follows as a basis of decision and finally, a decision is made based on statistical hypothesis tests. An application of the scheme is given in [163]. If this three-tier scheme encounters potentially unhealthy data, damage localization is the logical next step.

## Model updating for damage localization

If the response of a dynamic system alters due to damage, a numerical model may be adjusted to reproduce the new system response. The location where an algorithm changes stiffnesses in the numerical model may then be interpreted as

# 1. Introduction

the damage location. According to [102], the general approach can be partitioned via six steps:

1. Formulation of a numerical model of the examined structure
2. Measurement and processing of dynamic time series
3. Adjusting the numerical model to reproduce the measured data best possible
4. After damage event: repeat step 2
5. Re-adjust the numerical model to reproduce the measurements taken in step 4
6. Interpretation of changed model parameters as a damage indicator

Many studies focus on model updating for structural health monitoring, but often the investigated systems are purely numerical studies, neglecting the influence of measurement noise (see, for instance, [29,88,174]). Furthermore, modal properties vary with different environmental and operational conditions [68]. These studies can be seen as a proof of concept, but not as a validation of the methodology. This is also one of the central statements of Figure 1.3 [10], with measurement data being one of the three essential columns for model-based structural health monitoring.

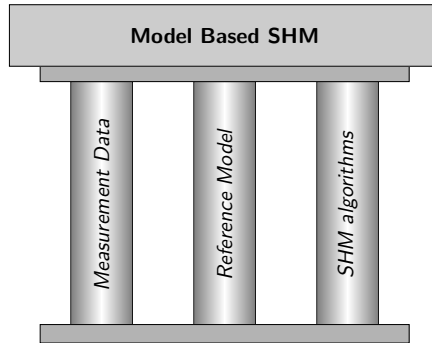


Figure 1.3.: Three columns of model-based structural health monitoring [10]

Different studies focused on model updating for damage localization in structural systems: In [167] damage quantification is performed using model updating techniques applied to simple reinforced concrete beams. The authors of [110] and [90] successfully aim to use model updating for damage localization in frame structures. Model updating for damage identification in lattice structures is used in [32], whereas damage quantification at an offshore jacket-structure is performed in [109].



In many cases, the damage is modeled using variable stiffnesses of elements, which is the simplest way to model the postulated stiffness decrease. The spot with a decreased stiffness is interpreted as the damage location [111]. Depending on the complexity of the model it may be extensive to model every single element with variable stiffness. This can be overcome by the use of damage functions [161]. This approach modifies the stiffnesses of several elements using functions instead of treating every element individually. The factors of these functions are used as optimization parameters, drastically reducing the number of parameters needed. Besides, this approach leads to well-conditioned system matrices which has advantages during the solution of the models.

### 1.3. Goals and objectives

Model updating is a widely used technique, and plenty of research effort has been put into the field of updating structural systems to achieve a higher concordance between numerical models and measurement data. However, what is missing is a strategy that can deal with the globality of the optimization problems in a numerically efficient way. Every evaluation of the objective function causes a time-consuming numerical analysis, resulting in long computational times usually needed to solve the optimization problem using state-of-the-art global optimization algorithms. If local algorithms are applied solely, computational times are low, but there is no guarantee that the global optimum is found. Thus, the main objective of this thesis is to develop, implement and analyze an advanced model updating strategy with special emphasis on large structural systems. Also, an approach for the interpretation of results is given. A general framework shall be developed, illustrating all essential steps that may be used for model updating, enabling a more general view on the methodology and a deeper understanding of model updating approaches. The algorithm presented in this thesis comprises a possible implementation of this scheme.

Though modal properties are known to be relatively insensitive to structural changes such as damages, they are still state-of-the-art with ongoing research focusing on metrics in the modal domain. Besides, the use of metrics in modal domain restricts the application to linear problems. Therefore, other metrics in both frequency and time domain are investigated, and their capability for use in model updating applications is compared to modal approaches with special emphasis on their capabilities to include and detect nonlinearities.

The structured evaluation and interpretation of the model updating results is another important topic that is covered in this thesis, focusing on the randomness of results generated using metaheuristic optimization methods by introducing ways

# 1. Introduction

to assert the solutions statistically and by their optimal objective function value. Many examples used in the literature lack applications of the methods to real measurement data, though the effects of measurement noise and experimental techniques play a substantial role. It is the authors believe that a practical application is of the highest importance to prove the functionality of model updating methods due to the difficulties that arise in real measurements only. Thus, different experimental structures are analyzed within this thesis to prove the investigated concepts in near-practice applications. The measurement data are analyzed and interpreted employing used practice techniques, showing methodologies to evaluate large scale experiments in structural dynamics. The algorithms presented are applied both to general model updating as well as damage localization, since all models are damaged during the experiments. Hence, the examples demonstrate both the functionality as well as limitations of the approach. Furthermore, recommendations for the design of experiments in future applications are given.

The central innovations in this thesis are:

- a new numerically efficient two-step optimization algorithm able to deal with all challenges arising in applications for model updating, especially the globality of optimization problems and constraints on the parameters
- the introduction of model to measurement comparison techniques that are new in model updating applications
- a general scheme for model updating, allowing a comprehensive overview of all methods and technologies needed to perform iterative model updating in structural dynamics
- suggestions on the choice of metrics for specific problems.

Further novelties are:

- the application of new metrics to both general model updating as well as model updating for damage localization
- the application of these metrics to nonlinear problems
- a new probabilistic interpretation approach for results of abbreviated meta-heuristic procedures
- new investigations on the capability of beam models for representation of local damages
- new approaches for the interpretation of results obtained from model updating analyses.

This thesis is intended to contribute to the model updating community in several ways: Firstly, to give an up-to-date overview of the literature and state-of-the-art techniques for updating structural systems to measurement data. Secondly, to

present a new, numerically efficient algorithm for model updating and demonstrate the application to different, partially nonlinear structural systems and to damage localization. Finally, to give advice and ideas on the choice of metrics for model to measurement comparison and discuss advantages and disadvantages of the different approaches for future applications. In the structural health monitoring context of model updating, damage quantification (Level III structural health monitoring according to Rytter's scale) is beyond the scope of this thesis.

## 1.4. Structure of the thesis

Model updating techniques are a result of the constantly growing need for more reliable models. The key task of this thesis is to develop a strategy for model updating in often complex structural systems. Based on the introduction and the state-of-the-art given within this chapter, the theoretical foundation for this thesis is outlined in chapter 2, including a general introduction to structural dynamics, various methods to compare measurement data and numerical model and a deep description of the optimization algorithms used throughout this thesis.

A general strategy for model updating is introduced in chapter 3, followed by two examples that verify the methodology on a theoretical basis. The first example is a numerically tested, simulated cantilever beam that is investigated using virtual damage. Damage is located using the model updating approach described in the previous section. The second example is the application to a virtual offshore wind turbine based on a monopile foundation.

The methods are applied parameter to parameter identification with real measured data in chapter 4, using two examples. The first example is a small scale model of a three-story building structure that was tested at the Los Alamos National Laboratory. The localization and quantification of ice accretion on a real scale 34m long rotor blade is the second example.

The concept is utilized for damage localization in chapter 5, using three examples. A sensitivity analysis on the damage localization capabilities of the strategy is demonstrated in the first example, a scaled model of an offshore tripile-structure. The 34m rotor blade of chapter 4 is driven to fatigue damage during the experiments. Thus, the damage is located using the model updating strategy. In addition, a scaled prestressed concrete tower is damaged by saw cuts and loosened screws at the basement clamping. Both damages are located in this section.

Chapter 6 closes the work, summarizing the major findings of this thesis and discussing open questions to provide a basis for future research.



## 2. Theoretical Background

Within this chapter, the theoretical background needed for the application of model updating as done in the following chapters is given. Starting with a general introduction to numerical modeling in dynamic analyses, metrics that quantify the deviation between numerical models and measurement data in different domains are introduced afterward. The metrics are utilized to formulate optimization problems and methods used to solve these problems are introduced. These methods aim to minimize the deviation of numerical and measured results subject to constraints via alterations of parameters of numerical models, yielding the parameters that result in a minimum deviation between model and measurement as their final result.

### 2.1. Basics of computational structural dynamics

#### 2.1.1. Numerical representation of dynamic systems

Mathematical descriptions of physical processes are essential in all engineering sciences. These mathematical models support a deep understanding of the physical behavior and allow predicting characteristics and performance of the studied system. Model updating in structural dynamics includes the adjustment of model parameters to match measured data. The dynamic response of a linear mechanical system with  $P$  degrees of freedom is described by the second order ordinary differential equation

$$M\ddot{\mathbf{u}}(t) + C\dot{\mathbf{u}}(t) + K\mathbf{u}(t) = \mathbf{f}(t), \quad (2.1)$$

where  $K$ ,  $C$  and  $M \in \mathbb{R}^{P \times P}$  stand for the stiffness, damping and mass matrices, respectively.  $\mathbf{f}$ ,  $\mathbf{u}$ ,  $\dot{\mathbf{u}}$  and  $\ddot{\mathbf{u}} \in \mathbb{R}^{P \times 1}$  represent the vector of forces acting on the system, the displacement, the velocity and the acceleration vector. The stiffness and mass matrices are usually assembled from local element-matrices that are formulated individually for each element connecting several degrees of freedom<sup>1</sup>, whereas

---

<sup>1</sup>In addition to local finite elements other concepts exist that formulate the global matrices directly

## 2. Theoretical Background

the determination of the energy dissipating damping terms is not as straightforward. Damping is a result of several physical processes working simultaneously. For instance, it is material, amplitude, and frequency-dependent. It can be caused by friction within the structure and friction with the surrounding medium. That is why the so-called Rayleigh damping

$$\mathbf{C} = c_1 \mathbf{M} + c_2 \mathbf{K} \quad (2.2)$$

is often employed due to missing information on the exact damping behavior [40], reducing the unknown damping parameters to two parameters  $\alpha$  and  $\beta$ . However, this formulation may be too simple for complex applications. If measurements are available and modal damping ratios are identified, these can be utilized to estimate the damping matrix [117] by computing

$$\mathbf{C}_n = \mathbb{1} [2\zeta_1 \omega_1 M_1 \cdots 2\zeta_i \omega_i M_i]^T, \quad (2.3)$$

where  $\mathbb{1}$  is the identity matrix and  $\zeta_i, \omega_i$  and  $M_i$  represent the  $i$ -th identified damping ratio, eigenfrequency and mass. The damping matrix used in (2.1) is then obtained using

$$\mathbf{C} = \mathbf{\Phi}^{-T} \mathbf{C}_n \mathbf{\Phi}^{-1}, \quad (2.4)$$

with  $\mathbf{\Phi}$  denoting the matrix of column-wise eigenvectors.

The undamped eigenfrequencies and eigenvectors are needed for this approach. These are computed by solving the eigenvalue problem

$$(\mathbf{K} - \omega_i^2 \mathbf{M}) \phi_i = 0. \quad (2.5)$$

The solution of equation (2.5) is referred to as modal analysis of the system. The resulting eigenfrequencies and mode shapes may be used to compare simulation results and measured data. Another approach is to compare the measured signals directly without a previous identification of the eigenfrequencies and mode shapes. The transient solution of the system is needed for this approach. The transient solution of the system (2.1) can be calculated using the implicit time integration algorithm proposed by Newmark [134]. Starting with given initial conditions for  $\mathbf{u}_0$  and  $\dot{\mathbf{u}}_0$ , the displacement at the next iterate  $\mathbf{u}_{k+1}$  is computed solving the linear equation system

$$\hat{\mathbf{K}} \mathbf{u}_{k+1} = \hat{\mathbf{f}}_{k+1}, \quad (2.6)$$

with the effective stiffness  $\hat{\mathbf{K}}$  being

$$\hat{\mathbf{K}} = \mathbf{K} + \frac{1}{\beta \Delta t^2} \mathbf{M} + \frac{\gamma}{\beta \Delta t} \mathbf{C}. \quad (2.7)$$

Here, the Newmark constants  $\gamma = 0.5$  and  $\beta = 0.1\bar{6}$  are used for the linear acceleration method and  $\Delta t$  denotes the time increment. The effective force  $\hat{\mathbf{f}}_{k+1}$  at time  $t_{k+1}$  is defined by

$$\begin{aligned} \hat{\mathbf{f}}_{k+1} = & \mathbf{f}_{k+1} + \mathbf{M} \left( \frac{1}{\beta \Delta t^2} \mathbf{u}_k + \frac{1}{\beta \Delta t} \dot{\mathbf{u}}_k + \left( \frac{1}{2\beta} - 1 \right) \ddot{\mathbf{u}}_k \right) \\ & + \mathbf{C} \left( \frac{\gamma}{\beta \Delta t} \mathbf{u}_k + \left( \frac{\gamma}{\beta} - 1 \right) \dot{\mathbf{u}}_k + \left( \frac{\gamma}{2\beta} - 1 \right) \Delta t \ddot{\mathbf{u}}_k \right). \end{aligned} \quad (2.8)$$

With the displacement vector of the next iterate known from equation (2.6), the velocity and acceleration at the next iterate are computed using

$$\dot{\mathbf{u}}_{k+1} = \dot{\mathbf{u}}_k + (1 - \gamma) \Delta t \ddot{\mathbf{u}}_k + \gamma \Delta t \ddot{\mathbf{u}}_{k+1} \quad (2.9)$$

and

$$\ddot{\mathbf{u}}_{k+1} = \frac{1}{\beta \Delta t^2} (\mathbf{u}_{k+1} - \mathbf{u}_k) - \frac{1}{\beta \Delta t} \dot{\mathbf{u}}_k - \left( \frac{1}{2\beta} - 1 \right) \ddot{\mathbf{u}}_k. \quad (2.10)$$

Equations (2.9) and (2.10) are called the prediction formulae.

Another representation of the system results from a transformation of the equation system (2.1) to state space. This representation is a more systematic approach that models the system by input, output and state variables. Originating from controls engineering, this formulation is useful in many system identification tasks such as the stochastic subspace identification due to its applicability to nonlinear systems and multiple input multiple output systems. The state-space formulation transfers the  $N$  second order differential equations of (2.1) to a system with  $2N$  first order differential equations. The state-space representation of equation (2.1),

$$\dot{\mathbf{x}}(t) = \mathbf{A}_c \mathbf{x}(t) + \mathbf{B}_c \mathbf{f}(t) \quad (2.11a)$$

$$\mathbf{y}(t) = \mathbf{C}_c \mathbf{x}(t), \quad (2.11b)$$

is obtained by multiplication of (2.1) with  $\mathbf{M}^{-1}$  and rearranging, using the definitions

$$\mathbf{x}(t) = \begin{bmatrix} \mathbf{u}(t) \\ \dot{\mathbf{u}}(t) \end{bmatrix}, \mathbf{A}_c = \begin{bmatrix} 0 & \mathbb{1} \\ -\mathbf{M}^{-1} \mathbf{K} & -\mathbf{M}^{-1} \mathbf{C} \end{bmatrix}, \mathbf{B}_c(t) = \begin{bmatrix} 0 \\ \mathbf{M}^{-1} \end{bmatrix}. \quad (2.12)$$

$\mathbf{C}_c$  denotes the *output matrix* of the system,  $\mathbf{A}_c$  is the *system matrix* and  $\mathbf{B}_c$  represents the *input matrix*. The subscript  $c$  denotes the formulation in continuous time<sup>2</sup>, whereas measurement data are in discrete time. To account for this,

---

<sup>2</sup>This formulation is continuous in time, but spatially discrete.

## 2. Theoretical Background

equation (2.11) can be transferred to discrete time using  $\mathbf{y}_k = \mathbf{y}(k\Delta t)$

$$\mathbf{x}_k = \mathbf{A}_d^k \mathbf{x}_0 + \mathbf{B}_d \mathbf{f}_k \quad (2.13a)$$

$$\mathbf{y}_k = \mathbf{C} \mathbf{A}_d^k \mathbf{x}_0, \quad (2.13b)$$

where  $\mathbf{A}_d = e^{\mathbf{A}_c \Delta t}$  and  $\mathbf{B}_d = \int_0^{\Delta t} e^{\mathbf{A}_c \tau} d\tau \mathbf{B}_c$ .

### 2.1.2. Data pre- and post-processing

Metrics are essential to determine how well a numerical model represents measured data. A metric is a nonnegative mathematical function that describes the 'distance' between two sets as a number. These sets may be eigenfrequencies, mode shapes, time series or other quantities derived from those. In order to compare measured data with simulation results, the data need to be preprocessed depending on the metric used for comparison. These preprocessing steps depend on the metric and the underlying physical simulation needed for model updating.

Cross-correlation is a measure of how much a signal looks like another when one of the signals is shifted by  $d$  data points.

$$\mathbf{v}_m \star \mathbf{v}_s = \frac{\sum_i (v_m^i - \mathcal{M}_m) \cdot (v_s^{i-d} - \mathcal{M}_s)}{\sqrt{(\sum_i v_s^i - \mathcal{M}_s)^2} \sqrt{(\sum_i v_m^{(i-d)} - \mathcal{M}_m)^2}}, \quad (2.14)$$

with  $\mathcal{M}$  being an operator for the expectation value of a signal and  $n = 0, 1, \dots, N-1$ .  $N$  represents the total number of data points within the time series  $\mathbf{v}$  and  $\star$  is an operator for cross-correlation of two time series. Subindices  $m$  and  $s$  denote the measured and simulated response, respectively. The formulation given in equation (2.14) includes a numerically costly evaluation of the sliding dot product. The convolution theorem, stating that the convolution of two signals in time domain is equivalent to pointwise multiplication in frequency domain, is utilized. This establishes a more effective way to compute the cross-correlation [21], resulting in

$$\mathbf{v}_m \star \mathbf{v}_s = \mathcal{F}^{-1}(\mathcal{F}(\mathbf{v}_m)^T \mathcal{F}(\bar{\mathbf{v}}_s)), \quad (2.15)$$

where  $\mathcal{F}(\bullet)$  is the Fourier transform operator and  $\bar{\bullet}$  symbolizes the conjugate complex of a signal  $\bullet$ . This method results in reductions of computational times up to factor 15 [93]. The index of the maximum value of  $\mathbf{v}_m \star \mathbf{v}_s$  is interpreted as the phase shift between these two signals. If a signal is correlated with itself (e.g.,  $\mathbf{v}_m \star \mathbf{v}_m$ ), cross-correlation becomes the *autocorrelation* of the signal, which is often used to emphasize periodicities of signals.



## 2.1. Basics of computational structural dynamics

In addition to the determination of periodicities in a signal, autocorrelation in combination with the Fourier transform is used to determine the Power Spectral Density  $\mathbf{s}^{aa}$  of this time series,

$$\mathbf{s}^{aa}(\omega) = \mathcal{F}(\mathbf{v}_a \star \mathbf{v}_a). \quad (2.16)$$

The Power Spectral Density contains the energy of the signal as a function of frequency. It is often used to validate results from system identification [67] and can also be formulated across two signals ( $\mathbf{s}^{ab}$ ) using cross-correlation.

Filters are techniques that are used in signal analysis to restrict the frequency bandwidth of a signal to a certain range [43]. This is especially useful to eliminate measurement noise or high-frequency responses from simulated time series. Filters, that suppress high-frequency content of a given signal while passing lower frequencies are called *low-pass* filters. Butterworth filters are one of the most basic and useful methods that are often used in filter design [43]. The basic frequency response function for analog Butterworth filters is

$$|\mathbf{H}(j\omega)| = \frac{1}{\sqrt{1 + \left(\frac{\omega}{\omega_c}\right)^{2n}}}, \quad (2.17)$$

where  $\omega_c$  denotes the cutoff frequency and  $n$  denotes the filter order. A higher filter order ensures a steep truncation of the signal after passing  $\omega_c$ . The filter is applied using

$$\mathbf{v}_f = \mathbf{H}\mathbf{v}, \quad (2.18)$$

with  $\mathbf{v}$  being an unfiltered signal and subscript  $f$  denoting the filtered signal.

If results generated by numerical models and measured data shall be compared using modal properties, these have to be identified from measured time series first. *Operational modal analysis* techniques are used in case the input excitation force is unknown, which is often the case in civil engineering structures. The excitation, e.g., by wind, waves or traffic loads, is complex and their modeling is not easy. Due to their size, it may be difficult to excite these structures with hammers or shakers, inducing enough energy above the level of ambient excitations. Hence, methods that do not require the input to identify eigenmodes of the structure are preferred. These methods are also referred to as *output-only* modal analysis [135]. The Stochastic Subspace Identification is such an operational modal analysis method. The method addresses the identification of a stochastic state-space model from output-only data. A detailed description of the method is given

## 2. Theoretical Background

in [67]. The model is assumed to be excited by white noise only. Thus, the time-discrete state-space system equations (see equation (2.11)) reduce to

$$\mathbf{x}_{k+1} = \mathbf{A}_d \mathbf{x}_k + \mathbf{w}_k \quad (2.19a)$$

$$\mathbf{y}_k = \mathbf{C}_d \mathbf{x}_k + \mathbf{v}_k, \quad (2.19b)$$

with  $\mathbf{w}_k$  and  $\mathbf{v}_k$  being zero mean white *process* and *measurement* noise terms. If the (measured) input to the system contains some dominant frequency signals (e.g., eigenfrequencies of a vibrating system) in addition to white noise, these frequencies will appear as additional poles of the system matrix  $\mathbf{A}_d$  [173]. Robust numerical techniques are used for stochastic subspace identification: QR-factorization is used to reduce the data, and singular value decomposition is used to reject the noise. Stochastic subspace identification methods usually result in many mathematical eigenmodes that have to be separated from the physical eigenmodes afterward. Both stability diagrams and modal validation parameters are employed for this purpose [67].

### 2.2. Metrics for comparison of numerical models and measured data

In order to compare numerical models and measurement data, sophisticated error metrics are needed. These metrics quantify the error of the model as a distance between measured data and simulation results. If these metrics are used for damage localization, special attention must be paid to their sensitivity to damages. Especially in damage detection, the metrics presented here are usually referred to as *condition parameters* or *damage features*. Due to the use of these quantities as metrics for the deviation between numerical model and measured data, as intended here, the term *error metrics* is regarded to be more suitable in this context. The aim is minimizing the error metric  $\rho$ , depending on a set of selected parameters  $\boldsymbol{\theta} \in \mathbb{R}^{n \times 1}$ . In model updating, these parameters manipulate properties of the model, for instance stiffnesses, masses or loads. The scalar value of  $\rho$  can be modified via alterations of the parameters of the numerical model. In mathematical terms, this leads to an optimization problem of the form

$$\min_{\boldsymbol{\theta}} \rho(\boldsymbol{\theta}) \quad (2.20a)$$

$$\text{subject to } c \geq 0, \quad (2.20b)$$

meaning that the objective function, equation (2.20a) shall be minimized by variations of the parameter vector  $\theta$ , while satisfying the constraint equations (equation (2.20b)) simultaneously. All parameters are restricted to vary within a certain range. For instance, physical feasibility demands many parameters to always remain positive. Furthermore, parameter values must often be restricted to remain within predefined boundaries. Therefore, the optimization problem is solved subject to a set of constraints.

The following section introduces metrics needed for model to measurement comparison in different domains, each providing individual advantages and disadvantages (see Table 3.1).

### 2.2.1. Error metrics in modal domain

The comparison of modal properties<sup>3</sup> can be considered as the 'classical approach' [10] to model-measurement comparison. Modal properties provide an easy possibility to perform model updating, because only information regarding the structural data is needed to solve the model and get a result that is comparable to measurement data. The most basic approach is to compare eigenfrequencies  $\omega \in \mathbb{R}^{H \times 1}$  with  $H$  being the number of considered eigenmodes. Usually, these are the lowest eigenfrequencies. They can be compared using the  $n$ -th norm of the deviations

$$\rho^\omega(\theta) = \left\| \frac{\omega_m - \omega_s(\theta)}{\omega_m} \right\|_n, \quad (2.21)$$

with the subindices  $m$  denoting measured and  $s$  denoting simulated quantities, respectively. Obviously, the properties of the simulation model depend on the set of parameters  $\theta$ . The denominator is used to normalize the differences.

Another technique is to formulate a metric based on mode shapes. Since being able to reconstruct the mode shapes causes additional complication in the measurement set up, this approach is not investigated as often as the eigenfrequency-based residuals. As a mode shape comparison measure

$$\rho^\phi(\theta) = \sum_{i \in \mathcal{Y}} \frac{1}{2} \frac{(\phi_m^i - \phi_s^i(\theta))^T (\phi_m^i - \phi_s^i(\theta))}{\phi_m^i T \phi_m^i}, \quad \phi \in \mathbb{R}^{K \times 1} \quad (2.22)$$

is used.  $\mathcal{Y}$  denotes the set of eigenvectors considered for the comparison of model to measurement and  $K$  represents the number of considered nodes, e.g., the number of sensors. (2.22) expresses the deviation of simulated and measured eigenvectors

---

<sup>3</sup>Eigenfrequencies and mode shapes are regarded as modal properties. Sometimes, modal damping is added to this set.

## 2. Theoretical Background

as the length of the difference vector of both. This length is squared for practical reasons and normalized by the denominator.  $\rho^\omega$  and  $\rho^\phi$  may be summed up in order to include as much information as possible to the optimization algorithm using the linear combination

$$\rho^{\omega+\phi}(\boldsymbol{\theta}) = \alpha_\omega \rho^\omega(\boldsymbol{\theta}) + \alpha_\phi \rho^\phi(\boldsymbol{\theta}), \quad (2.23)$$

with  $\alpha_\omega$  and  $\alpha_\phi$  denoting weighting factors. Throughout this thesis, these are set to 1.0. Both measured and simulated eigenvectors have to be normalized prior to evaluation of equation (2.22). This normalization is done using the biggest entry in all vectors

$$\phi = \frac{1}{\max(\phi)} \phi. \quad (2.24)$$

In addition, phase balance of the vectors must be ensured. This is achieved comparing the length of the difference vector  $\|\phi_m^i - \phi_s^i\|_2$  and  $\|\phi_m^i + \phi_s^i\|_2$ . If the last expression results in a smaller value than the first, the simulated eigenvector is multiplied by  $-1$ , otherwise the vectors are in phase. This is only valid for similar vectors and has to be checked prior to the application.

With changing parameters, the order of eigenmodes is subject to change. Thus, mode shape tracking is needed in order to compare only associated mode shapes and frequencies. The *Modal Assurance Criterion* is a measure for the similarity between two mode shapes [3].

$$MAC(\phi_m, \phi_s(\boldsymbol{\theta})) = \left( \frac{\phi_m^T \phi_s(\boldsymbol{\theta})}{\phi_m^T \phi_m \cdot \phi_s(\boldsymbol{\theta})^T \phi_s(\boldsymbol{\theta})} \right) \in [0, 1] \quad (2.25)$$

The Modal Assurance Criterion returns a value of 1, if two vectors  $\phi_m$  and  $\phi_s$  are linearly dependent and 0, if they are not. A modal assurance criterion value greater than 0.8 is supposed to indicate good conformity of two vectors [111]. If the measured mode shapes are in the same order as the numerical, the MAC-matrix computed using equation (2.25) has values close to 1 on its diagonal and close to 0 elsewhere. If this is not the case, the assignment of eigenmodes is changed according to the off-diagonal terms in the matrix.

### 2.2.2. Error metrics in frequency domain

For the definition of error metrics in frequency domain, the power spectral density of a signal is used. Power spectral density describes the energy of a signal over frequency (see equation 2.16). In practical applications, the power spectral density is often estimated using Welch's method [170]. A metric defined by power spectral

density is defined by

$$\rho^s = \sum_{j \in \mathcal{Z}} \left\| \mathbf{s}_m^j - \mathbf{s}_s^j(\boldsymbol{\theta}) \right\|_2, \quad (2.26)$$

where  $\mathbf{s}_m$  and  $\mathbf{s}_s$  denote the measured and simulated power spectral density, respectively. Here,  $\mathcal{Z}$  is the set of signals considered for the evaluation of the metric. Normalization of  $\mathbf{s}_m$  and  $\mathbf{s}_s$  may help reducing the influence of magnitudes of forces, yet it causes a loss of information.

A new frequency domain metric employs transmissibility functions [35] to define a measure for comparison between numerical model and measurement data. Ewins defines transmissibility as 'a quantity which is commonly used in vibration engineering practice to indicate the relative vibration level between two points' [40]. State-of-the-art techniques in vibration engineering often make use of the frequency response function, which is basically a measured quantity divided by the input signal (i.e., a force). In contrast to this definition, a transmissibility function  $\boldsymbol{\tau}$  is a measured quantity divided by a measured reference quantity [34],

$$\boldsymbol{\tau}^{ij}(\omega) = \frac{\mathbf{x}^i(\omega)}{\mathbf{x}^j(\omega)}. \quad (2.27)$$

In this equation,  $\mathbf{x}^i(\omega)$  and  $\mathbf{x}^j(\omega)$  denote the spectral signals recorded in channels  $i$  and  $j$ , respectively, depending on the frequency  $\omega$ . The recorded spectral signals are obtained using

$$\mathbf{x}^i(\omega) = \mathbf{H}^{ik}(\omega) \cdot \mathbf{f}^k(\omega), \quad (2.28)$$

with  $\mathbf{H}^{ik}(\omega)$  denoting the transfer function between measurement point  $i$  and a force  $\mathbf{f}^k(\omega)$  applied at point  $k$ . Inserting equation (2.28) in equation (2.27) yields

$$\boldsymbol{\tau}^{ij,k}(\omega) = \frac{\mathbf{H}^{ik}(\omega) \cdot \mathbf{f}^k(\omega)}{\mathbf{H}^{jk}(\omega) \cdot \mathbf{f}^k(\omega)} = \frac{\mathbf{H}^{ik}(\omega)}{\mathbf{H}^{jk}(\omega)}. \quad (2.29)$$

Equation (2.29) proves that  $\boldsymbol{\tau}^{ij,k}(\omega)$  is solely influenced by the location of loads acting on the structure and independent from their amplitude or phase. A practical way to define the transmissibility functions without knowing the transfer functions explicitly is

$$\boldsymbol{\tau}^{ij}(\omega) = \frac{\mathbf{s}^{ij}(\omega)}{\mathbf{s}^{ii}(\omega)}. \quad (2.30)$$

## 2. Theoretical Background

These transmissibility functions are computed for both simulation and measurement data and used for comparison of model to measurement. The actual comparison for several measurement channels is then done using

$$\rho^\tau(\boldsymbol{\theta}) = \sum_{p \in \mathcal{X}} \frac{\|\boldsymbol{\tau}_{m,p}^{ij} - \boldsymbol{\tau}_{s,p}^{ij}(\boldsymbol{\theta})\|_2}{\|\boldsymbol{\tau}_{m,p}^{ij}\|_2}, \quad (2.31)$$

where  $\mathcal{X}$  denotes the set of all reasonable combinations of measurement channels.

### 2.2.3. Error metrics in time domain

Time series provide another source of information that can be employed for the comparison between numerical model and measured data. Many authors utilize the  $l_2$ -norm

$$\rho^{l_2}(\boldsymbol{\theta}) = \|\mathbf{v}_m - \mathbf{v}_s(\boldsymbol{\theta})\|_2 \quad (2.32)$$

to define an objective function for optimization (as in [76]), where  $\mathbf{v}_m \in \mathbb{R}^{D \times 1}$  denotes any signal recorded in a real structure and  $\mathbf{v}_s$  is the corresponding signal from a simulation, depending on the parameters  $\boldsymbol{\theta}$ .  $D$  represents the number of data points within this signal. Before the direct comparison of signals is performed, the signals have to be adjusted to provide the same sampling frequency. This is done using downsampling<sup>4</sup> of  $\mathbf{v}_s$  or  $\mathbf{v}_m$ , respectively. In addition, filtering of the measured signals (see equation (2.18)) may be beneficial. These signals may be any quantity that is measurable, typically acceleration or strain time series. If signals from more than one channel are compared, the function is extended to

$$\rho^{l_2}(\boldsymbol{\theta}) = \sum_{j \in \mathcal{Z}} \left\| \mathbf{v}_m^j - \mathbf{v}_s^j(\boldsymbol{\theta}) \right\|_2, \quad (2.33)$$

with  $\mathcal{Z}$  being the set of considered time series. Due to the fact that initial conditions may be unknown, the signals may be out of phase, leading to time series incomparable using equation (2.33). This is circumvented using the cross-correlation (see equation 2.15) [168]. Prior to the computation of the actual deviation of the time series using equation (2.33), the simulated time series is shifted according to the results of the cross-correlation.

The Mahalanobis distance is another error measure that may be employed to quantify the difference between time series. [58] successfully employ a metric as a weighted vector norm to identify damages in plate structures. The main difference is the formulation of the weighting matrix, which is done using the covariance

---

<sup>4</sup>Downsampling is the term for a reduction of the sampling rate of a signal. E.g., only every  $n$ -th sample of a signal is kept

matrix in the Mahalanobis distance. In the Mahalanobis distance, the error  $e_i$  between simulated and measured time series is defined using

$$|\mu_i(\boldsymbol{\theta})| = \sqrt{\sum_{j=1}^l (\mathbf{v}_m^{ij} - \mathbf{v}_s^{ij}(\boldsymbol{\theta}))^T \mathbf{W} (\mathbf{v}_m^{ij} - \mathbf{v}_s^{ij}(\boldsymbol{\theta}))}, \quad (2.34)$$

where  $l$  denotes the number of sensor channels,  $\mathbf{W}$  is the weighting matrix.  $\mathbf{W}$  is defined by the covariance matrix, which is a quantification of direction and extent of dependence of the signals. A metric  $\rho^\mu$ , quantifying the difference of all channels, is then formulated employing the  $l_2$ -norm on the vector  $\boldsymbol{\mu}$

$$\rho^\mu(\boldsymbol{\theta}) = \left\| \sum_{j=1}^l (\mathbf{v}_m^{ij} - \mathbf{v}_s^{ij}(\boldsymbol{\theta}))^T \mathbf{W} (\mathbf{v}_m^{ij} - \mathbf{v}_s^{ij}(\boldsymbol{\theta})) \right\|_2. \quad (2.35)$$

An advantage of the Mahalanobis Norm over the Euclidean Norm are the dimensionless distance values, which account for more consistent comparisons. Furthermore, the difference between simulated and measured response is weighted by the existing correlations. Variables with high variance and highly correlated variables are given less weight.

## 2.3. Optimization algorithms for model updating

The aim of finite element model updating is to minimize the deviation  $\rho$  between measured and simulated results. This is done by solving the general optimization problem (2.20). The objective function formulated in the previous sections is minimized subject to constraints. These constraints can be formulated in arbitrary form. The constraints that are used in most constrained model updating applications are the so called boxed constraints

$$l_i \leq \theta_i \leq u_i \quad \forall i \in [1..n], \quad (2.36)$$

ensuring that the parameters remain within a certain range around the initial configuration. In addition to these constraints, summarizing constraints may include further information to the optimization problem. These constraints are introduced in subsequent chapters and formulated individually per problem.

### 2.3.1. Simulated Annealing and Simulated Quenching

The central idea of Simulated Annealing is to transfer the annealing process in metallurgy to an optimization problem. In metallurgy, the controlled cooling of a metal grants the particles enough time to build stable crystal lattices with few defects. At a certain state of the annealing process, particles can be in the lattice or leave it with a certain probability, dependent on the actual temperature. The Simulated Annealing method is used for the exploration of the search domain defined by the optimization problem (2.20). Simulated Annealing is a metaheuristic optimization method that can approximate solutions of large optimization problems with many local minima [89]. In contrast to other global optimization algorithms, convergence to the correct optimum can be proven [64]. However, this can only be done for certain theoretical conditions, causing endless computational times.

The annealing process means transferred to optimization that better solutions are always accepted, whereas worse solutions are accepted with a certain probability. A solution is regarded to be better if the associated objective function value is smaller than in the previous solution. In Simulated Annealing, a slowly decreased temperature is interpreted as a decrease of the probability to accept worse solutions. Simulated Annealing has widely been used in the chip industry to find the optimal arrangement of microchips components [141] or solving the famous traveling salesman problem [38].

In the Simulated Annealing algorithm, the next parameters are created using a random neighbor of the actual variables, see Figure 2.1. Since the new parameters are independent of the current, consideration of constraints is simple. A random vector is added to the actual parameter vector  $\theta_k$ . It is then checked if the new solution fulfills all constraints. Otherwise, a new solution is created randomly. Other, more advanced methods for finding a valid neighbor may be applied, but for model updating, this approach yields satisfying results. If the actual solution is better than the previous ( $\delta < 0$ ), it is accepted. If it is worse, its acceptance depends on the actual temperature  $T$  and the size of the descent  $\delta$  (see the purple diamond in Figure 2.1). This is the most important step of Simulated Annealing, since it allows the algorithm to leave local minima. At the same time, this decision is slowing down convergence of the method, because at low temperatures many solutions are rejected after the numerically costly evaluation of the objective function. According to [141], the initial parameters are chosen to  $T_0 = 500$  and  $N = 50$ , meaning an initial temperature of 500 and 50 repetitions at each temperature step. The main disadvantage of Simulated Annealing is that it is known to require long time periods to reach the exact optimum [164].

An exponential cooling scheme can be used instead of a linear in order to accel-



erate the algorithm (see Figure 2.2). Using this approach, the next temperature  $T_{k+1}$  is obtained using  $T_{k+1} = T_0 \cdot e^{((C-1)k)}$  with an appropriately chosen value for the annealing constant  $C$ . Sometimes, this procedure is referred to as Simulated Quenching [164]. Due to the fact that an exponential curve never reaches zero, an additional restriction has to be defined as a stop criterion for the algorithm, whereas the linear approach usually is stopped when it reaches zero. Simulated Quenching is a procedure based on randomness. Therefore, it can never be guaranteed that the algorithm approximates the correct solution. The algorithm is started several times for this reason. The results are then compared using the final objective function.

### 2.3.2. Sequential Quadratic Programming

Because Simulated Quenching approximates solutions that may be remote to the actual solution, a local optimization algorithm is started from the solution generated by Simulated Quenching. For solving the local, constrained,  $C^2$ -continuous nonlinear optimization problem, or, more commonly, *nonlinear program*

$$\min_{\boldsymbol{\theta}} \rho(\boldsymbol{\theta}) \quad (2.37a)$$

$$\text{subject to } c_i(\boldsymbol{\theta})=0 \quad \forall i \in \mathcal{E} \quad (2.37b)$$

$$c_i(\boldsymbol{\theta}) \geq 0 \quad \forall i \in \mathcal{I} \quad (2.37c)$$

Sequential Quadratic Programming is employed.  $\mathcal{E}$  represents the indices of equality- and  $\mathcal{I}$  the indices of inequality constraints. Sequential Quadratic Programming methods are a class of iterative methods that combine the basic ideas of optimizing an unconstrained function using Newton's method with Lagrange's method for constraint consideration. They are known to need fewer evaluations of the objective function than most other local optimization algorithms. At the same time, they reveal high numerical stability, even for badly scaled problems [126]. This is why they are especially useful in model updating, where the evaluation of the objective function is numerically expensive regarding computational time. The basic idea of Sequential Quadratic Programming methods is to construct a quadratic optimization subproblem around an actual iteration point  $\boldsymbol{\theta}_k$ . The solution of this subproblem can be used as an iteration step (defining the new iterate  $\boldsymbol{\theta}_{k+1}$ ) towards the solution (2.37). The Lagrangian of (2.37) is

$$\mathcal{L}(\boldsymbol{\theta}, \boldsymbol{\lambda}) = \rho(\boldsymbol{\theta}) - \sum_{i \in \mathcal{E} \cup \mathcal{I}} \lambda_i c_i(\boldsymbol{\theta}). \quad (2.38)$$

## 2. Theoretical Background

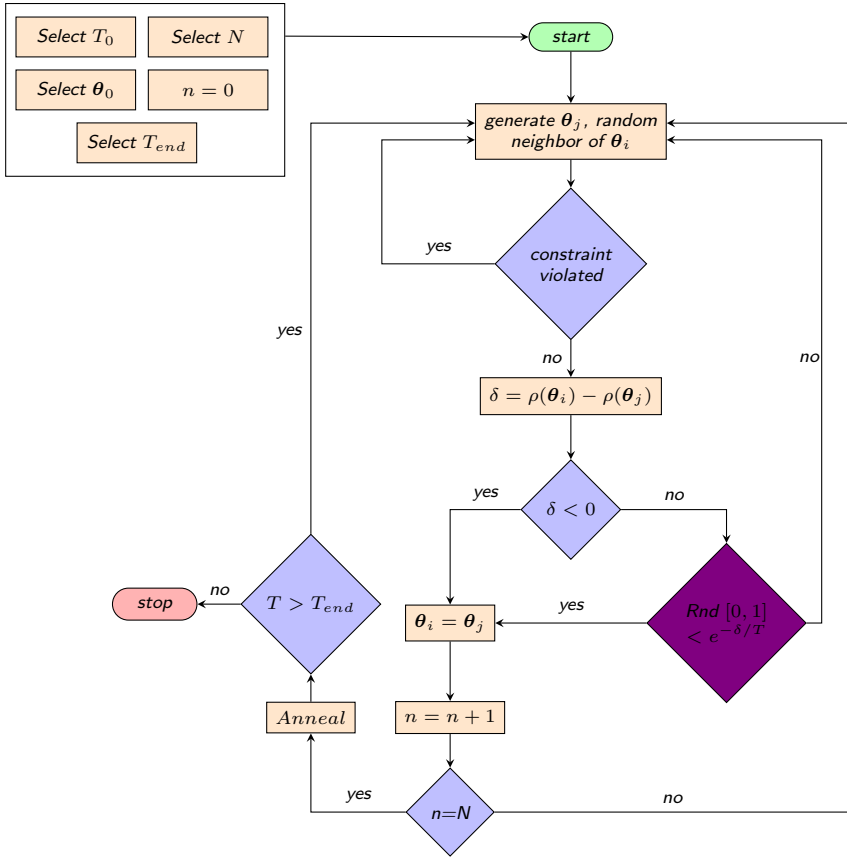


Figure 2.1.: Flow Chart of the Simulated Quenching Algorithm. The most important step of the algorithm is indicated by the purple diamond. This decision generally allows to leave local minima, whereas the probability to accept worse solutions decreases with a falling temperature  $T$ .

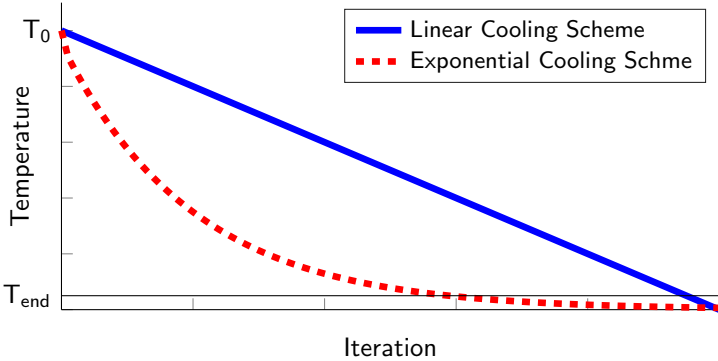


Figure 2.2.: Comparison of linear (Simulated Annealing) and exponential (Simulated Quenching) cooling schemes.

The first order optimality conditions for constrained optimization<sup>5</sup> postulate

$$\nabla_{\theta} \mathcal{L}(\theta^*, \lambda^*) = 0 \quad (2.39a)$$

$$c_i(\theta^*) = 0 \quad \forall i \in \mathcal{E} \quad (2.39b)$$

$$c_i(\theta^*) \geq 0 \quad \forall i \in \mathcal{I} \quad (2.39c)$$

$$\lambda_i^* \geq 0 \quad \forall i \in \mathcal{I} \quad (2.39d)$$

$$\lambda_i^* c_i(\theta^*) = 0 \quad \forall i \in \mathcal{E} \cup \mathcal{I}, \quad (2.39e)$$

with  $\nabla_{\theta} \mathcal{L}(\theta, \lambda) = \nabla \rho(\theta) - \lambda \nabla \mathbf{c}(\theta)$ . Solving the nonlinear equation system (2.39) leads to the optimum of (2.37). Because there are no analytical methods to do so directly, this is done iteratively using Newton's method known from unconstrained optimization [48]. Using this method, the Newton-step towards the solution is defined as

$$\begin{bmatrix} \theta_{k+1} \\ \lambda_{k+1} \end{bmatrix} = \begin{bmatrix} \theta_k \\ \lambda_k \end{bmatrix} + \begin{bmatrix} \mathbf{p}_k^{\theta} \\ \mathbf{p}_k^{\lambda} \end{bmatrix}. \quad (2.40)$$

In accordance with Newton's method, the step size  $\mathbf{p}_k$  is obtained from the solution of

$$\nabla_{\theta\theta}^2 \mathcal{L}(\theta_k, \lambda_k) \mathbf{p}_k = -\nabla_{\theta} \mathcal{L}(\theta_k, \lambda_k), \quad (2.41)$$

while fulfilling the remaining first order optimality conditions (equations (2.39c) to (2.39e)) simultaneously.

<sup>5</sup>These conditions are known as the Karush-Kuhn-Tucker- or KKT-conditions [91].

## 2. Theoretical Background

### Definition of the quadratic optimization subproblem

An optimization problem of the form

$$\min_{\mathbf{p}} \frac{1}{2} \mathbf{p}^T \mathbf{Q} \mathbf{p} + \mathbf{c}^T \mathbf{p} + d \quad (2.42a)$$

$$\text{subject to } \mathbf{a}_i^T \mathbf{p} - b_i = 0 \quad \forall i \in \mathcal{E} \quad (2.42b)$$

$$\mathbf{a}_i^T \mathbf{p} - b_i \geq 0 \quad \forall i \in \mathcal{I} \quad (2.42c)$$

is called *Quadratic Program*. It consists of a quadratic objective function with linear equality and inequality constraints with  $\mathbf{Q} \in \mathbb{R}^{n \times n}$  being the matrix holding the quadratic terms,  $\mathbf{c}, \mathbf{p}, \mathbf{a}_i \in \mathbb{R}^{n \times 1}$  containing the linear terms of the objective function, the solution vector and the linear constraint vectors.

The nonlinear program (2.37) can be approximated using Taylor's expansion at  $\boldsymbol{\theta}_k$ . For the definition of the objective function of the quadratic program the expansion is used up to the second order terms. The constraint equations ((2.37b) and (2.37c)) are approximated using the first order terms only. The resulting sub-problem has the form

$$\min_{\mathbf{p}} \frac{1}{2} \mathbf{p}^T \nabla_{\boldsymbol{\theta}\boldsymbol{\theta}}^2 \mathcal{L}_k \mathbf{p} + \nabla \mathbf{r}_k^T \mathbf{p} + r_k \quad (2.43a)$$

$$\text{subject to } \nabla \mathbf{c}_i(\boldsymbol{\theta}_k)^T \mathbf{p} + c_i(\boldsymbol{\theta}_k) = 0 \quad \forall i \in \mathcal{E} \quad (2.43b)$$

$$\nabla \mathbf{c}_i(\boldsymbol{\theta}_k)^T \mathbf{p} + c_i(\boldsymbol{\theta}_k) \geq 0 \quad \forall i \in \mathcal{I}, \quad (2.43c)$$

where  $r_k$  is the objective function (2.37a) evaluated at the  $k$ -th iteration. In general, the  $\nabla$ - operator contains all partial derivatives, in this case the objective function is derived with respect to the optimization variables. The solution of (2.43) is equivalent to the solution of (2.41), while fulfilling the remaining first order optimality conditions (equations (2.39c) to (2.39e)) simultaneously [105].

Comparison of (2.43) and (2.42) reveals that (2.43) is a quadratic program. Therefore, this resulting subproblem can be solved using the according quadratic programming algorithms. The solution vector  $\mathbf{p}$  of (2.43) is the Newton-step towards the solution of (2.37) that is used in equation (2.40).

### Solution of the quadratic optimization subproblem using active set methods

Both *active-set* and *interior-point* methods are reliable methods for solving the general quadratic program (2.42). For small optimization problems ( $\dim(\mathbf{p}) < 10000$ ), as it is the usual case in model updating, especially active-set strategies reveal their potential, whereas interior-point algorithms have advantages at big optimization

problems [48]. Therefore, an active-set method is used for the solution of (2.43). The idea of active-set methods is to use only those inequality constraints of  $\mathcal{I}$  that are active at a current iterate and treat them as equality constraints. Thus, problem (2.42) can be reduced to a quadratic program with solely equality constraints at every iteration. Optimization problems holding no inequality constraints can be solved easily via the solution of equation systems (see equation (2.45)), whereas problems having inequality constraints must be challenged using additional effort by conversion of the problem holding both equality and inequality constraints to a system with only equality constraints. The set of all equality constraints and the inequality constraints active at the current iteration is called active set  $\mathcal{A}(\mathbf{p})$ . At the beginning of the solution process it is unknown which constraints belong to  $\mathcal{A}(\mathbf{p}^*)$  of the optimal solution  $\mathbf{p}^*$ . Therefore, this optimal active set has to be found, which is done iteratively. Initially, an arbitrary working set  $\mathcal{W}_0$  containing all equality constraints and some of the inequality constraints is defined.  $\mathcal{W}_0$  can even be chosen as  $\emptyset$ , if no equality constraints are present. Using the definitions

$$\mathbf{q} = \mathbf{p}_{k+1} - \mathbf{p}_k, \quad \mathbf{g}_k = \mathbf{Q}\mathbf{p}_k + \mathbf{c},$$

the objective function (2.42a) can be rearranged to

$$h(\mathbf{p}_k + \mathbf{q}) = \frac{1}{2}\mathbf{q}^T \mathbf{Q}\mathbf{q} + \mathbf{g}_k^T \mathbf{q} + \rho_k,$$

where  $\rho_k = \frac{1}{2}\mathbf{p}_k^T \mathbf{Q}\mathbf{p}_k + \mathbf{p}_k^T \mathbf{c}$  is independent of  $\mathbf{q}$ . Therefore,  $\rho_k$  can be dropped from the objective function without altering the solution. The resulting subproblem at the  $k$ -th<sup>6</sup> iteration is

$$\min_{\mathbf{q}} \frac{1}{2}\mathbf{q}^T \mathbf{Q}\mathbf{q} + \mathbf{g}_k^T \mathbf{q} \tag{2.44a}$$

$$\text{subject to } \mathbf{a}_i^T \mathbf{q} = 0 \quad i \in \mathcal{W}_k. \tag{2.44b}$$

All inequality constraints in  $\mathcal{W}_k$  are treated as equality constraints. Therefore, the problem does not contain inequalities. Using the first order necessary optimality conditions for constrained optimization (equations 2.39), problem (2.44) can be solved using the equation system

$$\begin{bmatrix} \mathbf{Q} & \mathbf{A}^T \\ \mathbf{A} & \mathbf{0} \end{bmatrix} \begin{bmatrix} -\mathbf{t} \\ \boldsymbol{\lambda}^* \end{bmatrix} = \begin{bmatrix} \mathbf{g}_k + \mathbf{Q}\mathbf{p} \\ \mathbf{0} \end{bmatrix}, \tag{2.45}$$

---

<sup>6</sup>Note that this iteration counter  $k$  is not the same as in the Sequential Quadratic Programming iteration, it is restarted at every quadratic subproblem.

## 2. Theoretical Background

where the optimal solution  $\mathbf{q}^*$  of the subproblem (2.44) is found using  $\mathbf{q}^* = \mathbf{q} + \mathbf{t}$ . The so called *KKT-matrix*  $\begin{bmatrix} \mathbf{Q} & \mathbf{A}^T \\ \mathbf{A} & 0 \end{bmatrix}$  is always nonsingular in Sequential Quadratic Programming as long as the matrix  $\mathbf{Q}$  is nonsingular which is ensured using appropriate methods to approximate  $\mathbf{Q}$  and if the lines and columns of  $\mathbf{A}$  are linearly independent. Thus, this equation system is solved using LU-decomposition. In case the number of constraints in  $\mathcal{W}$  is smaller than the number of optimization variables, the null-space approach is used<sup>7</sup>. This approach does not postulate nonsingularity of the KKT-matrix and is numerically more efficient since no inversion or factorization of the full equation system is needed [126].

Any step along  $\mathbf{q}$  decreases the objective function of the quadratic subproblem (2.43). In addition to a decrease of the objective function, the algorithm has to ensure that none of the constraints are violated by the step. If a step  $\mathbf{p}_{k+1} = \mathbf{p}_k + \mathbf{q}_k$  is feasible, it is done. Otherwise, the step length is restricted via

$$\mathbf{p}_{k+1} = \mathbf{p}_k + \alpha_k \mathbf{q}_k. \quad (2.46)$$

$\alpha_k$  is chosen to be the maximum value in  $[0, 1]$  that satisfies all constraints such that none of the so-called *blocking constraints* is violated. The blocking constraints are then added to the working set  $\mathcal{W}_{k+1}$ , making the algorithm introduced here a line-search method. Line search methods determine a search direction first and then a seek to minimize the problem along this direction. Other constraints are dropped from the working set, and a new iteration towards the solution of the quadratic problem (2.42) is started. The contrary class to line-search, trust-region methods, are not introduced here in detail. The basic idea of trust-region methods is to presume the quadratic approximation to be sufficiently accurate only in a defined region and set this region as the maximum step length, adding a supplemental constraint to the optimization problem. It is still unclear which approach results in faster convergence speeds [48]. One of the most advanced Sequential Quadratic Programming algorithms uses a line-search implementation [62], whereas others use trust-region approaches [27].

### Sequential Quadratic Programing iteration

When the subproblem (2.43) is solved, the next iterate is computed using equation (2.40). In order to construct the quadratic subproblem, the objective function  $\rho_{k+1}$ , the Jacobian  $\nabla \rho_{k+1}$  and the Hessian  $\nabla_{\theta\theta}^2 \mathcal{L}_{k+1}$  have to be evaluated at the

---

<sup>7</sup>Several methods exist to identify the null-space of the KKT-matrix. A common way is to employ the QR-decomposition of  $\mathbf{Q}$ .

### 2.3. Optimization algorithms for model updating

new iterate  $\boldsymbol{\theta}_{k+1}$ . First order derivatives are approximated using finite differences

$$\frac{\partial \rho}{\partial \theta_i} = \frac{\rho(\boldsymbol{\theta} + \mathbf{h}) - \rho(\boldsymbol{\theta} - \mathbf{h})}{2h} \quad (2.47)$$

with  $\mathbf{h} = h\mathbf{e}_i$  and a small value  $h$ , where  $\mathbf{e}_i$  is the unit vector. A central difference approximation is chosen here. This has been found to perform better in model updating algorithms than forward differences [146]. Therefore, the use of central differences is worth the additional numerical effort in comparison to forward or backward differences. Being numerically extensive, finite differences should be avoided if possible. For instance, analytical derivatives may be employed as it is the case when modal properties are employed (see equation (2.52)).

Due to the fact that an approximation of second order derivatives using finite differences, including at least  $n \times n$  evaluations of the objective function, is numerically costly in model updating and positive definiteness of the Hessian can not be guaranteed, other methods are considered to find this matrix. In the *BFGS-method*<sup>8</sup>, the Hessian is approximated using quasi-Newton formula, making use of curvature information being generated during the process of iteration. The major drawback of this approach is the loss of quadratic convergence. An extension to this method are the damped BFGS- formula [126]. The BFGS-update starts with a given, symmetric and positive definite matrix  $\mathbf{Q}_k$ . For the update, the definitions

$$\mathbf{s}_k = \boldsymbol{\theta}_{k+1} - \boldsymbol{\theta}_k \quad (2.48a)$$

$$\mathbf{y}_k = \nabla_{\boldsymbol{\theta}} \mathcal{L}(\boldsymbol{\theta}_{k+1}, \lambda_{k+1}) - \nabla_{\boldsymbol{\theta}} \mathcal{L}(\boldsymbol{\theta}_k, \lambda_k) \quad (2.48b)$$

$$\mathbf{r}_k = \alpha_k \mathbf{y}_k + (1 - \alpha_k) \mathbf{Q}_k \mathbf{s}_k, \quad (2.48c)$$

with  $\alpha_k = 1$  if  $\mathbf{s}_k^T \mathbf{y}_k \geq 0.2 \mathbf{s}_k^T \mathbf{Q}_k \mathbf{s}_k$  and  $\alpha_k = (0.8 \mathbf{s}_k^T \mathbf{Q}_k \mathbf{s}_k) / (\mathbf{s}_k^T \mathbf{Q}_k \mathbf{s}_k - \mathbf{s}_k^T \mathbf{y}_k)$ , else, are needed. The BFGS-update of the matrix  $\mathbf{Q}_{k+1}$  is then determined using

$$\mathbf{Q}_{k+1} = \mathbf{Q}_k - \frac{\mathbf{Q}_k \mathbf{s}_k \mathbf{s}_k^T \mathbf{Q}_k}{\mathbf{s}_k^T \mathbf{Q}_k \mathbf{s}_k} + \frac{\mathbf{r}_k \mathbf{r}_k^T}{\mathbf{s}_k^T \mathbf{r}_k} \quad (2.49)$$

The included damping term  $\alpha_k$  ensures validity of the curvature condition and subsequently positive definiteness of the approximated Hessian<sup>9</sup>. A valid initial

<sup>8</sup>Named by R. Broyden [26], C. G. Fletcher [47], D. Goldfarb [63] and D. F. Shanno [153], who developed and published similar variations of the method independently in 1970.

<sup>9</sup>This is important when solving the resulting quadratic sub-program(2.42), since finding the solution of positive definite equation systems is easier to find than in semidefinite or indefinite systems.

## 2. Theoretical Background

guess for the Hessian is the unity matrix.

In case the objective function is formulated in modal domain, the Jacobian  $\nabla \boldsymbol{\rho}_{k+1}$  of the objective function may be computed using Nelson's method for derivatives of eigenvalues and eigenvectors [125] making use of the structure of the eigensystem. This method was later expanded by Friswell [52] to higher order derivatives. The derivative of the undamped eigensystem

$$[\mathbf{K} - \lambda_i \mathbf{M}] \boldsymbol{\phi}_i = 0, \quad i = 1, \dots, n \quad (2.50)$$

with respect to the set of design parameters  $\boldsymbol{\theta}$  yields

$$[\mathbf{K} - \lambda_i \mathbf{M}] \frac{\partial \boldsymbol{\phi}_i}{\partial \theta_k} + \left[ \frac{\partial \mathbf{K}}{\partial \theta_k} - \lambda_i \frac{\partial \mathbf{M}}{\partial \theta_k} \right] \boldsymbol{\phi}_i - \frac{\partial \lambda_i}{\partial \theta_k} \mathbf{M} \boldsymbol{\phi}_i = 0. \quad (2.51)$$

Multiplication of the eigenvector, using (2.50) and assuming mass normalized eigenvectors, the derivative of the eigenvalues with respect to the design parameters yields

$$\frac{\partial \lambda_i}{\partial \theta_k} = \boldsymbol{\phi}_i^T \left[ \frac{\partial \mathbf{K}}{\partial \theta_k} - \lambda_i \frac{\partial \mathbf{M}}{\partial \theta_k} \right] \boldsymbol{\phi}_i \quad (2.52)$$

Insertion of the eigenvalue derivative in (2.51) yields the derivatives of the eigenvectors.

### The big M method for quadratic optimization problems

During the solution of optimization problems using Sequential Quadratic Programming, infeasible constraint sets appear on a regular basis. This is due to linearization of the constraints of the original problem for formulation of quadratic subproblems. If two constraints  $\rho \leq 1$  and  $\rho^2 \geq 0$  are linearized at  $\rho_k = 3$ , the linearization inequalities constraints of the subproblem are  $3 + p \leq 1$  and  $9 + 6p \geq 0$ , which are inconsistent [126]. Furthermore, an initial point satisfying all constraints is unknown when starting the iteration for solving the quadratic subproblem. These difficulties may be faced using the *big M*-method, which was originally designed for linear optimization problems. In contrast to many other methods, the *big M*-method is a single-phase method that solves the optimization problem directly without an additional phase needed to find an initial solution, as it is done in many methods derived from the famous two-phase simplex algorithm for linear optimization [126].

The basic idea of the *big M*-method is to allow a violation  $\eta$  of the constraints and to penalize  $\eta$  with a big value  $M$  that is added to the objective function.



### 2.3. Optimization algorithms for model updating

A linear penalization of the maximum constraint penalization is the classical approach for this method [48], being referred to as an exact penalty method using the  $l_\infty$  norm<sup>10</sup>. Following this approach, the basic quadratic program (see equation (2.42)) is expanded to

$$\begin{aligned} \min_{\mathbf{p}, \eta} \quad & \frac{1}{2} \mathbf{p}^T \mathbf{Q} \mathbf{p} + \mathbf{c}^T \mathbf{p} + d + \eta M \\ \text{subject to} \quad & \mathbf{a}_i^T \mathbf{p} - b_i \leq \eta \quad \forall i \in \mathcal{E} \\ & -(\mathbf{a}_i^T \mathbf{p} - b_i) \leq \eta \quad \forall i \in \mathcal{E} \\ & b_i - \mathbf{a}_i^T \mathbf{p} \leq \eta \quad \forall i \in \mathcal{I} \\ & 0 \leq \eta. \end{aligned} \tag{2.53}$$

Setting  $\mathbf{y} = [\mathbf{p} \ \eta]^T$ , the objective function of (2.53) is reformulated to

$$\min_{\mathbf{y}} \quad \frac{1}{2} \mathbf{y}^T \begin{bmatrix} \mathbf{Q} & 0 \\ 0 & 0 \end{bmatrix} \mathbf{y} + [\mathbf{c}^T \ M] \mathbf{y} + d. \tag{2.54}$$

Being in standard format, this optimization problem can be solved using state of the art solvers for quadratic optimization problems. A problem that arises with the linear penalization of constraint violation is that the expanded matrix holding the quadratic terms becomes singular. This is avoided with a quadratic penalization of the maximum constraint violation. The objective function (2.54) then becomes

$$\min_{\mathbf{y}} \quad \frac{1}{2} \mathbf{y}^T \begin{bmatrix} \mathbf{Q} & 0 \\ 0 & 1 \end{bmatrix} \mathbf{y} + [\mathbf{c}^T \ M] \mathbf{y} + d, \tag{2.55}$$

resulting in an optimization problem in standard-format that holds a nonsingular matrix for the quadratic terms. It can be shown that the solution  $\mathbf{y}^*$  converges to the solution of the original problem,  $\mathbf{p}^*$ , with  $\eta = 0$  for large values of  $M$ <sup>11</sup> [48]. If there are infeasible constraints, the violation of all these constraints is as small as possible, yet still this solution can be taken as a Newton-step towards the solution of the initial problem (2.37) [126].

---

<sup>10</sup>Other penalization methods employing the  $l_1$  or  $l_2$ -norm are also existent, but these introduce an additional variable for every constraint, possibly resulting in bigger optimization problems than with the  $l_\infty$ -norm.

<sup>11</sup> $M = 10^4$  has proven to be big enough in typical model updating applications.

## 2. Theoretical Background

### Merit function

Merit functions provide an essential addition to Sequential Quadratic Programming algorithms to ensure a global convergence of line-search algorithms. Another approach to ensure global convergence, filter methods [126], is not considered here. The merit function ensures that every iteration step decreases the objective function value 'sufficiently'. A special class of Merit functions can be seen as the extension of the Armijo-condition to constrained optimization problems [48]. For unconstrained optimization problems, the Armijo-condition is

$$\rho(\boldsymbol{\theta}_k + \alpha_k \mathbf{p}_k) \leq \rho(\boldsymbol{x}_k) + \eta \alpha_k \nabla \rho_{\mathbf{p}_k}^T \mathbf{p}_k, \quad (2.56)$$

with  $\eta \in (0, 1)$ . This condition ensures that a reduction in  $\rho$  is proportional to both the step length  $\alpha_k$  and the directional derivative  $\nabla \rho_{\mathbf{p}_k}^T \mathbf{p}_k$ . For expanding equation (2.56) to the constrained case, a function that penalizes all constraint violations using

$$\phi_1(\boldsymbol{\theta}, \mu) = \rho(\boldsymbol{\theta}) + \mu \sum_{i \in \mathcal{E}} |c_i(\boldsymbol{\theta})| + \mu \sum_{i \in \mathcal{I}} [c_i(\boldsymbol{\theta})]^- \quad (2.57)$$

is introduced first, with  $\mu$  being a parameter chosen sufficiently large to penalize constraint violations.  $[c_i(\boldsymbol{\theta})]^-$  is an operator for violations of inequality constraints, being zero, if  $c_i(\boldsymbol{\theta}) > 0$  and  $-c_i(\boldsymbol{\theta})$ , otherwise. This is a  $l_1$ -penalization of constraint violations. Joining equations (2.56) and (2.57) results in

$$\phi_1(\boldsymbol{\theta}_k + \alpha_k \mathbf{p}_k, \mu_k) \leq \phi_1(\boldsymbol{\theta}_k, \mu_k) + \eta \alpha_k D(\phi_1(\boldsymbol{\theta}_k, \mu_k), \mathbf{p}_k). \quad (2.58)$$

Here,  $D(\phi_1(\boldsymbol{\theta}_k, \mu_k), \mathbf{p}_k)$  denotes the directional derivative of  $\phi_1$  in the direction  $\mathbf{p}_k$ . Any step  $\mathbf{p}_k$  fulfilling this inequality is accepted, otherwise  $\alpha_k$  is reduced iteratively. Assumptions for the choice of  $\mu$  and  $\eta$  are given in [62] and [126].

### 2.3.3. Adaptive combination of Simulated Quenching and Sequential Quadratic Programming

The solutions approximated by the Simulated Quenching algorithm are usually not located exactly at the local optimum. Hence, Sequential Quadratic Programming is executed after running Simulated Quenching, starting with the solution generated by Simulated Quenching. If Model Updating is used for damage localization, it is often assumed that damage is present at a single spot in the structure. This spot is roughly estimated by Simulated Quenching, using the stiffnesses of the elements as optimization parameters. Subsequently, Sequential Quadratic Programming is started adaptively and the optimization problem is solved again with a reduced set

of parameters. Adaptively means here that the entry with the lowest stiffness parameter is interpreted as the possibly damaged area. The stiffness of this element and the neighbored elements are considered as variable, whereas the remaining elements are treated as non-variable elements (see Figure 2.3). This results in only three variable element stiffnesses. Therefore, a Jacobian of the objective function is computable fast. In doing so, a window is opened that is supposed to contain the actual damaged area. At the same time, the number of optimization variables is decreased, greatly reducing the effort for solving the problem. For the variable elements, the stiffness resulting from Simulated Quenching is used, whereas the stiffness parameters of the non-variable elements are set back to the initial values of 1.0. This strategy may easily be adopted to higher dimensions, e.g., two or three dimensional elements, but these are not considered within this thesis.

Simulated Quenching is a heuristic optimization procedure, meaning that randomness is always present in the solutions generated by the algorithm. If the global algorithm approximates a local instead of the global optimum, the local algorithm is stuck in this local optimum and will converge to the 'wrong' solution. The combination of Simulated Quenching and Sequential Quadratic Programming is started multiple times to allow statistical evaluation of the results generated by the algorithm. In this context, Simulated Quenching can be regarded as a technique to create a deliberate initial parameter vector for the local algorithm.

## 2. Theoretical Background

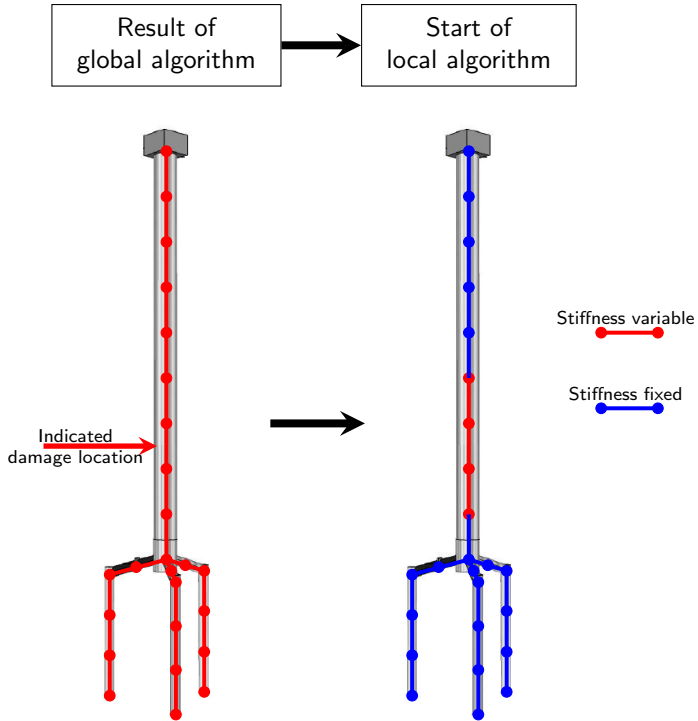


Figure 2.3.: Adaptive reduction of the parameter set for damage localization. Only the sections neighbored to the indicated area are set variable during the local optimization run.

# 3. Effective Application of Model Updating

A general perspective on the methods and techniques needed to perform model updating effectively is introduced in this chapter. Subsequently, two sections focus on important questions that often arise in applications of model updating. These sections comprise the possible globality of the optimization problems and the choice of metrics used for comparison of simulation results and measurement data. The general effectiveness and the evaluation of results of the proposed algorithm are demonstrated using theoretical examples of a tubular cantilever beam model and a numerical model of a real scale offshore wind turbine. The latter is used to prove the performance in an environment with more complex load and control requirements. Both models are damaged virtually, and the model updating approach is used to locate these damages. Since damage localization can be regarded as a special case of model updating, this approach proves both the general capability for parameter identification and the effectiveness of damage localization simultaneously.

## 3.1. General considerations on model updating

This section focuses on general questions that may arise when model updating is to be applied. The topics discussed here are- to the best knowledge of the author- unanswered in the literature. Firstly, a general overview of model updating and the methods needed is given, focusing on updating itself as well as all preliminary steps needed to initialize the updating problem. Subsequently, the need for global optimization methods to solve model updating problems is proven using a straightforward example of a simple harmonic oscillator. Even in recent literature, many authors still use local optimization methods to solve the problems, although it is known that the problems provide several local minima. The section aims to deliver a contribution to this finding. The third section introduces background knowledge on the choice of metrics used to compare simulation results and measured data and lists all items that influence the decision.

### 3. Effective Application of Model Updating

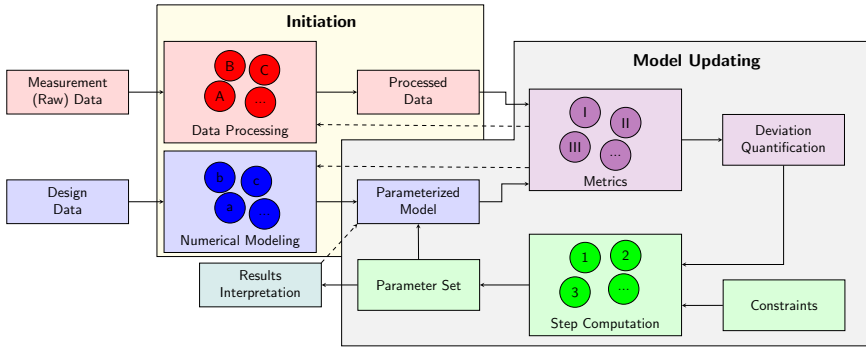


Figure 3.1.: Workflow for iterative deterministic model updating. The initiation phase consists of two steps: the application of data processing methods and numerical modeling. Both steps are influenced by the metrics chosen. The model updating phase is characterized by choice of metrics and optimization methods that modify parameters of a numerical model. In case a sequential algorithm is used, the result of the optimization algorithm may be used to modify the parameter set and start a new optimization run.

#### 3.1.1. Comprehensive workflow for model updating

Any model updating method starts with unprocessed measurement data and design data of the investigated structure (see Figure 3.1). Different methods or combinations of those may be used for processing the raw measurement data. The selection of data processing methods such as data cleansing, filtering, and outlier analysis is an important step, making the results of measurement and simulation comparable. If, for instance, the objective function employed to compare numerical model and measured data is formulated in modal domain, the associated methods used to identify modal parameters from measurement data are also part of the data preprocessing. Thus, it is obvious that the choice of data processing methods is influenced by the metrics applied to update a model.

Based on the design data, a numerical model is built. This step is strongly influenced by the executive engineer and the assumptions made during modeling. Different methods may be used depending on the application, covering all state-of-the-art techniques to build numerical models in structural dynamics. Furthermore, the modeling techniques are influenced by the metrics intended to use. For instance, modeling the loads acting on the structure is necessary if the metric is defined in the time domain, whereas this often complex modeling can be skipped

in the modal domain. Another important step in numerical modeling is an appropriate parameterization of the model that covers all inaccuracies of the model. Again, engineering judgment is important in this step. Any model that is not able to represent the underlying physics of measured data to a certain accuracy level is useless in model updating.

After the essential preparation steps, data processing, numerical modeling, and parameterization, are completed, updating of the numerical model is started. Different metrics or combinations of those come into account, each having different advantages and disadvantages (see Section 3.1.3). These metrics are utilized to quantify the deviation between numerical model and measured data. The computation of steps towards the optimum can be entered with this information, which is the core of the optimization algorithm used for model updating. Depending on the algorithm, this computation may be affected by predefined constraints. Since many parameters that modify physical properties of the model must remain within a certain range, constraints are necessary to maintain physical feasibility of the model or restrict parameters to remain within a reasonable range. Performing the computed step results in updated parameters which are used to update the numerical model. In iterative environments, this loop is repeated multiple times until a convergence criterion is fulfilled and the iteration is aborted, if this criterion is reached. The metrics may be reutilized to classify the results of the optimum parameters in case several solutions are created by the algorithm. Afterwards, updating may be started again, using a different optimization algorithm or a modified parameter set for computation of iteration steps. If an adaptive strategy is implemented (as in Section 2.3.3), the results are interpreted automatically, and the parameterization of the numerical model is adjusted accordingly. The computation of steps mentioned in Figure 3.1 should involve a global optimization algorithm, although many authors still use local algorithms for model updating. Hence, the next section focuses on the globality of optimization problems used in model updating.

#### 3.1.2. On the globality of the optimization problem

Though it is known that problems arising in model updating are nonlinear and provide several local minima [54, 102, 162], authors still employ local algorithms for model updating, even in current publications [44, 49, 79, 108, 110, 127, 156, 159]. This section aims to prove the need for global algorithms for model updating using the mathematical concept of convexity. If the objective function of an optimization problem is convex, then any local solution is a global solution. The feasible set described by the constraints must also be convex if constraints are added to this

### 3. Effective Application of Model Updating

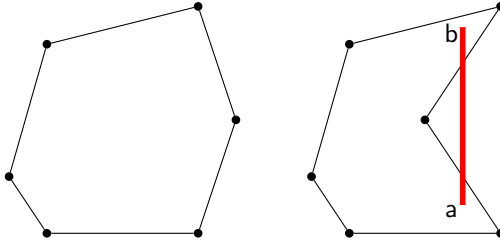


Figure 3.2.: Convex(left) and non-convex(right) sets.

optimization problem [48]. Otherwise, convexity is lost, even for a convex objective function. Both features can not be guaranteed in model updating. The term convex can be applied to both sets and functions. An arbitrary set  $S \in \mathbb{R}^n$  is convex if any line connecting two points  $a$  and  $b$  in  $S$  lies entirely inside  $S$ . If not so, the set is regarded to be non-convex. Transferred to functions, this can be expressed using

$$f(\alpha a + (1 - \alpha)b) - \alpha f(a) - (1 - \alpha)f(b) \leq 0 \quad \forall \alpha \in [0, 1], \quad (3.1)$$

where  $f$  is any function to be tested for convexity.

Assume a simple harmonic oscillator where both the mass  $m$  and the stiffness  $k$  are unknown. The eigenfrequency of this system is determined by  $\omega_s = \sqrt{\frac{k}{m}}$ . A measured eigenfrequency is determined to  $\omega_m = 1.5Hz$  and the model shall be adjusted via variations of  $k$  and  $m$ . The metric  $\rho^\omega$  is applied to compare measurement and simulation results, hence

$$\rho^\omega = \frac{1.5 - \sqrt{\frac{k}{m}}}{1.5}. \quad (3.2)$$

Suppose two parameter combinations  $a$  and  $b$ , with  $a = (k \ m) = (3 \ 2)$  and  $b = (2.5 \ 4)$ . For evaluation of equation (3.1),  $\alpha$  is chosen to 0.2. Evaluation of (3.1) using these arbitrarily chosen values yields  $\rho^\omega(\alpha a + (1 - \alpha)b) = 0.4335$ ,  $f(a) = 0.1835$  and  $f(b) = 0.4733$ . Evaluation of equation (3.1) yields  $\rho^\omega(\alpha a + (1 - \alpha)b) - \alpha \rho^\omega(a) - (1 - \alpha)\rho^\omega(b) = 0.0184 > 0$ , which proves the non-convexity of the objective function.

A visualization of the objective function (3.2) under variations of  $m$  and  $k$  is drawn in Figure 3.3. The illustrated straight red line breaks through the surface multiple times, proving the non-convexity of the function optically. Other objective functions introduced in chapter 2 reveal a similar behavior.

With this proof of non-convexity of the model updating optimization problem,



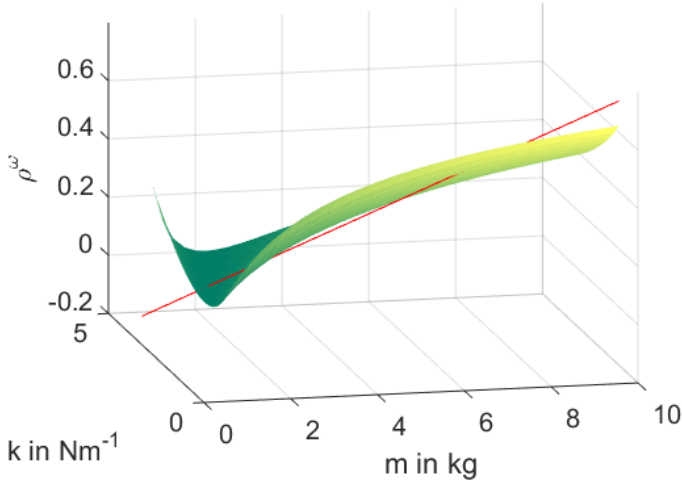


Figure 3.3.: Non-convex shape of  $\rho^\omega$  used as objective function at simple harmonic oscillator system.

it is obvious that a global optimization method is needed to guarantee to find the global optimum, since the problem may exhibit more than a single optimum. Global optimization methods often provide a slow convergence towards the exact optimum. Afterwards, a local optimization method may be used to converge towards the exact optimum. The choice of metrics used for comparison of measurement and simulation data influences the convexity of the function. Hence, the subsequent section gives information on the choice of metrics employed for updating a numerical model.

### 3.1.3. On the choice of error metrics for model updating

The choice of metrics is essential for successful model updating. Any metric must reliably be able to identify differences between model and measurement data. In case model updating is employed for damage localization, the metrics should provide sensitivity to the occurring damage. In applications in structural dynamics, metrics may be defined based on modal or transient simulations, each providing different advantages and disadvantages (see Table 3.1).

In addition to the sensitivity to changes in the system, the objective function must supply a certain level of continuity, depending on the optimization algorithm that

### 3. Effective Application of Model Updating

is employed in order to solve the problem. For instance, if an algorithm employs the Hessian<sup>1</sup>, the function must provide  $C^2$ -steadiness at least.

The numerical effort needed to quantify the deviation between numerical model and measured data is essential. There are quite advanced techniques to compare measurement data and models, such as the dynamic time warping algorithm known from speech recognition [137]. Since every optimization run consists of several thousand evaluations of the objective function, the computational cost needed for its evaluation should be kept in mind, although in most cases the solution of the numerical model consumes the major part of the time needed for a single iteration. The choice of metrics influences the signal processing methods used to process the raw measurement data, as stated in Section 3.1.1. In case eigenvectors are used for model updating, additional methods with manifold underlying mathematics may be needed to identify these from measurement data such as the stochastic subspace identification. If time series are compared, advanced filtering methods may be beneficial to filter both results from the numerical model and measured data. The quality and effect of signal processing are often heavily influenced by the experience and qualification of the engineer assigned to model updating. If these methods have to be implemented for model updating, the implementation effort becomes another important argument that may influence decisions on metrics.

The choice of metrics is essential and yet will always be influenced by the engineer, available soft- and hardware and especially by the investigated problems. To illustrate this choice, the next section introduces the main ideas of model updating using a theoretical example.

## 3.2. Plausibility test of damage localization using a simulated cantilever beam

Any damage is supposed to alter the physical properties of a structure, including the stiffness [42]. On the other hand, most model updating applications use beam models to localize damages, which is a strong simplification of the real physical behavior. With the beam representation being a formulation to capture global structural behavior, the local effect of damage induced stiffness reduction can only be considered inaccurately. Hence, this section aims to verify the hypothesis that beam elements may be used for localization of local structural changes employing the example of a cantilever system.

---

<sup>1</sup>The Sequential Quadratic Programming method used as a local algorithm throughout this thesis employs the Hessian matrix.

### 3.2. Plausibility test of damage localization using a simulated cantilever beam

Table 3.1.: Advantages and disadvantages of different analysis types for comparison of measurement data and numerical models in structural dynamics. Transient signals may be compared either in time or frequency domain

Analysis	Domain	Numerical Modeling	Measurement data
Modal		+Fast solution procedures	+averaging of measurements
		+damping may be neglected	-mode shape tracking needed
		+analytical solutions possible	-system identification needed
		-linear time invariant models	-subset of measured information
Transient	Freq.	+nonlinear signature	+averaging may be possible
		+no phase balancing needed	-amplitudes load dependent
		+fully nonlinear models	+full measured information
	Time	-damping formulation needed	-load measurements needed
		-phase balancing needed	-advanced signal processing needed
-slow solution procedures		-nontrivial choice of metrics	
	-load modeling needed		

Therefore, a model consisting partially of linear four-node shell and linear two-node Bernoulli-beam elements is simulated (see Figure 3.4). The shell section is modeled using 72 elements in the circumferential direction and 60 elements along its length  $L$ . The cantilever has tubular cross-sectional properties with a diameter of  $200\text{mm}$  and a wall thickness of  $1.5\text{mm}$ . It is  $4000\text{mm}$  long and assumed to be made of steel ( $E = 2.1 \cdot 10^{11} \frac{\text{N}}{\text{mm}^2}$ ,  $\mu = 0.3$ ,  $\rho = 7850 \frac{\text{kg}}{\text{m}^3}$ ). An impulse load with a magnitude of  $10^5 \text{N}$  is applied to the free end of the structure. This load is released after  $0.05\text{s}$ . A total time of  $0.5\text{s}$  is simulated with a time increment of  $0.001\text{s}$ . Certain shell elements are deleted to simulate the effect of a local crack in the material, located  $L/2$  from the clamping. Elements are deleted in a single row to simulate a local stiffness decrease. Three different damage severities are simulated, with two, four and six elements being deleted radially<sup>2</sup>. The transition from sections modeled by beam and shell elements is implemented using a flexible contact surface approach. By this approach, the flexibility of the tube is included in the transition while warping effects are not considered.

In a second model, the shell section is also modeled by beam elements to validate the methodology, using the same boundary conditions, loads and cross-sectional properties. Six beam elements are used to represent the dynamic behavior of the structure. These are numbered consecutively from 1 to 6, starting at the clamping.

<sup>2</sup>Since 72 elements are used in the circumferential direction, this yields an angular defect of  $10^\circ$ ,  $20^\circ$  and  $30^\circ$

### 3. Effective Application of Model Updating

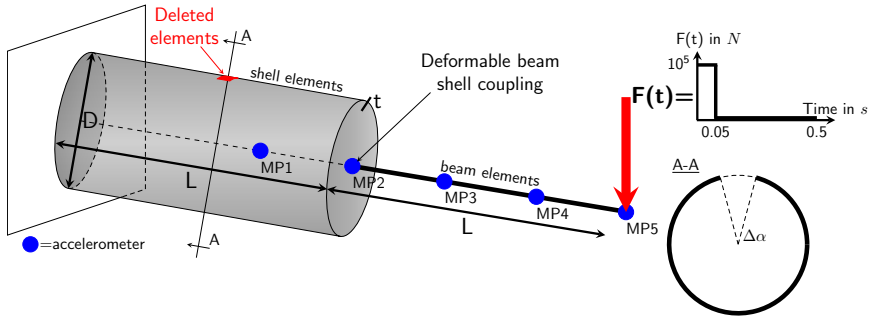


Figure 3.4.: Simulated cantilever beam, modeled partially using shell elements and beam elements, with the beam section providing the same geometrical properties as the shell section. The structure is clamped at the left-hand side. Damage is simulated gradually at  $L/2$  in the shell segment with  $\Delta\alpha = 10^\circ, 20^\circ, 30^\circ$ .  $D=200\text{mm}$ ,  $L=2000\text{mm}$ ,  $t=1.5\text{mm}$ .

Hence, the damage is located in element number 2. This simplified model is then updated to reproduce the response of the more complex, damaged shell model. Damping and gravitation are neglected in both models.

The structural response is evaluated and compared using the accelerations at  $2/3L$ ,  $L$ ,  $4/3L$ ,  $5/3L$ , and  $2L$ , representing locations of five assumed accelerometers (MP1 - MP5 in Figure 3.4) recording with a frequency of  $1000\text{Hz}$ . Figure 3.5 illustrates time series from both the shell model with  $\Delta\alpha = 0$  and the beam model at MP3. The plot reveals that high-frequency amplitudes of the beam model are bigger than those of the shell model, whereas low-frequency contents agree well. This is assumed to be caused by activation of the Poisson effect in the shell elements, which expends a part of the total energy induced to the system by  $F(t)$ . Since beam theory is a rather abstract representation, the Poisson effect is not considered in beam theory, and the entire energy is released in translational vibrations. Due to the amplitude difference, a direct comparison of time series using the time-domain metric  $\rho^{l^2}$  is regarded to be arguable, although it could be circumvented using filters. Therefore, the signals are transferred to the frequency domain using power spectral density and  $\rho^s$  is employed to quantify the difference between shell and beam models throughout this section. Comparison of normalized power spectral densities from both models is drawn in Figure 3.6. The impression that high-frequency contents of the signals differ more is confirmed by this plot, though peaks at high frequencies are smaller than the low-frequency content by

### 3.2. Plausibility test of damage localization using a simulated cantilever beam

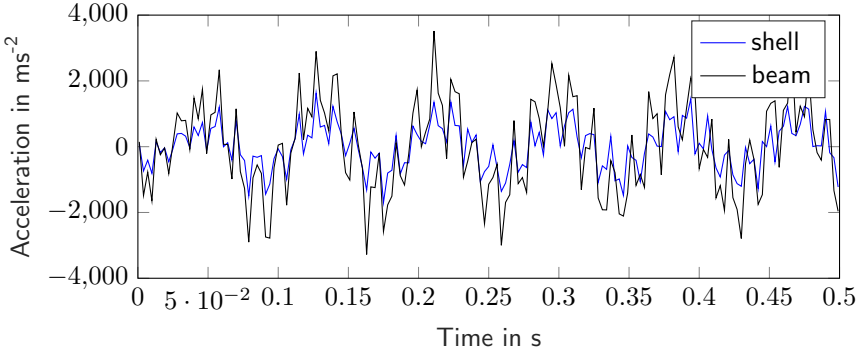


Figure 3.5.: Comparison of time series computed using beam and shell representations of cantilever beam, evaluated at MP3 without damage ( $\Delta\alpha = 0$ ).

Table 3.2.: Comparison of eigenfrequencies of the shell model in Hertz for different damage severities. Eigenfrequencies of perpendicular bending mode shapes in damaged configurations differ due to the damage representation (Figure 3.4) (b=bending shape, t=torsional shape)

		$\Delta\alpha = 0^\circ$	$\Delta\alpha = 10^\circ$	$\Delta\alpha = 20^\circ$	$\Delta\alpha = 30^\circ$
1 <sup>st</sup>	b	11.819	11.810/11.819	11.792/11.819	11.763/11.819
2 <sup>nd</sup>	b	72.908	72.910/72.911	72.911/72.912	72.906/72.911
3 <sup>rd</sup>	b	196.63	196.57/196.68	196.38/196.72	196.08/196.76
4 <sup>th</sup>	t	200.91	200.80	200.65	200.45
5 <sup>th</sup>	t	324.45	324.33	324.08	323.69
6 <sup>th</sup>	b	370.75	370.62/370.80	370.32/370.85	369.82/370.89

three powers of ten.

The eigenfrequencies of the shell model are listed in Table 3.2 for different damage severities. Due to the relatively small damage, the eigenfrequencies alter only up to a few percent. The eigenfrequencies with mode shapes in the direction of the damage drop, whereas some frequencies in perpendicular direction raise somewhat (see Table 3.2). A visual check of the mode shapes reveals that these do not change significantly with the damage.

The beam model is parameterized using six parameters ( $\boldsymbol{\theta} \in \mathbb{R}^{6 \times 1}$ ). Each parameter modifies the stiffness of a single beam element. These parameters are then adjusted to match the responses of the damaged shell model using the two-step model updating algorithm introduced in chapter 2. Since element number two

### 3. Effective Application of Model Updating

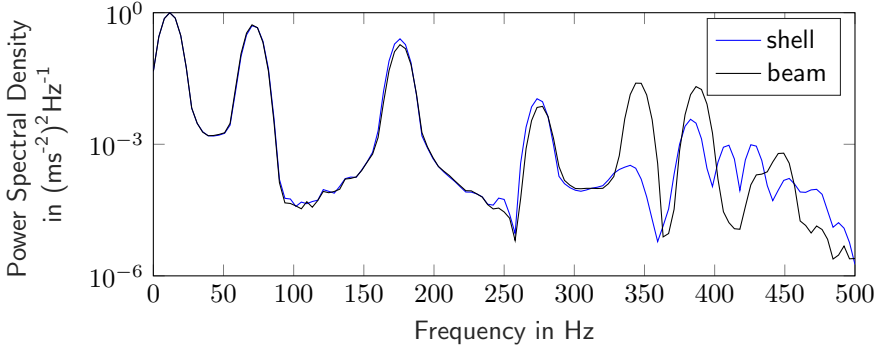


Figure 3.6.: Comparison of normalized power spectral density computed using beam and shell representations of cantilever beam, evaluated at MP3 without damage ( $\Delta\alpha = 0$ ).

of the beam model covers the area where elements are deleted in the shell model, the stiffness parameter  $\theta_2$  should be reduced by the model updating algorithm, indicating the damage to be in the section covered by this element.

The optimization problem being solved to localize the damage is

$$\min_{\theta} \rho^s(\theta) \quad (3.3a)$$

$$\text{subject to } \theta_i \geq 0.9 \quad \forall i \in [1..6] \quad (3.3b)$$

$$\theta_i \leq 1.01 \quad \forall i \in [1..6] \quad (3.3c)$$

$$\sum_{i=1}^6 (1 - \theta_i) \leq 0.1, \quad (3.3d)$$

meaning that the objective function (equation (3.3a)) shall be minimized while fulfilling the constraints (equations (3.3b)-(3.3d)) simultaneously. The constraint equations (3.3b) and (3.3c) are box-constraints that restrict all parameters to remain within a certain range. This is useful to ensure physical feasibility of the parameters<sup>3</sup> and to keep the values within a realistic range. Again, engineering judgment is needed to define this range. All parameters are enforced to be greater than 0.9, meaning a maximum stiffness decrease of 10%. A small increase is allowed for numerical reasons for all parameters. Constraint equation (3.3d) is introduced in [148]. It is added assuming that damage is present at a single spot only. The

<sup>3</sup>For instance, a numerical model would fail if a mass becomes negative.

### 3.2. Plausibility test of damage localization using a simulated cantilever beam

Table 3.3.: Minimal objective function values and corresponding stiffness parameters from ten Simulated Quenching runs using  $\rho^s$  at the cantilever model with  $\Delta\alpha = 10^\circ$ . The objective function value at the initiation of the optimization is normalized to one, all other objective function values are adjusted accordingly. Minimum values are highlighted in gray.

SQ run number	Objective Function Value	element number					
		1	2	3	4	5	6
1	0.597	1.008	0.953	1.009	1.004	0.993	0.983
2	0.636	1.010	0.936	1.006	1.000	0.996	0.995
3	0.627	1.009	0.968	1.000	1.005	1.000	0.947
4	0.579	1.009	0.948	1.008	1.006	0.996	0.988
5	0.588	1.008	0.941	1.006	1.004	1.002	0.982
6	0.579	1.009	0.942	1.01	1.006	0.992	1.004
7	0.607	1.008	0.942	0.999	1.006	1.005	0.98
8	0.649	1.004	0.942	1.001	1.008	1.009	0.993
9	0.58	1.008	0.957	1.004	1.010	0.996	0.973
10	0.614	1.005	0.931	0.998	1.009	1.003	0.989
$\mathcal{M}$	0.606	1.008	0.946	1.004	1.006	0.999	0.983
$\sigma$	0.024	0.002	0.01	0.004	0.003	0.005	0.015

summation ensures that a parameter can reach values close to the maximum stiffness reduction allowed (10%) only if all other parameters are close to the initial value 1.0.

Figure 3.7 illustrates the evaluated objective function normalized to the initial objective function value throughout a single Simulated Quenching run to solve problem (3.3). The plot exposes the ability of the algorithm to leave local minima. It also reveals that the final solution must not necessarily be the solution with the smallest objective function value. This can only be guaranteed for an infinite starting temperature [64]. Hence, the solution with the smallest objective function value is taken as the optimum solution of a Simulated Quenching run instead of the final one. Results of ten Simulated Quenching runs to solve problem (3.3) for the case  $\Delta\alpha = 10^\circ$  are illustrated in Table 3.3. This table lists the normalized objective function values and the according parameter vectors for the optimum solution of each run. All runs are started from the initial solution (all parameters

### 3. Effective Application of Model Updating

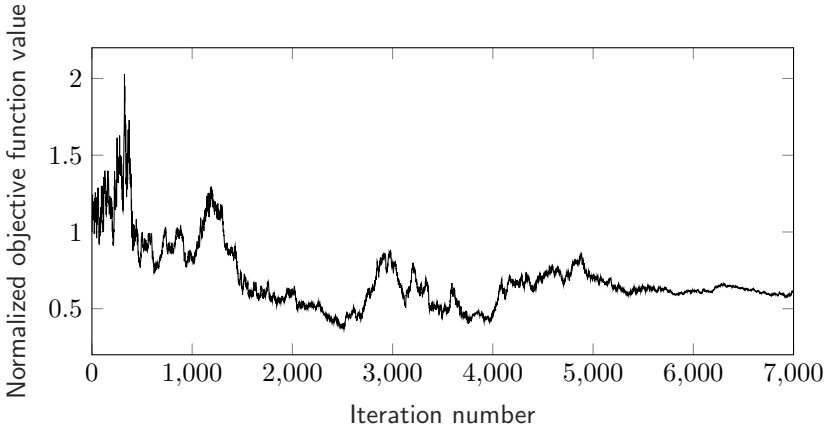


Figure 3.7.: Objective function values of a single Simulated Quenching run to solve problem (3.3), normalized with respect to the initial value.

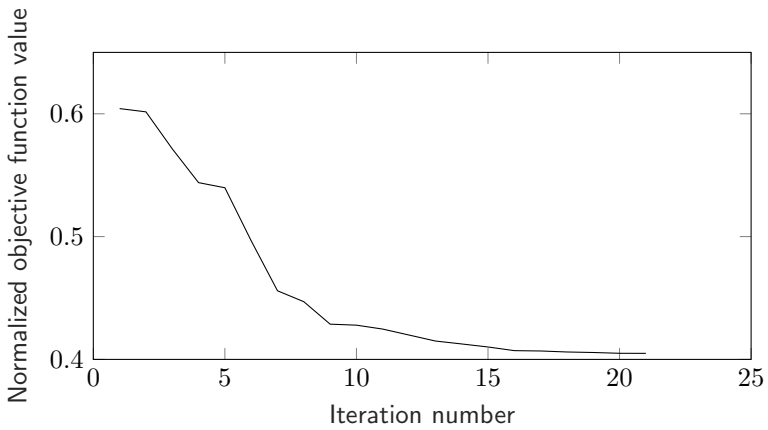


Figure 3.8.: Objective function values of a single Sequential Quadratic Programming run to solve problem (3.3), normalized with respect to the initial value.



### 3.2. Plausibility test of damage localization using a simulated cantilever beam

Table 3.4.: Minimal objective function values and corresponding stiffness parameters from ten Sequential Quadratic Programming runs using  $\rho^s$  at the cantilever model with  $\Delta\alpha = 10^\circ$ , starting with the results from Table 3.3. The objective function value at the initiation of the optimization is normalized to one, all other objective function values are adjusted accordingly.

SQP run number	Objective Function Value	element number					
		1	2	3	4	5	6
1	0.493	1.01	0.913	1.01	1.0	1.0	1.0
2	0.443	1.01	0.93	1.007	1.0	1.0	1.0
3	0.601	1.0	1.0	1.0	1.0	0.992	0.907
4	0.438	1.01	0.943	1.0	1.0	1.0	1.01
5	0.419	1.01	0.929	1.01	1.0	1.0	1.0
6	0.417	1.01	0.932	1.01	1.0	1.0	1.0
7	0.417	1.01	0.932	1.01	1.0	1.0	1.0
8	0.521	1.009	0.914	1.008	1.0	1.0	1.0
9	0.498	1.01	0.914	1.009	1.0	1.0	1.0
10	0.511	1.009	0.914	1.008	1.0	1.0	1.0

set to 1.0). The different solutions are caused by the randomness of the Simulated Quenching algorithm. From a probabilistic point of view, finding the correct solution can not be guaranteed using 10 runs, but the experience of the various examples presented in this thesis reveals that 10 runs are enough to find the correct solution. If the correct solution can not be found using ten runs, it will most likely not be found using more runs. Furthermore, expected values and standard deviations are given for each parameter and the objective function values in Table 3.3. The objective function value may be used to distinguish wrong from correct solutions. In this case, all parameters modify element stiffnesses. Hence, a small parameter entry indicates a reduced stiffness in this area and thus the estimated damaged area. A clear tendency towards element two being the damaged area is visible in these results since it has the lowest stiffness value in nine runs. Another optimum seems to be located at element six by looking at run number three. Furthermore, the expectation value of parameter two is the lowest of all six parameters.

Following the adaptive strategy introduced in chapter 2.3.3, Sequential Quadratic Programming is started, taking the parameters from Table 3.3 as start vectors. All parameters being outside of the adaptive window are reset to 1.0. Figure 3.8 illustrates the convergence of a single Sequential Quadratic Programming run.

### 3. Effective Application of Model Updating

The normalized objective function value is reduced by 30% in this run. The distinct quadratic convergence of the method is lost due to the damped BFGS-approximation of the Hessian. Especially in the first step, the convergence is slow due to erroneous choices of the Hessian. The convergence speeds up after few iterations because the approximation gains precision.

Resulting parameters from ten runs are illustrated in Table 3.4. Sequential Quadratic Programming reduces the objective function values further which confirms the statement that solutions are approximated by the Simulated Quenching methods whereas the Sequential Quadratic Programming method converges towards the real optimum. The final objective function value is used to distinguish correct from wrong solutions. Run number three is assumed to be a wrong solution since its final objective function value is 30% higher than the values of the correct solutions. This difference is only visible after running the local algorithm, proving the usefulness of its application, compare Tables 3.3 and 3.4. Damage localization is successful in all investigated scenarios and element 2 is reliably identified as the damaged area. Parameter two is lower for increased damages (see Table 3.5). Effects of damages can only be considered in an inaccurate manner because the length of the crack is small (local scale) in comparison to the length of each beam element (global scale). Only the bending stiffness of complete beam elements may be changed using this approach. Furthermore, increasing  $\Delta\alpha$  has a big influence on the geometrical moment of inertia in the beginning (see Figure 3.9(a) and Appendix A.2) and its influence is decreasing nonlinearly with growing values for  $\Delta\alpha$  due to the nonlinear nature of the geometrical moment of inertia. Hence, the rather global representation of damages and the nonlinear, rather local effect of damage prevents quantification of damages.

In addition to damage severity, results are also influenced by the location of damage within the shell (see Figure 3.9). If the damage location is rotated by  $\alpha = 45^\circ$  around the center of the tubular section in the cross sectional plane<sup>4</sup>, the according stiffness parameter gets a higher value (see column  $\Delta\alpha = 10^\circ, 45^\circ$  in Table 3.5) due to the smaller influence of the stiffness reduction in the direction contemplated for the evaluation of  $\rho^s$ . In this study, only the signals in x-direction are utilized for the evaluation of the metric. The practical way to deal with this would be to simply use both x- and y-direction for the evaluation of the objective function. Comparison with the analytical stiffness reductions reveals that small damages are overestimated whereas bigger damages are underestimated. This observation confirms Rytter's assumption [142] that additional and often more com-

---

<sup>4</sup>A rotation of  $45^\circ$  is the most disadvantageous configuration. A rotation of  $90^\circ$  would imply to use the perpendicular direction for the evaluation. Most accelerometers used in structural systems support this by allowing to record signals from three spatial directions.

### 3.3. Application to a simulated real scale offshore wind turbine

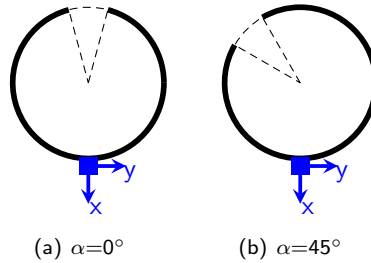


Figure 3.9.: Influence of damage location on measured signal at the tubular beam. Assuming excitation in x-direction, only the measured signal in x-direction is influenced by the damage in case (a), whereas both x- and y-directions are influenced in case (b). However, the signal solely in x-direction is less influenced in case (b).

Table 3.5.: Averaged stiffness parameters of the damaged area after model updating for different damage severities and according analytical stiffnesses.

Damage scenario	$\Delta\alpha = 30^\circ$	$\Delta\alpha = 20^\circ$	$\Delta\alpha = 10^\circ$	$\Delta\alpha = 10^\circ, \alpha = 45^\circ$
<b>Analytical remaining stiffness</b>	0.837	0.890	0.945	0.972
<b>Stiffness parameter 2</b>	0.911	0.920	0.926	0.931

plex methods are needed to enter a higher level of structural health monitoring.

### 3.3. Application to a simulated real scale offshore wind turbine

The OC3-Phase I wind turbine [81] is chosen as an example to demonstrate the functionality of the algorithm using a purely numerical study employing a model with more complex, transient loads and control algorithms. While these are fully controlled in the previous example, the loading conditions are much more complex in this example. Loading conditions are simulated by an artificial wind field. Resulting loads are generated by the simulation code. Geometric properties of this 5-MW wind turbine are given in Table 3.6. This section is aimed to demonstrate the capability of the algorithm to be functional in a more complex environment such as a wind turbine in operation, including aerodynamic loads, complex damping and coupled dynamic characteristics. All results presented in this section are

### 3. Effective Application of Model Updating

published in [147]. The investigated structure is made of steel. Hence, Young's modulus of  $210GPa$  and a shear modulus of  $80.8GPa$  are assumed. Following [81], the density is increased to  $8500 \frac{kg}{m^3}$  to account for paint, bolts, welds, and flanges, which are not considered in the tower data. The tower and monopile are modeled using thirteen linear two-node Timoshenko beam elements, three modeling the monopile and ten modeling the tower. Although being quite coarse, the mesh is found to be sufficiently fine employing a convergence analysis. The structure is clamped at the ground. The rotor-nacelle assembly is modeled as a single mass point. Validity of this assumption for substructure dynamics is proven in [157]. Simulated damage is induced using a stiffness reduction of 10% in the area of the grouted joint, a component that is known to be quite prone to damage. The elements are numbered consecutively from one to thirteen, beginning from the ground (see Figure 3.10). Hence, element number four, the tower base element, has a reduced stiffness. The resulting differences in the natural frequencies are illustrated in Table 3.7.

Since the comparison of model and measurement using a modal approach is regarded as the 'classical approach', these frequencies and the corresponding mode shapes are recorded and treated as measured quantities subsequently. Only the first three eigenmodes are considered in this study, which are known to be identified on a regular basis in real offshore environments [68]. Four sensors are assumed for this study at a height of  $10m$ ,  $31m$ ,  $59m$  and  $87.6m$  above mean sea level. As a consequence, the mode shapes are known at these four nodes.  $\rho^{\omega+\phi}$  (see equation (2.23)) is used as objective function to account for both eigenfrequencies and mode shapes, resulting in the optimization problem

$$\min_{\theta} \rho^{\omega+\phi}(\theta) \quad (3.4a)$$

$$\text{subject to } \theta_i \geq 0.75 \forall i \in [1..n] \quad (3.4b)$$

$$\theta_i \leq 1.01 \forall i \in [1..n] \quad (3.4c)$$

$$\sum_i (1 - \theta_i) \leq 0.25. \quad (3.4d)$$

Each optimization parameter in  $\theta \in \mathbb{R}^{n \times 1}$  controls Young's and shear modulus of one element. The validity of this simplified damage representation is demonstrated in the previous section. The individually allowed stiffness reduction is restricted to 25 percent (3.4b), for numerical reasons a small increase of one percent is allowed (3.4c). Without this increase, finding a new random solution starting from 1.0 would be numerically hard in the way implemented in the algorithm. It is assumed that only one element is damaged, hence an additional constraint is defined

### 3.3. Application to a simulated real scale offshore wind turbine

Table 3.6.: Geometric properties of the OC3 monopile model.

Rotor-Nacelle-Assembly mass	350t
Nacelle height	87.6m
Tower length	77.6m
Tower base diameter	6m
Tower base wall thickness	0.027m
Tower top diameter	3.87m
Tower top wall thickness	0.019m
Monopile length	30m
Monopile diameter	6m
Monopile wall thickness	0.06m



Figure 3.10.: Element numbering of the simulated monopile model. Damage is simulated by a decreased stiffness (10%) of the element marked in black.

Table 3.7.: Comparison of damaged and undamaged eigenfrequencies at the monopile model resulting from a stiffness reduction of 10% in element four (see Figure 3.10).

	undamaged	damaged	Deviation in %
1 <sup>st</sup>	0.30469	0.30265	0.67
2 <sup>nd</sup>	2.2293	2.2285	0.04
3 <sup>rd</sup>	6.2556	6.2180	0.60

Table 3.8.: Resulting minimal objective function values and corresponding stiffness parameters from ten Simulated Quenching runs using  $\rho^{\omega+\phi}$  at the monopile model. The objective function value at the initiation of the optimization is normalized to one. All other objective function values are adjusted accordingly. Minimum values are highlighted in gray.

SQ run number	Objective Function Value	element number												
		1	2	3	4	5	6	7	8	9	10	11	12	13
1	0.748	0.992	1.001	0.997	0.955	1.009	0.975	1.003	0.982	0.981	1.006	0.979	1.009	1.005
2	0.919	0.993	0.993	0.993	0.993	0.999	1.008	0.997	0.989	1.005	0.997	0.990	1.004	0.993
3	0.888	0.988	0.997	0.993	0.978	0.923	0.979	0.984	1.009	0.997	0.987	0.995	0.977	0.960
4	0.770	0.995	1.004	0.9691	0.9698	1.001	0.982	0.987	1.004	0.989	0.987	1.009	0.995	0.975
5	0.817	0.982	1.000	1.007	0.974	0.98	1.000	0.998	0.990	0.975	0.989	0.988	1.006	0.997
6	0.776	0.977	1.002	0.975	0.986	0.964	1.002	1.009	0.988	1.002	0.987	1.001	1.006	1.001
7	0.887	1.002	0.999	1.008	0.967	0.992	1.008	0.979	1.004	0.99	0.987	0.985	0.994	0.986
8	0.777	0.977	0.996	1.006	0.956	0.982	0.990	1.000	0.999	1.004	0.994	0.995	0.977	0.999
9	0.919	1.000	0.992	0.985	0.993	1.007	0.992	1.004	0.984	0.997	0.996	1.001	0.996	1.000
10	0.880	0.999	1.006	0.989	0.957	0.938	0.989	0.994	0.998	0.982	1.001	0.986	0.949	0.995

Table 3.9.: Resulting minimal objective function values and corresponding stiffness parameters from ten Sequential Quadratic Programming runs, using  $\rho^{\omega+\phi}$  at the monopile model, starting adaptively with the results from Table 3.8. The lower section of the Table contains the runs with a shifted window. In the last row, the Sequential Quadratic Programming algorithm is started with the same window, with all parameters set back to 1.0 initially.

SQP run number	Objective Function Value	element number												
		1	2	3	4	5	6	7	8	9	10	11	12	13
1	0.00074	1.0	1.0	0.997	0.910	0.992	1.0	1.0	1.0	1.0	1.0	1.0	1.0	1.0
2	0.19452	1.0	1.0	1.0	1.0	1.0	1.0	0.969	1.010	0.99138	1.0	1.0	1.0	1.0
3	0.00454	1.0	1.0	1.0	0.919	0.907	0.971	1.0	1.0	1.0	1.0	1.0	1.0	1.0
4	0.00811	1.0	0.993	0.945	0.929	1.0	1.0	1.0	1.0	1.0	1.0	1.0	1.0	1.0
5	0.00093	1.0	1.0	0.976	0.913	0.975	1.0	1.0	1.0	1.0	1.0	1.0	1.0	1.0
6	0.00048	1.0	1.0	1.0	0.906	0.950	1.010	1.0	1.0	1.0	1.0	1.0	1.0	1.0
7	0.00051	1.0	1.0	0.982	0.909	0.982	1.0	1.0	1.0	1.0	1.0	1.0	1.0	1.0
8	0.00048	1.0	1.0	0.987	0.909	0.966	1.0	1.0	1.0	1.0	1.0	1.0	1.0	1.0
9	0.21446	1.0	1.0	1.0	1.0	1.0	1.0	1.004	0.984	0.997	1.0	1.0	1.0	1.0
10	0.00245	1.0	1.0	1.0	0.914	0.929	0.980	1.0	1.0	1.0	1.0	1.0	1.0	1.0
3	0.00431	1.0	1.0	0.982	0.919	0.962	1.0	1.0	1.0	1.0	1.0	1.0	1.0	1.0
4	0.00031	1.0	1.0	1.010	0.893	0.999	1.0	1.0	1.0	1.0	1.0	1.0	1.0	1.0
6	0.00489	1.0	1.0	0.947	0.931	0.950	1.0	1.0	1.0	1.0	1.0	1.0	1.0	1.0
10	0.00253	1.0	1.0	0.972	0.921	0.923	1.0	1.0	1.0	1.0	1.0	1.0	1.0	1.0
starting from 1.0	0.00007	1.0	1.0	0.999	0.902	0.983	1.0	1.0	1.0	1.0	1.0	1.0	1.0	1.0

### 3. Effective Application of Model Updating

ensuring that only a single parameter can be close to the maximum estimated stiffness reduction (3.4d).

Beginning with the undamaged configuration, Simulated Quenching is started to solve the optimization problem (3.4). According to [64], the initial temperature  $T_0$  is chosen to 500 and  $N$  to 50. Based on expert knowledge, the annealing factor  $C$  and the final temperature  $T_{end}$  are chosen to 0.95 and 0.5, respectively<sup>5</sup>. The resulting parameter vectors with the lowest corresponding objective function value of ten Simulated Quenching runs, all starting with the initial parameter vector, are shown in Table 3.8. Simulated Quenching finds two local minima, one located around the correct solution (element four) and one at element eight. Although in a similar range, the objective function values are smaller for the solutions being closer to the correct location. This can be taken as the first indication of element four being the correct damage location.

Subsequently, the optimization problem (3.4) is modified according to section 2.3.3 and Sequential Quadratic Programming is started with a reduced set of parameters. The modification contains the assumption that the minimum parameter is the possibly damaged area and only this parameter and the direct neighbors are treated as variable. For the variable elements, the stiffness resulting from Simulated Quenching is used, whereas the stiffness parameters of the non variable elements are set back to the initial value 1.0. The resulting objective function values are displayed in Figure 3.11 and the parameter vectors are drawn in Table 3.9. Figure 3.11 reveals the two solutions that are far away from the actual solution (run number two and nine) as wrong solutions. After running Sequential Quadratic Programming, the objective function values of right and wrong solutions are in a different range. If Simulated Quenching estimates the correct solution (runs number one, five, seven and eight), only the correct value is decreased (see Table 3.9), the other values remain close to 1.0. Even the stiffness reduction is estimated with an accuracy of 1.5% (see Table 3.9, element number 4) in these cases. Although this may be seen as a hint towards damage quantification, please note that a beam model is updated to reproduce the response of the same beam model with reduced stiffness in this example. Hence, there are no modeling errors in this theoretical study. Nevertheless, this analysis is useful to demonstrate the strength of the approach. All solutions that point in the neighborhood of the correct solution (runs number three, four, six and ten) reveal that two stiffness parameters are decreased simultaneously, pointing to the damaged area. Based on these results, the adaptive window (compare section 2.3.3) can be moved towards the direction with low stiffnesses, and a new Sequential Quadratic Programming run can be started. The

---

<sup>5</sup>These values have been found to perform well in the applications presented within this thesis. Therefore, this set up is employed in all examples presented throughout the thesis.



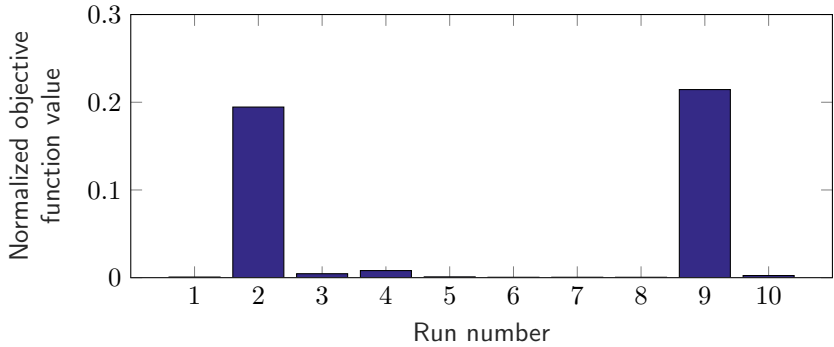


Figure 3.11.: Final objective function values after running ten Simulated Quenching runs and Sequential Quadratic Programming adaptively, using  $\rho^{\omega+\phi}$  as objective function.

results of this optimization with a shifted window are shown in the lower section of Table 3.9. The most distinctive result is achieved, if the original stiffnesses (see Table 3.9, line 'starting from 1.0') are used as a start vector of the new Sequential Quadratic Programming iteration with a shifted window instead of the values generated using the adaptive Sequential Quadratic Programming approach with the original parameter window.

For comparison of the 'classical approach' using modal properties and a metric using a direct comparison of time series, the aero-servo-hydro-elastic computer-aided engineering tool FAST [80] is used to simulate transient dynamics of the wind turbine. The model has the same geometric properties, as described in the previous section (see Figure 3.12). Furthermore, the consideration of aerodynamic loads requires a more sophisticated model of the rotor and the wind turbine control which is given by the software. Hence, the rotor is modeled as described in [81]. A steady wind field with a velocity of  $12 \frac{m}{s}$  is simulated, the controller given in FAST is employed and periodic waves with a significant height of  $6m$  are modeled to account for hydrodynamic loads. Following the preceding section, the tower and monopile are built out of thirteen beam elements, and the stiffness of the tower base element is reduced by ten percent. Again, four measurement sensors are assumed to be placed in the previously described locations. The acceleration signals at these locations are used to evaluate the objective function. The difference of the tower top acceleration signal of the damaged and undamaged system state is illustrated in Figure 3.13, revealing slight differences between the two signals graphically.

### 3. Effective Application of Model Updating

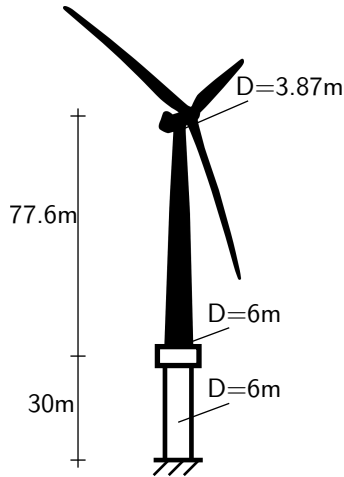


Figure 3.12.: Overview on geometric properties of the NREL 5MW wind turbine.

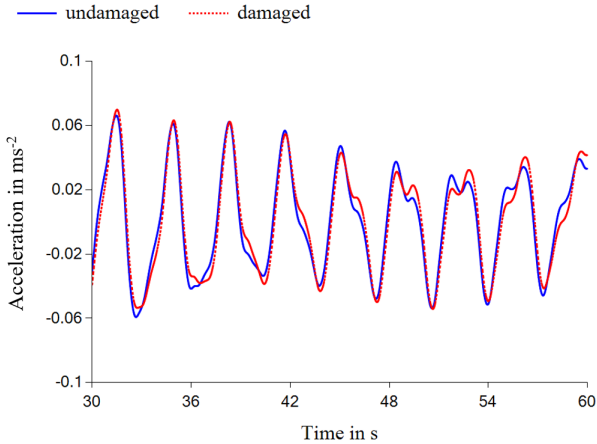


Figure 3.13.: Comparison of the monopiles damaged and undamaged tower top acceleration time series in wind direction, filtered with a Butterworth filter. The initial 30 seconds are skipped due to the transient procedure in this phase.

Table 3.10.: Resulting minimal objective function values and corresponding stiffness parameters from eight Simulated Quenching runs using  $\rho^{l_2}$  at the monopile model. Minimum values are highlighted in gray.

SQ run number	Objective Function Value	element number												
		1	2	3	4	5	6	7	8	9	10	11	12	13
1	0.0091	0.995	0.989	0.998	1.005	0.986	0.999	0.995	1.009	0.996	1.001	0.999	0.995	0.991
2	0.0624	1.008	1.007	0.983	0.996	1.003	1.00	0.989	0.995	0.985	0.999	0.980	0.992	1.004
3	0.0786	0.989	0.9866	1.001	0.998	0.991	0.993	1.009	0.990	0.9862	0.995	1.001	1.008	0.993
4	0.0143	0.997	0.984	1.004	0.982	0.982	1.005	1.005	1.002	0.991	0.992	1.008	1.002	0.994
5	0.0948	0.992	0.993	1.007	1.006	1.001	0.991	0.986	0.996	0.996	0.995	0.993	0.997	1.003
6	0.0053	0.990	1.000	0.989	0.981	0.986	0.995	1.00254	0.999	0.994	0.995	1.000	0.998	1.002
7	0.0196	0.991	0.991	0.999	1.007	1.001	0.998	0.994	0.9981	0.964	1.006	0.989	1.000	0.987
8	0.0085	0.998	0.984	0.978	0.984	1.002	1.002	0.999	0.989	0.996	1.003	0.993	1.004	0.999



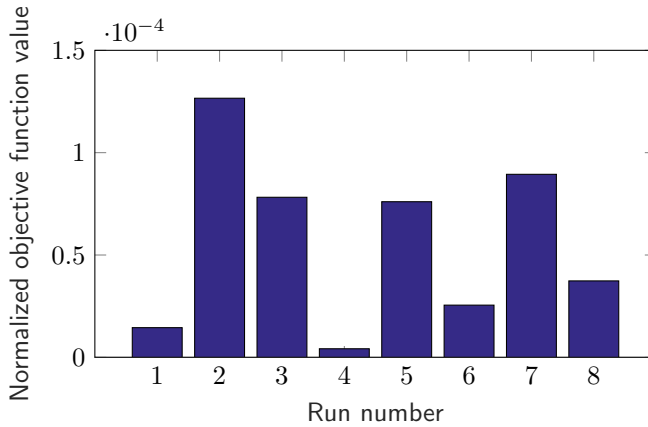


Figure 3.14.: Final objective function values after running eight Simulated Quenching runs and Sequential Quadratic Programming adaptively using  $\rho^{l_2}$  at the monopile model.

For damage localization,  $\rho^{l_2}$  is used as an objective function and the constraints (3.4b)-(3.4d) from the modal-based example are reused. The results of eight Simulated Quenching runs are illustrated in Table 3.10. In 50 percent of the Simulated Quenching runs, the solution points to the damaged area, whereas the remaining four solutions point to areas located at a higher position in the tower. Based on these results, Sequential Quadratic Programming is started adaptively. Table 3.11 provides an overview of the results of the Sequential Quadratic Programming algorithm. In case Simulated Quenching points to the correct location (runs number four and six), Sequential Quadratic Programming decreases the correct stiffness parameter, but the decrease is not as distinct as in the modal-based example. If the solutions generated by Simulated Quenching point close to the correct solution (run number one and eight), the solutions generated by Sequential Quadratic Programming point to the correct solution. The final objective function values of the damage localization using time series are compared in Figure 3.14. This diagram can easily be used to distinguish correct from wrong solutions, the objective function values of the correct solutions (run number one, four, six and eight) are up to 50% smaller than the objective function values of the wrong solutions. The difference between correct and wrong solutions is not as distinctive as in the modal-based example, but different enough to draw a clear decision. This example proves that damage localization is possible with both modal properties and time

### 3. Effective Application of Model Updating

series employed as the objective function. Since many error sources are excluded in updating model-to-model, the objective function values are close to zero.

## 3.4. Conclusion

This chapter starts with general thoughts on model updating. Firstly, a global view of iterative model updating is given, and a comprehensive overview on all methods and equipment needed to effectively update numerical models to measured data using iterative optimization algorithms in structural dynamics is introduced. A second section focuses on the globality of optimization problems arising in model updating, proving that the objective functions are non-convex and hence a global optimization algorithm is needed to solve the problems accurately. Thirdly, advantages and disadvantages of different metrics used to compare measurement data and results of numerical models are given.

In the following sections, the adaptive two-step model updating algorithm introduced in chapter 2 is utilized to two theoretical examples: a simulated cantilever beam with a more realistic damage representation than usually used in model updating and a simulated offshore wind turbine. The simulated cantilever beam is partially modeled by shell elements. Several shell elements are deleted to simulate a crack in the material more realistically than with beam elements. This damage is then successfully located using a beam representation of the structure, verifying this often used simplification for damage localization. The second example is a simulated offshore wind turbine on a monopile foundation that is damaged in the area of the grouted joint, an assembly that is known to be quite prone to damage. This example demonstrates the functionality in more complex environments with complex loads and controls acting on the structure. Damage is simulated using a stiffness decrease of 10%.

Damage localization is successful in both examples. Furthermore, the optimization problems in both examples reveal to have at least two local minima, approving the need for a global optimization algorithm for model updating. The final objective function value is used to distinguish correct from wrong solutions. A metric defined in the frequency domain is employed to update the cantilever, whereas metrics in modal and time domain are compared using the example of a simulated offshore wind turbine. Though damage localization is in focus here, the effectiveness of the algorithm for parameter adjustments is proven simultaneously, since a stiffness decrease is also a modified parameter that has to be identified and adjusted by the algorithm. The cantilever model proves that even the rather global beam representation can capture the local effects of damages. While the damage representation fits perfectly to the reference data in the wind turbine example, this is not the case

in the cantilever beam example. This correlation is visible in the final objective function values. Note that these are normalized. The value is close to zero in the wind turbine example, whereas this is not the case in the cantilever example. This emphasizes the high importance of accurate numerical modeling for effective model updating.

Although being successful in the wind turbine example, damage quantification is not feasible due to the simplified modeling of damages using decreased stiffnesses of beam models. In the wind turbine, a beam model is updated to reproduce a beam model. Hence, modeling errors are excluded in this case. A workaround towards damage quantification would be to use more accurate damage models after the exact damage location is known, placing the more exact damage representation in areas identified using the approach presented here. Afterward, the model updating algorithm may be restarted to adjust the more complex damage models to quantify damages, but damage quantification is beyond the scope of this thesis. Within this chapter, all examples comprise only simulated data, eliminating some of the effects and issues that arise if real measured data are used for model updating. Hence, the application to real measurement data is demonstrated in the next chapter.





# 4. Concept Validation for Parameter Identification

This chapter presents the application of the approach for parameter identification in two practical examples. The result of these studies is an estimated set of parameters that adjust the given model to represent the measured data as good as possible, indicating which parameter causes a potential structural change. The first example is a scaled model of a three-story building structure with four degrees of freedom, whereas, in the second example, ice masses accreting on a real scaled wind turbine rotor blade are quantified.

## 4.1. Model Updating at a three-story building structure

This section proves the functionality of the model updating algorithm at a model of a three-story frame that was installed and tested at the engineering institute of Los Alamos National Laboratories [45]. Measured and constructional data is stored in a database that is publicly available<sup>1</sup>. Different metrics for model-measurement comparison introduced in chapter 2 are applied, and their performance for parameter identification is compared with special emphasis on artificial nonlinearities that may be added to the frame setup.

### 4.1.1. Experimental set up of the frame structure

The three-story frame (see Figure 4.1) is constructed using four aluminum plates ( $30.5 \cdot 30.5 \cdot 2.5\text{cm}$ ) that are connected using four aluminum columns ( $17.7 \cdot 2.5 \cdot 0.6\text{cm}$ ) for each floor. Each plate represents a floor. The columns are arranged to be bent about their weak axis. An additional aluminum column ( $15.0 \cdot 2.5 \cdot 2.5\text{cm}$ ) that hits a bumper fixed at the second floor (see Figure 4.1(b)) can be

---

<sup>1</sup>For download visit <http://www.lanl.gov/projects/national-security-education-center/engineering/ei-software-download/thanks.php>

#### 4. Concept Validation for Parameter Identification

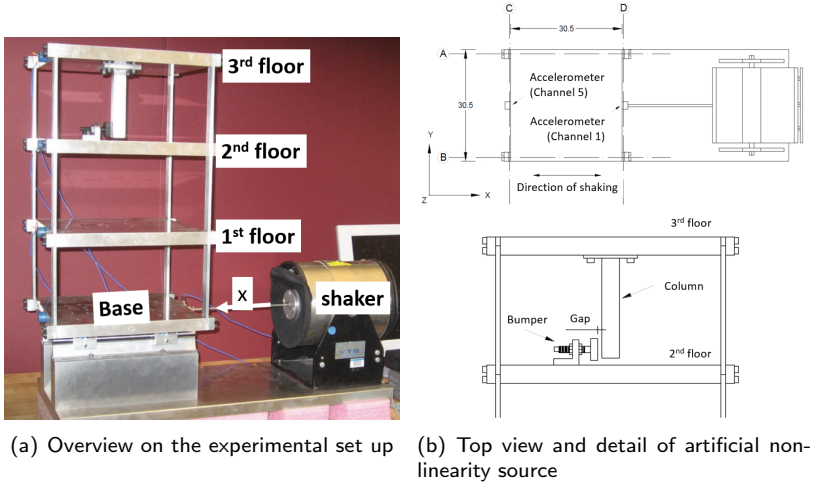


Figure 4.1.: Experimental set up of the three-story building structure.

mounted under the top floor to be able to include artificial nonlinearities. The position of the bumper is adjustable to increase the impact of the nonlinearity. Additional masses can be mounted at the base and the first floor. The structure is excited using an electrodynamic shaker that provides lateral displacements of the base plate along its centerline. The base plate is mounted on rails to enable a simple excitation of the structure, allowing rigid body motions. It is modified using additional masses, stiffness reductions, contact-nonlinearity and a combination of contact and additional mass. The test program is depicted in Table 4.1. State 1 represents the baseline system, states 2 and 3 have an additional mass attached to one single floor, states 4 to 9 provide stiffness reductions of different columns of the structure, states 10 to 14 have the additional nonlinearity activated whereas states 15 to 17 provide combinations of nonlinearity and additional masses, respectively. The measurement signals are recorded with a sampling frequency of  $322.58Hz$  on all four floors. The system is excited using a shaker attached to the base floor with a band-limited random excitation within a range of  $20 - 150Hz$  with a level of  $2.6V$  root mean square. The lower frequency boundary is chosen in order not to excite the rigid body eigenmodes that are present below  $20Hz$  [45]. These excitation boundaries are clearly visible in the power spectral density of the uppermost accelerometer (see Figure 4.4). An exemplary time series for the force that was applied in one run in baseline condition is illustrated in Figure 4.2.

## 4.1. Model Updating at a three-story building structure

Table 4.1.: Overview on structural states investigated in the three-story frame by Los Alamos National Laboratories.

Label	State Cond.	Description
State 1	Undamaged	Baseline condition
State 2	Undamaged	Mass=1.2kg at the base
State 3	Undamaged	Mass=1.2kg at the first floor
State 4	Undamaged	87.5% stiffness reduction in column 1BD <sup>a</sup>
State 5	Undamaged	87.5% stiffness reduction in column 1AD <sup>a</sup> and 1BD <sup>a</sup>
State 6	Undamaged	87.5% stiffness reduction in column 2BD <sup>a</sup>
State 7	Undamaged	87.5% stiffness reduction in column 2AD <sup>a</sup> and 2BD <sup>a</sup>
State 8	Undamaged	87.5% stiffness reduction in column 3BD <sup>a</sup>
State 9	Undamaged	87.5% stiffness reduction in column 3AD <sup>a</sup> and 3BD <sup>a</sup>
State 10	Damaged	Gap=0.20mm
State 11	Damaged	Gap=0.15mm
State 12	Damaged	Gap=0.13mm
State 13	Damaged	Gap=0.10mm
State 14	Damaged	Gap=0.05mm
State 15	Damaged	Gap=0.20mm and Mass=1.2kg at the base
State 16	Damaged	Gap=0.20mm and Mass=1.2kg at the first floor
State 17	Damaged	Gap=0.10mm and Mass=1.2kg at the first floor

<sup>a</sup> XYZ = the column on floor X at the intersection of axis Y and Z (see Figure 4.1(b)) is modified

## 4. Concept Validation for Parameter Identification

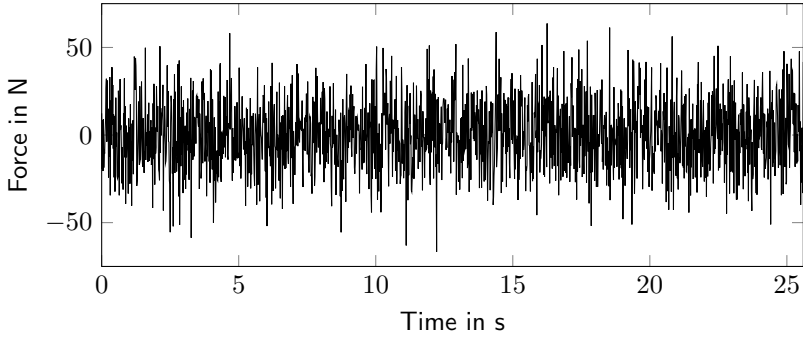


Figure 4.2.: Example force time series applied to baseline condition (band-limited random excitation within 20-150 Hz).

### 4.1.2. Numerical model of the three-story frame

Vibrations in  $y$ - and  $z$ -direction are very small due to the missing excitation in this direction and the design which avoids these motions by means of geometric and inertial decoupling. As only a single accelerometer is attached centered in the excitation direction, these accelerometers are insensitive to torsional vibrations of the structure. Compared to the bending-deflection of the columns, their deformation is negligible for the numerical model. These assumptions result in a one-dimensional shear-frame model with four degrees of freedom ( $u_0$ - $u_3$ ) and a lumped mass at each node (see Figure 4.5). The according mass and stiffness matrices ( $M$  and  $K$ ) are written as

$$\mathbf{M} = \begin{bmatrix} m_0 & 0 & 0 & 0 \\ 0 & m_1 & 0 & 0 \\ 0 & 0 & m_2 & 0 \\ 0 & 0 & 0 & m_3 \end{bmatrix}, \quad \mathbf{K} = \begin{bmatrix} k_0 + k_1 & -k_1 & 0 & 0 \\ -k_1 & k_1 + k_2 & -k_2 & 0 \\ 0 & -k_2 & k_2 + k_3 & -k_3 \\ 0 & 0 & -k_3 & k_3 \end{bmatrix}. \quad (4.1)$$

The base stiffness ( $k_0$ ) can be neglected because of the low stiffness of the gliders on the rails. The stiffnesses of the beams connecting the floors ( $k_1$  to  $k_3$ ) are modeled using four clamped-clamped beams, summing up to a single stiffness

$$k_i = 4 \cdot \frac{12E_i I_i}{l_i^3}, \quad (4.2)$$

where  $E$  represents Young's Modulus (65GPa),  $I$  is the geometrical moment of inertia and  $l$  is the free length of the columns (17.7cm – 2.5cm). The masses vary

#### 4.1. Model Updating at a three-story building structure

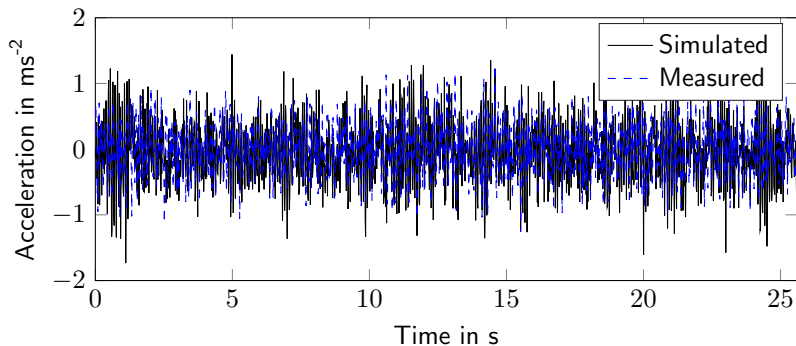


Figure 4.3.: Comparison of measured and simulated baseline condition acceleration at the top floor as a response to the force illustrated in Figure 4.2.

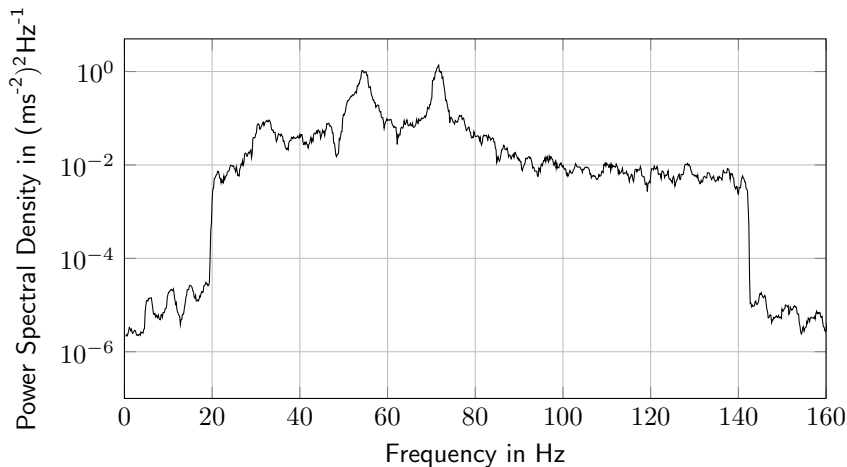


Figure 4.4.: Averaged power spectral density of the uppermost accelerometer of the frame structure in baseline condition.

#### 4. Concept Validation for Parameter Identification

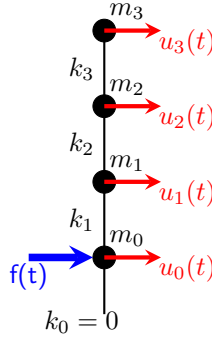


Figure 4.5.: Numerical model of the three-story frame.

Table 4.2.: Masses of components used for building the frame structure.

Component	Mass in kg
Floor ( $m_{flr}$ )	$0.305 \cdot 0.305 \cdot 0.025 \cdot 2710 = 6.30$
Column ( $m_{col}$ )	$0.025 \cdot 0.006 \cdot 0.177 \cdot 2710 = 0.072$
Column Screw Block ( $m_{csb}$ )	0.04
Bumper ( $m_b$ )	0.2
Suspended Column ( $m_{sc}$ )	$0.025 \cdot 0.025 \cdot 0.15 \cdot 2710 = 0.254$

for each floor due to the nonlinearity sources installed (see Table 4.2), resulting in

$$m_0 = m_{flr} + 4 \cdot 0.5 \cdot m_{col} + 4 \cdot m_{csb} \quad (4.3)$$

$$m_1 = m_{flr} + 4 \cdot m_{col} + 4 \cdot m_{csb} \quad (4.4)$$

$$m_2 = m_{flr} + 4 \cdot m_{col} + 4 \cdot m_{csb} + m_b \quad (4.5)$$

$$m_3 = m_{flr} + 4 \cdot 0.5 \cdot m_{col} + 4 \cdot m_{csb} + m_{sc}. \quad (4.6)$$

Modal properties are identified from the measured data using enhanced frequency domain decomposition. The results for the baseline condition are illustrated and compared to the results of the numerical model in Table 4.3 and Figure 4.6. The first eigenmode is a rigid body mode. Therefore, it is not considered further in the evaluation of the objective function. The results reveal numerical model and measured structure (see Figure 4.3) to be in good agreement, the maximum deviation of eigenfrequencies accounts to 2.5% and the minimum value of the modal assurance criterion is 0.98.

Table 4.3.: Comparison of measured and simulated eigenfrequencies of the three-story frame. In addition, damping ratios identified from the measurements are given.

Eigenmode	$\omega_m$ in Hz	$\omega_s$ in Hz	Deviation in %	$\zeta_m$ in %
2	30.40	29.65	-2.47	5.65
3	54.08	54.60	+0,96	3.18
4	70.87	71.15	+0,40	1.39

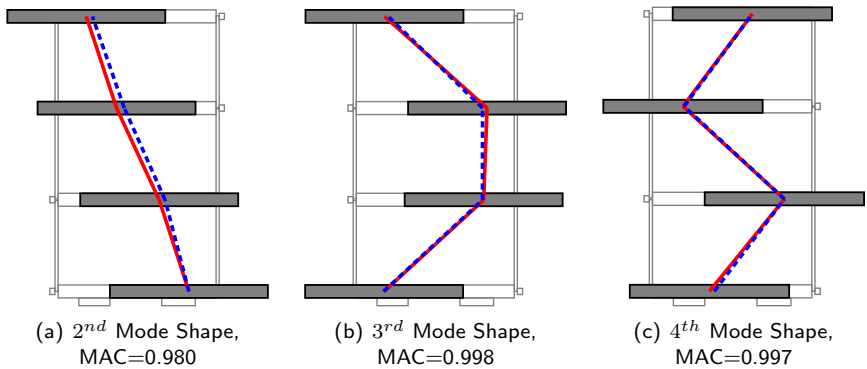


Figure 4.6.: Comparison of measured (blue, dashed) and simulated (red) mode shapes of the frame structure and according modal assurance criterion values.

## 4. Concept Validation for Parameter Identification

According to [117], the damping matrix can be obtained employing the modal damping ratios identified from the measured data using

$$\mathbf{C}_n = \begin{bmatrix} 2\zeta_1\omega_1 M_1 & 0 & 0 & 0 \\ 0 & 2\zeta_2\omega_2 M_2 & 0 & 0 \\ 0 & 0 & 2\zeta_3\omega_3 M_3 & 0 \\ 0 & 0 & 0 & 2\zeta_4\omega_4 M_4 \end{bmatrix}, \quad (4.7)$$

where  $\zeta_i$ ,  $\omega_i$  and  $M_i$  represent the  $i$ -th modal damping ratio, natural frequency and modal mass, respectively. The damping matrix used in a finite element analysis is then obtained using equation (2.4)

$$\mathbf{C} = \mathbf{\Phi}^{-T} \mathbf{C}_n \mathbf{\Phi}^{-1}, \quad (4.8)$$

with  $\mathbf{\Phi}$  being the matrix of undamped eigenvectors, resulting in the set of equations of motion of the system

$$\mathbf{M}\ddot{\mathbf{u}}(t) + \mathbf{C}\dot{\mathbf{u}}(t) + \mathbf{M}\mathbf{u}(t) = \mathbf{f}(t), \quad (4.9)$$

where  $\mathbf{f}(t)$  denotes the vector of forces acting on each node of the system. Besides the force of the shaker acting on node 0, which is recorded by the measurement system (see Figure 4.2), all input forces are zero.

The gap nonlinearity (states #10-17) is modeled using an additional stiffness being added to the stiffness of the uppermost story,  $k_3$ . With the bumper being quite stiff, this additional stiffness is chosen to  $8 \cdot 10^5 \frac{N}{m}$  using an initial convergence analysis. The gap-nonlinearity is activated, if the inequality

$$u_3(t_i) - u_2(t_i) \geq g \quad (4.10)$$

is fulfilled at time step  $t_i$ , with  $g$  denoting the gap width. In case this equation is activated during the actual time step, this time step is repeated with the additional stiffness.

### 4.1.3. Updating the numerical model of the frame structure

As illustrated in Table 4.1, an additional mass of  $1.2kg$  is added to the first floor in state 3, raising  $m_1$  by 19%. Due to its big effect on the structural dynamics and the nonlinearity not being activated, this state is investigated here, using the basic objective functions that are introduced in section 2.2, namely  $\rho^{\omega+\phi}$ ,  $\rho^s$  and  $\rho^{l_2}$ . In case the nonlinearity is activated, the concept of modal analysis is no longer valid. Hence,  $\rho^{\omega+\phi}$  is not used in these states. All masses and stiffnesses are treated



as variable, resulting in an optimization problem containing seven variables. The variation of the variables is restricted using boxed constraints with a lower value of 0.7 and an upper boundary of 1.3.

### Parameter identification based on modal data

For parameter identification using modal properties, both eigenfrequencies and mode shapes are considered (equation (2.23)). Although there is very good agreement between numerical model and eigenmodes identified from the measurement (see Table 4.3 and Figure 4.6), the model is adjusted to the measured eigenmodes of baseline condition first to ensure maximum compatibility of numerical model and measured data. Furthermore, this plot reveals the low stiffness of the gliders on the rails, since the mode shapes affirm free-free boundary conditions. Baseline condition contains nine measurement sets, the modal parameters are averaged over these sets.

The constraints of the optimization problem are chosen quite broad in order to let the optimization solver do its work, just ensuring solvability of the numerical model<sup>2</sup>. Combining the constraints with the metric results in the optimization problem

$$\min_{\boldsymbol{\theta}} \rho^{\omega+\phi}(\boldsymbol{\theta}) \quad (4.11a)$$

$$\text{subject to} \quad \boldsymbol{\theta} \geq 0.4 \forall i \in [1..n] \quad (4.11b)$$

$$\boldsymbol{\theta} \leq 1.6 \forall i \in [1..n] \quad (4.11c)$$

to be solved. Results of ten runs of the algorithm to solve the problem are listed in Table 4.4. Being a random search algorithm, Simulated Quenching returns different solutions. Comparison of the parameters reveals that small changes in the parameters strongly influence the objective function values. Although measured and simulated eigenmodes are very close, the objective function value of ten runs is still reduced by a mean of 14%. The boundary conditions (eqns. (4.11b) and (4.11c)) are not activated in any run. The mean values of the parameters are close to one with a maximum deviation of 5.6 percent. Computing the objective function value using the mean values of the optimum solutions from ten Simulated Quenching runs returns a normalized objective function value of 0.699, returning the best solution in this example. This is not always the case, but recommended. Starting Sequential Quadratic Programming using optimum vectors as a

---

<sup>2</sup>In case the parameter values differ in several powers of ten, the matrices become close to singularity. This is prevented using the parameter bounds given here

#### 4. Concept Validation for Parameter Identification

Table 4.4.: Normalized minimal objective function values and according parameters for ten Simulated Quenching runs, using  $\rho^{\omega+\phi}$  to identify parameters of baseline condition. The last two lines reveal the mean and standard deviation of the values listed in the respective column.

SQ run number	Objective Function Value	mass number				stiffness number		
		0	1	2	3	1	2	3
1	0.921	0.992	0.983	0.999	1.018	0.999	1.000	1.006
2	0.699	0.918	0.969	1.043	1.032	0.95	1.052	1.018
3	0.878	1.006	0.997	0.999	1.261	0.962	1.191	1.082
4	0.836	0.946	1.004	0.984	1.025	0.985	1.011	1.028
5	0.813	0.938	1.017	1.016	1.021	0.994	1.033	1.008
6	0.886	0.941	0.999	0.999	0.976	0.992	1.086	1.002
7	0.864	0.955	0.99	0.981	0.998	0.962	0.996	0.985
8	0.828	1.046	0.979	0.992	1.118	1.032	1.051	1.081
9	0.986	0.999	0.996	1.000	1.018	1.009	0.99	1.008
10	0.877	0.919	0.934	1.006	1.095	0.986	0.872	1.136
$\mathcal{M}$	0.859	0.966	0.987	1.002	1.056	0.987	1.028	1.036
$\sigma$	0.075	0.040	0.022	0.017	0.079	0.023	0.077	0.046

starting point results in a minimal objective function value of  $\rho^{\omega+\phi}(\theta^*) = 0.303$  with  $\theta^* = [0.911, 1.104, 1.105, 1.102, 0.986, 0.753, 1.08]^T$ . With this set of parameters, the eigenfrequencies become  $29.89Hz$ ,  $54.19Hz$  and  $70.87Hz$ . The according Modal Assurance Criterion values are 0.991, 0.999 and 0.996. The mode shapes of the second and third eigenmodes are represented more accurately by the model, whereas it performs somewhat worse for the fourth eigenmode. Being the optimum parameter set with the smallest according objective function value and the starting configuration for subsequent analyses, the values of  $\theta^*$  are set to 1.0. Note that this analysis aims to identify the parameters that build the best representation of the measured eigenfrequencies and mode shapes, not to estimate parameters correctly. Otherwise, a stiffness decrease of 24.7% of stiffness number 2 can not be explained by physical means. Nevertheless, the identification of other states investigated in the experiment is attempted with this parameter set.

Having found the optimum parameter set for baseline condition, the algorithm is applied to state 3. The according results of this run are listed in Table 4.5. An increase of the mass decreases the eigenfrequencies of the structure, whereas stiffnesses must be decreased to obtain reduced eigenfrequencies. Hence, typically all masses and stiffnesses are modified by the algorithm, leading to a representation with all parameters being changed slightly. The parameter with the highest

Table 4.5.: Normalized minimal objective function values and according parameters for ten Simulated Quenching runs, using  $\rho^{\omega+\phi}$  to identify parameters of state 3.

SQ run number	Objective Function Value	mass number				stiffness number		
		0	1	2	3	1	2	3
1	0.478	0.945	1.239	1.009	1.092	1.067	1.035	0.85
2	0.519	1.014	1.078	0.986	1.033	0.985	0.839	0.935
3	0.303	0.911	1.104	1.105	1.102	0.986	0.753	1.08
4	0.809	0.989	1.012	1.05	0.984	0.999	0.946	1.032
5	0.857	0.885	1.262	1.074	0.823	0.848	1.254	0.804
6	0.909	1.002	0.994	1.001	1.008	1.007	0.996	0.997
7	0.806	0.999	1.032	0.957	1.015	1.034	1.002	0.982
8	0.305	0.918	1.297	1.293	1.21	0.913	0.992	0.982
9	0.351	0.761	1.237	0.992	1.134	0.838	0.7	0.801
10	0.641	0.948	1.075	1.058	1.064	1.055	0.997	1.1
$\mathcal{M}$	0.598	0.937	1.133	1.052	1.047	0.973	0.951	0.956
$\sigma$	0.023	0.072	0.108	0.091	0.098	0.077	0.149	0.102

deviation is regarded as the parameter that is changed in the experiment. The focus is on identification here, not on quantification. Since the effect of changing parameters other than the parameter modified in the experiment has a positive influence on the objective function value, the real parameter change is underestimated. This can be seen in the mean parameter values: Except for  $m_0$ , all masses are increased and all stiffness parameters are decreased. A closer look at the parameters reveals that the objective function is low (say, below 0.5 in runs number 1,3,8 and 9), if the mass  $m_1$  is high. Furthermore, the mean value of  $m_1$  reveals the biggest deviation from 1.0, indicating this parameter to be the place with an additional mass. Starting Sequential Quadratic Programming from this point results in a final objective function value of 0.167 with a parameter vector of  $\theta^* = [0.991, 1.170, 1.076, 0.960, 0.955, 1.015, 0.952]^T$ , with  $m_1 = 1.17$  being fairly close to the real mass increase (18%). Looking at runs 3 and 9 in Table 4.7, the impression that stiffness number 2 is the parameter to be changed might appear, but the parameter has minor influence on the objective function value (compare runs 1 and 8) and its mean value is 0.951. This disproves the impression.

## 4. Concept Validation for Parameter Identification

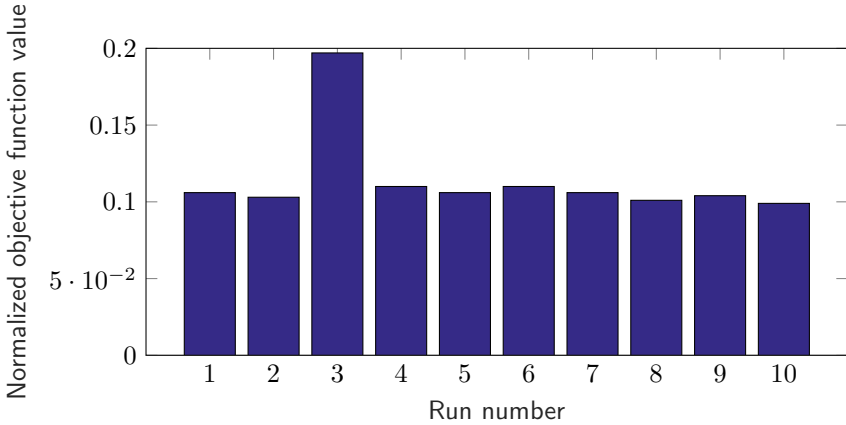


Figure 4.7.: Final objective function values after running the model updating algorithm using  $\rho^s$  for state 3.

### Parameter identification based on frequency domain data

For updating the model based on frequency domain data, the steps from the previous section are repeated using the metric  $\rho^s$  (see equation (2.26)) for comparison of model and measurement with the same constraints as in (4.11). The results for adjusting the model to baseline condition are listed in Table 4.6. In contrast to the previous section, no averaging is done, because it does not yield significant improvements in this example. Within this analysis, a single optimization run consisting of running Simulated Quenching and Sequential Quadratic Programming is performed for each of the nine measurement sets available in the database for state 3, resulting in nine runs. The vector with the lowest objective function value (run number 6) is chosen as the baseline condition, and the masses and stiffnesses of the model are adjusted accordingly for the following analyses. Again, the differences from the initial model are quite high (mass 1 is reduced by 13%), but this analysis focuses on finding a model that represents the spectral density as good as possible. Subsequently, the model previously being updated to baseline condition is updated to state 3. The results of this analysis are illustrated in Table 4.7. For state number 3, 10 data sets are available in the LANL database, resulting in ten optimization runs. The final objective function values are similar to the objective function value of baseline condition, indicating that the change in the system is detected and the model is adjusted accordingly. The remaining objective function value of 10% of the initial value is caused by measurement imperfections and mod-

Table 4.6.: Normalized minimal objective function values and according parameters for ten Simulated Quenching and subsequent Sequential Quadratic Programming runs, using  $\rho^s$  to identify baseline condition.

Run number	Objective Function Value	mass number			stiffness number			
		0	1	2	3	1	2	3
1	0.621	0.946	1.193	0.662	1.701	1.003	0.886	1.259
2	0.635	1.102	1.438	0.562	0.562	1.452	0.562	1.6
3	0.134	0.932	0.973	0.957	0.94	1.045	1.191	0.993
4	0.129	0.875	0.895	0.968	1.05	0.956	1.134	1.075
5	0.139	0.861	0.841	0.882	0.897	0.905	1.046	0.966
6	0.11	0.869	0.871	0.924	0.98	0.943	1.087	1.023
7	0.366	0.927	0.835	0.625	1.472	1.071	0.857	0.671
8	0.237	0.939	1.067	1.011	1.527	1.16	1.251	1.17
9	0.127	0.874	0.873	0.941	1.038	0.936	1.097	1.062
$\mathcal{M}$	0.278	0.98	0.999	0.837	1.13	1.052	1.012	1.091
$\sigma$	0.202	0.221	0.192	0.161	0.342	0.16	0.2	0.236

eling errors. Again, the total mass is raised, and the total stiffness is decreased. Being the biggest change, the increase in mass number 1 is successfully detected, with a mean mass increase of 14% being close to the additional mass mounted in the experiment. Being almost twice as big, the final objective function values as illustrated in Figure 4.7 reveal the solution of run number 3 as a wrong solution. Obviously, there is another local optimum here. In run number 3, the wrong mass number 0 is raised by 16% instead of mass number 1, which is raised by only 3%. The remaining entries of the parameter vector are similar to the other runs.

### Parameter identification based on time domain data

The steps from the previous sections are repeated with  $\rho^{l^2}$  to account for an objective function formulated in time domain. The results from updating towards baseline condition are given in Table 4.8. While the use of  $\rho^{\omega+\phi}$  and  $\rho^s$  returns quite similar results, the results generated by  $\rho^{l^2}$  are different. The mean base mass is raised by a mean of 72%, while the other masses are reduced and the mean base stiffness is also raised distinctively. The standard deviations of the parameters vary from 0.15 to 0.46 which is about ten times higher than in the previous examples, making the results and the uniqueness of the solution doubtful. This may be caused by the relatively high loads acting on the structure. These induce vibrations dominated by the loads whereas the vibration behavior of the system

## 4. Concept Validation for Parameter Identification

Table 4.7.: Normalized minimal objective function values and according parameters for ten Simulated Quenching and subsequent Sequential Quadratic Programming runs, using  $\rho^s$  to identify state 3.

Run number	Objective Function Value	mass number				stiffness number		
		0	1	2	3	1	2	3
1	0.106	1.131	1.201	0.875	0.819	1.078	0.928	0.841
2	0.103	0.997	1.133	0.973	0.93	0.952	0.949	0.984
3	0.197	1.161	1.031	0.988	0.836	1.005	0.887	0.958
4	0.11	0.998	1.142	1.017	1.009	0.945	0.973	1.05
5	0.106	1.001	1.149	0.982	0.944	0.964	0.961	0.991
6	0.11	0.99	1.144	1.006	0.96	0.948	0.969	1.022
7	0.106	0.983	1.137	1.003	0.995	0.942	0.963	1.032
8	0.101	0.999	1.155	0.995	0.997	0.965	0.964	1.022
9	0.104	1.005	1.162	0.997	0.947	0.967	0.972	1.004
10	0.099	0.997	1.143	0.981	0.941	0.961	0.954	0.992
$\mathcal{M}$	0.114	1.026	1.14	0.982	0.938	0.973	0.952	0.99
$\sigma$	0.028	0.061	0.041	0.038	0.061	0.039	0.025	0.056

plays a subordinated role. Hence, the measured vibration signals contain mostly induced vibrations. Comparing power spectral densities or eigenfrequencies and mode shapes focuses more on the dynamics of the system itself instead of the overall dynamics as the direct comparison of time series does.

### Application to other system states

The previous sections discuss results of updating the numerical model to match state number 3 in detail. This section aims to give a comprehensive overview on the results of updating the model with the aim of parameter identification for all system states described in Table 4.1. Therefore, results of updating the model using three different metrics considered in this section are gathered in Figure 4.8 for comparison. If the parameter to be changed cannot be identified from the results, the solution is regarded to be wrong. If the correct parameter is changed the most, it is regarded as the correct parameter. An additional status is introduced for correct parameters that are within  $\pm 10\%$  of the change introduced in the experiment. Since it is not possible to consider the nonlinearity in a modal analysis directly, no parameter identification and hence no model updating is done in states 10 to 17 for  $\rho^{\omega+\phi}$ . In case the model is linear (states 1 to 9), the identification based on this metric delivers best results. The correct parameter is identified within  $\pm 10\%$

Table 4.8.: Normalized minimal objective function values and according parameters for ten Simulated Quenching and subsequent Sequential Quadratic Programming runs, using  $\rho^{l2}$  to identify baseline condition.

Run number	Objective Function Value	mass number				stiffness number		
		0	1	2	3	1	2	3
1	0.768	1.635	0.94	0.768	1.199	0.869	0.45	0.501
2	0.761	1.553	0.899	0.484	1.537	1.351	0.748	0.481
3	0.756	1.933	0.958	0.961	1.145	1.042	0.519	1.354
4	0.815	1.913	0.406	0.762	0.909	1.507	1.287	1.459
5	0.758	1.835	1.199	0.401	0.908	1.564	0.665	0.512
6	0.796	1.821	0.426	0.743	0.576	1.099	1.015	1.318
7	0.746	1.773	1.125	1.331	1.522	1.143	0.406	1.024
8	0.741	1.597	1.238	0.655	0.523	1.25	0.572	1.849
9	0.767	1.494	1.249	1.352	0.448	1.093	0.821	0.962
$\mathcal{M}$	0.768	1.728	0.938	0.829	0.974	1.213	0.72	1.051
$\sigma$	0.022	0.153	0.305	0.315	0.386	0.213	0.27	0.459

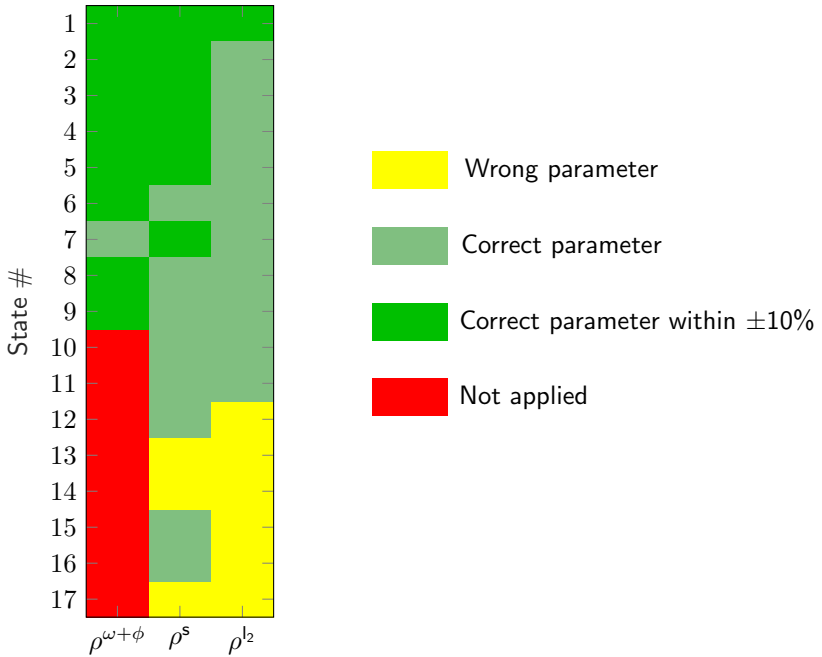


Figure 4.8.: Overview on the success of different metrics for model updating at the frame structure.

## 4. Concept Validation for Parameter Identification

in all states except state 7. In this state, the parameter deviation is 10.5% and hence only slightly outside the 10%-window considered a good identification. In case  $\rho^{l^2}$  is used, parameter identification works to a certain degree. Although mass 0 is estimated to be more than 70% bigger than it should be in baseline condition, only the parameter that needs to be changed is identified in most examples. With smaller gaps or combinations of added masses and smaller gaps, the parameters are not estimated correctly, or results become non-unique. Best results are achieved, if  $\rho^s$  is employed for parameter identification. Model updating using this metric yields correct parameter estimations for most of the linear cases. The algorithm successfully identifies the correct elements as long as the gap is wide and hence the influence of the nonlinearity is small. The algorithm fails to identify correct parameters with growing influence of nonlinearities (state 13, 14 and 17). This is assumed to be caused by imprecise modeling of the nonlinearity. An improvement of the approach used in this analysis<sup>3</sup> (see equation (4.10)) would be to use a more advanced modeling approach for the contact of the nonlinearity. This is expected to improve the functionality of using  $\rho^{l^2}$ , too.

### 4.2. Ice accretion at a full-scale rotor blade

This section demonstrates the functionality of the model updating methodology at the example of a full-scale structure, using a 34.2m long rotor blade that is tested in a rotor blade test rig in Bremerhaven, Germany. In cold environments, ice may be accumulated along the rotor blade starting from the blade tip (see Figure 4.9). This behavior is typical, caused by the high speed at the blade tip due to the angular motion of the rotor. The added masses cause mass imbalances and hence additional structural loads that may not be considered during the design process of the turbine. If the ice masses get too big, pieces with masses up to several kilograms may be thrown off the blade due to the angular movement of the rotor, causing danger within the surroundings of turbines [150]. A detailed description of the blade test is given in [163]. The classical objective function employing modal properties ( $\rho^{\omega+\phi}$ ) is employed and compared to a new metric based on transmissibility functions ( $\rho^\tau$ ) throughout this section for quantification of the deviation between measurement and simulation data. In contrast to the approaches presented in [163] that detect if ice is present on the blade, the focus of this section is on ice mass localization and quantification.

---

<sup>3</sup>Adding stiffness if there is contact is a linearization for two different system states.



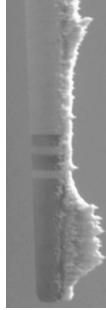


Figure 4.9.: Heavy icing at a wind turbine rotor blade [150].

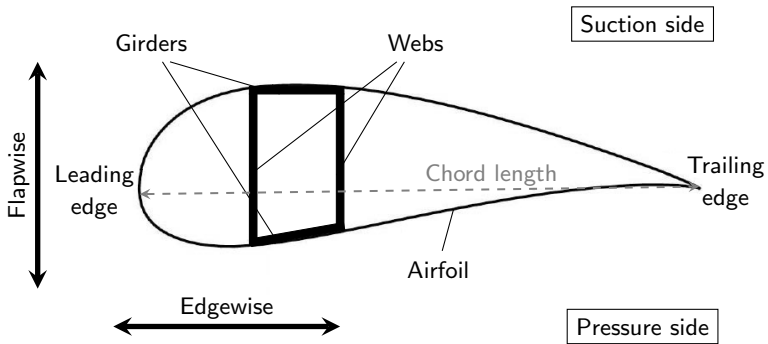


Figure 4.10.: Nomenclature at a cross-section of a wind turbine rotor blade.

### 4.2.1. Experimental set up of the rotor blade test

The rotor blade (see Figure 4.11) is made from glass fiber composite. Six sensors are mounted along the rotor blade to account for its dynamic behavior, each measuring in edgewise and flapwise direction. The measurement setup comprises two geophones measuring vibration velocities and four accelerometers (see Table 4.9 and Figure 4.12). Incoming velocity signals are derived with respect to time, yielding a total of twelve acceleration signals. All sensors are mounted along the web toward the trailing edge (see Figure 4.10) of the blade and operated with a sampling frequency of  $100\text{Hz}$ . Three sensors being close to the tip of the blade are mounted on the outside of the blade because these sections are not accessible from the inside due to the blade geometry. The dynamic behavior of the blade is investigated for different states. After the initial recording of the unmodified blade, ice

#### 4. Concept Validation for Parameter Identification



Figure 4.11.: Rotor blade installed in test rig. Load frame connected to blade at 17.5m from blade root [163].

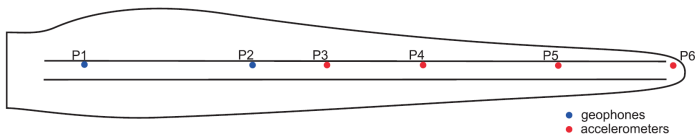


Figure 4.12.: Sensor positions on rotor blade [163].

Table 4.9.: Positions of geophones and accelerometers on rotor blade.

Sensor position	P1	P2	P3	P4	P5	P6
Distance from root in m	3.7	12	15.5	20.5	27.4	34.2
Measured quantity	Vel.	Vel.	Acc.	Acc.	Acc.	Acc.
Location	In	In	In	Out	Out	Out

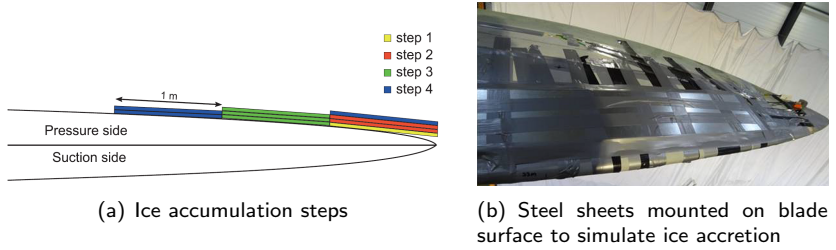


Figure 4.13.: Ice accretion steps and installation of additional masses for simulation of ice accretion [163].

accretion is simulated using steel plates added to the structure in four steps (see Figure 4.13). Copying the behavior of natural ice accretion, ice is accumulated in a pseudo-triangular shape, starting from the blade tip at the leading edge and on the pressure side. Each added plate has a mass of  $4.8\text{kg}$ , summing up to a total mass of  $43.2\text{kg}$  in step four. This accounts to  $0.9\%$  of the total blade mass.

The structure is excited using a load frame (see Figure 4.11), hand excitation of the first eigenmodes and impulse hammer excitations at different locations. The analysis presented here focuses on flapwise hammer excitations at a position  $33\text{m}$  from the blade root.

#### 4.2.2. Numerical model of the blade

Due to confidentiality reasons, only the bending stiffnesses and chord lengths of the rotor blade are given at certain points along the blade. Furthermore, all information concerning the blade geometry is normalized throughout this section. Based on this information, a beam model is built with boxed cross-sectional properties. This assumption is valid, because the load transport in a blade is done by the girders and webs to a large extent, whereas the shape of the airfoil is designed for optimum aerodynamic performance. The moment of inertia of such a box frame is given as

$$I_1 = \frac{bh^3}{12}; I_2 = \frac{hb^3}{12}. \quad (4.12)$$

Table 4.10.: Normalized geometry properties of the blade and the according numerical model.

z in m	Mass in kg	$EI_1$ in kNm <sup>2</sup>	$EI_2$ in kNm <sup>2</sup>	Width in m	Height in m	Element- number	Element height in m	Element width in m	Element Volume in m <sup>3</sup>	Element Density in $\frac{\text{kg}}{\text{m}^3}$
0	100	100	100	0.8308	0.8308					
1	84.634	40.5766	38.3307	0.6491	0.6678	1	0.7399	0.7493	0.4158	36.9534
2	77.5666	36.7961	32.4351	0.6172	0.6573	2	0.6331	0.6626	0.4195	16.8477
3	71.4629	34.0757	23.9610	0.5562	0.6633	3	0.5867	0.6603	0.3874	15.7553
3.7	66.734	27.0690	15.3402	0.4843	0.6433	4	0.5203	0.6533	0.3399	13.9125
5	62.8638	29.2558	12.8557	0.4489	0.6771	5	0.4666	0.6602	0.3081	12.5626
7	59.0794	23.5947	11.3768	0.4405	0.6343	6	0.4447	0.6557	0.2916	12.9793
8	51.7884	22.4487	8.3646	0.3949	0.6470	7	0.4177	0.6406	0.5352	13.6237
9	48.251	19.9728	7.1466	0.3778	0.6315	8	0.3863	0.6392	0.2470	14.3233
11	41.6142	14.9143	5.1062	0.3454	0.5903	9	0.3616	0.6109	0.4418	15.0221
14.5	31.1235	8.8988	2.8647	0.2966	0.5228	10	0.3210	0.5566	0.6253	16.7758
17	24.4396	5.9703	1.8091	0.2624	0.4768	11	0.2795	0.4998	0.3493	19.1356
18	21.9756	4.9341	1.4519	0.2475	0.4562	12	0.2550	0.4665	0.1189	20.7154
19.75	18.0504	3.4863	0.9926	0.2241	0.4200	13	0.2358	0.4381	0.1808	21.7094
20.5	15.506	2.7124	0.7442	0.2076	0.3963	14	0.2159	0.4082	0.1101	23.1028
22	13.6122	2.2192	0.5984	0.1961	0.3777	15	0.2019	0.3870	0.0781	24.2392
24	10.2369	1.402	0.3703	0.1735	0.3376	16	0.1848	0.3577	0.1322	25.5269
25	8.7336	1.0815	0.2881	0.1631	0.3161	17	0.1683	0.3269	0.0550	27.3233
26	7.3451	0.8002	0.2194	0.1530	0.2921	18	0.1581	0.3041	0.0481	28.8889
27.4	6.0646	0.6782	0.1669	0.1409	0.2841	19	0.1470	0.2881	0.0423	30.2486
28	4.8852	0.5705	0.1240	0.1288	0.2763	20	0.1349	0.2802	0.0378	31.2057
29	3.8062	0.4721	0.0905	0.1172	0.2677	21	0.1230	0.2720	0.0335	32.2500
30	2.8469	0.3884	0.0652	0.1062	0.2592	22	0.1117	0.2635	0.0294	32.5896
31	1.9818	0.3155	0.0454	0.0952	0.2509	23	0.1007	0.2551	0.0257	33.6832
32	1.2096	0.2514	0.0320	0.0859	0.2407	24	0.0905	0.2458	0.0223	34.7012
33	0.5366	0.1944	0.0218	0.0767	0.2293	25	0.0813	0.2350	0.0191	35.2095
34.2	0	0.003	0.0002	0.0228	0.0853	26	0.0498	0.1573	0.0098	54.8067

## 4.2. Ice accretion at a full-scale rotor blade

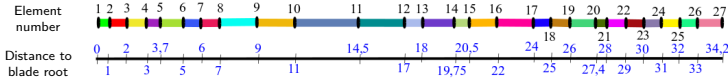


Figure 4.14.: Discretization of the model according to blade construction plans.

Rearranging these equations yields

$$h = \frac{12I_2}{b^3}; b = \sqrt[8]{\frac{12^2 I_2^3}{I_1}}. \quad (4.13)$$

With the information on the geometry (see Table 4.10 and Figure 4.14), a model of the blade is created using 26 linear two-node Timoshenko beam elements using the engineering software Ansys APDL. The mass of each element is known (see Table 4.10). Hence, the material density of each element needed to set up a numerical model can be computed using the geometry information. Since the cross-sectional properties do not coincide with the real blade, these densities vary and are not in a realistic range, only the overall mass of the element is considered to be decisive for the global dynamic behavior. The structure is assumed to be clamped at the base. Damping is considered using material damping. The damping is adjusted to the measured time series, yielding a damping of 10%. A signal of sensor P6 under impulse load at 33m from the blade root in flapwise direction is drawn in Figure 4.15. The according power spectral density is illustrated in Figure 4.16. This load is also the load that is considered in the updating process. This plot reveals the flapwise eigenfrequencies of the structure around 3.1Hz, 6.6Hz and 11.5Hz. Data-driven Stochastic Subspace Identification is used to identify eigenfrequencies and mode shapes needed for model updating from the measured signals. In addition to those frequencies visible in Figure 4.16, the identification locates another eigenmode at 1.069Hz. Furthermore, edgewise eigenmodes are identified at 1.679, 5.643 and 13.140Hz. The numerical model coincides with these identified results (see Table 4.11), regardless of the limited information available to formulate the numerical model.

Although there is good coincidence between measured data and numerical model, the model is updated to achieve maximum agreement between numerical model and measured data in baseline condition prior to using the algorithm for ice accretion. The optimization problem for updating the model to baseline condition is

#### 4. Concept Validation for Parameter Identification

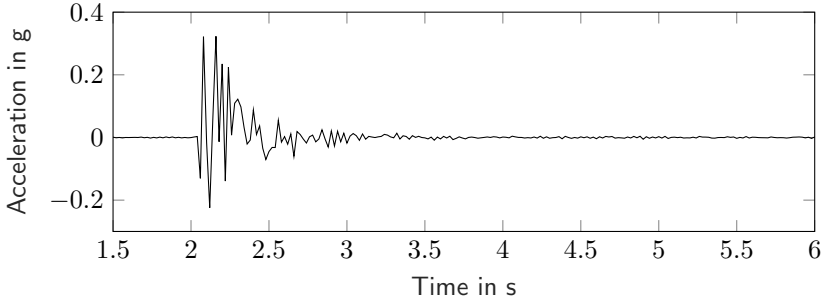


Figure 4.15.: Time series of sensor P6 (flapwise) after impulse load at 33m of the blade.

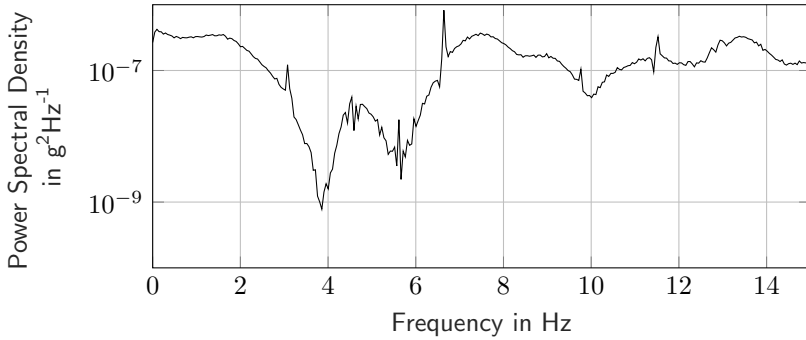


Figure 4.16.: Power spectral density of sensor P6 in flapwise direction after impulse load at 33m of the blade.

Table 4.11.: Comparison of rotor blade eigenfrequencies and mode shapes identified from measurement data and simulation model prior and after updating.

	$\omega_m$ in Hz	$\omega_s$ in Hz	$\pm$ in %	$\omega_s^u$ in Hz	$\pm$ in %	Dir.	MAC	MAC <sup>u</sup>
1.	1.069	1.109	3.6	1.048	2.0	flap	0.99957	0.99895
2.	1.679	1.829	8.2	1.726	2.7	edge	0.99618	0.99747
3.	3.113	3.186	2.3	3.128	0.5	flap	0.99558	0.99731
4.	5.643	5.497	3.1	5.390	4.5	edge	0.99515	0.99727
5.	6.644	6.923	4.0	6.811	2.5	flap	0.99674	0.99847
6.	11.536	12.412	7.1	11.999	3.9	flap	0.99198	0.99712
7.	13.140	12.635	3.8	12.383	5.8	edge	0.98728	0.99118
$\mathcal{M}$			4.58		3.12		0.99478	0.99682

u=updated

$$\min_{\theta} \rho^{\omega+\phi}(\theta) \quad (4.14a)$$

$$\text{subject to } \theta_i \geq 0.85 \forall i \in [1\dots n] \quad (4.14b)$$

$$\theta_i \leq 1.15 \forall i \in [1\dots n]. \quad (4.14c)$$

Since both masses and stiffnesses may slightly vary, both quantities are added to the set of parameters. Hence,  $\theta$  contains 26 parameters that modify the stiffnesses and masses<sup>4</sup> of each section as illustrated in Figure 4.17 in the numerical model. Table 4.11 reveals that the mean deviation of eigenfrequencies is reduced to 3% whereas the values of the modal assurance criterion are raised, meaning that the updated model builds a better representation of the measured signals than the initial one. Since the initial model is a quite good representation of the eigensystem identified from the measured data, the accordance can only be raised marginally. The updating process is always a trade-off, the deviation of some frequencies after updating may be bigger than in the initial model (see Table 4.11, eigenmodes 4 and 7). The parameters of the updated model are listed in Table 4.12, revealing small deviations of eigenfrequencies and mode shapes.

The model is still erroneous. These errors may be caused by several reasons, compare section 1.1: errors in the modeling approach (model inadequacy), errors in the modeling assumptions or parameter uncertainty (since only cross-sectional and mass properties of the blade are known, the information on the blade geometry is limited), errors in the evaluation of the time series and observation errors. The summation of all error sources is quantified by the metrics used to compare numerical model and measurement data ( $\rho$ ). Limited information on the error sources makes a differentiation between these errors hard or even impossible. As mentioned in section 1.1, model updating influences the parameter uncertainties, all other uncertainties remain untouched and are within the responsibility of the executive engineer. These uncertainties are the reason why the metrics can never be reduced to zero by model updating in practical environments. In case no damages occur, these uncertainties may be considered to remain constant. If structural changes (such as damages) occur, these damages may increase the modeling error due to the imprecise consideration of these alterations, for instance, using modified stiffnesses of elements as done within this thesis. This can usually be seen in objective function values being higher after the algorithm is applied to damage localization than if employed to estimate parameters of baseline condition.

---

<sup>4</sup>The stiffness is altered using Young's modulus and the masses using the material density of the elements

## 4. Concept Validation for Parameter Identification

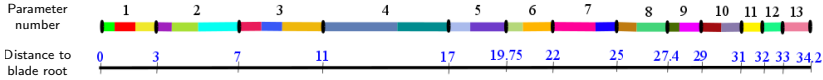


Figure 4.17.: Parameterization of the blade model according to blade construction plans and discretization.

Table 4.12.: Parameters after updating the numerical model to measured properties, using  $\rho^{\omega+\phi}$  as objective function.

	Section												
	1	2	3	4	5	6	7	8	9	10	11	12	13
Young's mod.	0.854	0.908	0.856	0.927	0.937	1.120	1.127	1.008	0.991	1.059	1.075	1.042	1.024
Density	1.038	0.998	1.040	0.862	0.992	0.915	0.952	1.035	1.008	1.018	0.998	1.123	1.146

### 4.2.3. Model updating for ice detection and quantification

#### Updating using modal properties

To reduce the number of parameters for model updating, several beam elements are grouped as illustrated in Figure 4.17. It is known that ice accretion initiates at the blade tip. Therefore, the parameterization is refined in the area close to the tip. In this study, the parameters modify the densities of elements in order to account for changes in the mass of the sections. The optimization problem solved to localize ice assembles to

$$\min_{\theta} \rho^{\omega+\phi}(\theta) \quad (4.15a)$$

$$\text{subject to } \theta_i \geq 0.99 \forall i \in [1...n] \quad (4.15b)$$

$$\theta_i \leq 1.75 \forall i \in [1...n]. \quad (4.15c)$$

A small decrease of 1% is allowed for numerical reasons for each parameter. The maximum increase is constrained to 75%. The analysis of each ice step consists of 10 optimization runs. In the first step, a mass of  $4.8kg$  is attached to the tip of the blade. Adaptive reduction of the parameter set is applied after running Simulated Quenching. Thus, many parameters are set to 1.0 in the results (see Table 4.13).



Table 4.13.: Results of ten runs, using Simulated Quenching and Sequential Quadratic Programming adaptively, employing  $\rho^{\omega+\phi}$  as objective function for investigation of ice step 1. Objective function values are normalized to the initial values.

SQP run number	$\rho^{\omega+\phi}$	Parameter												
		1	2	3	4	5	6	7	8	9	10	11	12	13
1	0.0304	1.024	1.049	0.999	1.00	1.00	1.00	1.00	1.00	1.00	1.00	1.00	1.00	1.00
2	0.0305	1.014	1.031	1.010	1.00	1.00	1.00	1.00	1.00	1.00	1.00	1.00	1.00	1.00
3	0.0300	1.00	1.00	1.00	1.00	1.00	1.00	1.00	1.00	1.00	1.00	1.00	1.047	1.053
4	0.0305	1.00	1.00	1.00	1.00	1.00	1.00	1.00	1.00	1.00	1.018	1.045	0.995	1.00
5	0.0305	1.00	1.00	1.00	1.00	1.00	1.00	0.990	1.013	0.999	1.00	1.00	1.00	1.00
6	0.0300	1.00	1.00	1.00	1.00	1.00	1.00	1.00	1.00	1.00	1.00	1.00	1.047	1.053
7	0.0300	1.00	1.00	1.00	1.00	1.00	1.00	1.00	1.00	1.00	1.00	0.993	1.038	1.065
8	0.0305	1.056	1.012	1.00	1.00	1.00	1.00	1.00	1.00	1.00	1.00	1.00	1.00	1.00
9	0.0301	1.00	1.00	1.00	1.00	1.00	1.00	1.00	1.00	1.00	1.00	0.994	1.075	1.120
10	0.0306	1.00	1.00	1.00	1.00	1.00	1.00	1.00	1.00	1.020	1.028	1.012	1.00	1.00

## 4. Concept Validation for Parameter Identification

In order to illustrate the results comprehensively, the vector parameter  $\psi$  is introduced, averaging the mean deviation of the parameters from the initial value 1.0 for all optimization runs.

$$\psi_i = \frac{|\mathcal{M}_{\mathbf{p}_i} - 1|}{\max(\psi)}, \quad (4.16)$$

where  $\mathbf{p}_i$  denotes the vector of parameter  $i$  in all optimum solutions. This vector parameter is useful to illustrate results from the parameter tables comprehensively, but interpretation is also possible without this parameter. However, it is applied to some examples presented in this thesis. The according values for  $\psi$  of ice steps 1 to 4 are illustrated in Figure 4.18. The plot reveals a clear location of added masses in parameters 12 and 13, which represents the blade tip. In ice sets 1 and 3,  $\psi$  is also raised in the root section of the blade (parameter number 1 and 2), caused by single solutions that locate the additional mass here (compare Table 4.13, runs number 1,2 and 8). Quantification of additional masses provides useful information for turbine operators regarding possible shutdowns of wind turbines due to critical icing conditions. The parameter vectors generated using model updating are used to quantify the added mass. The masses added in the experiment are contrasted with the averaged masses determined using model updating in Figure 4.19. Both the added masses of the experiment and the masses identified using model updating reveal a behavior close to linearity within the range considered. The identified masses overestimate the masses added during the experiment by the factor two to three. However, this linear relationship may be used to estimate the real mass growth on the structure with a correction factor. This factor must be adjusted with big care.

### Updating using transmissibility functions

As introduced in equation (2.31), measurement data and numerical model may also be compared using transmissibility functions. The following section shows the application of model updating using transmissibility functions to the rotor blade and ice detection. Starting from the tip, transmissibility functions are built for all possible measurement combinations towards the root of the blade (see Figure 4.20). For the six measurement sensors, this results in a total of 30 transmissibility functions, 15 flapwise and 15 edgewise. Although model updating using transmissibility functions is successful theoretically (see [158] and Section 5.2), it is not successful for the localization of additional masses. Results for the different ice steps applied to the structure even locate the additional mass in different elements. In ice step 1, the mass is located in element 2, step 2 locates it in element 12, step 3 in 11 and

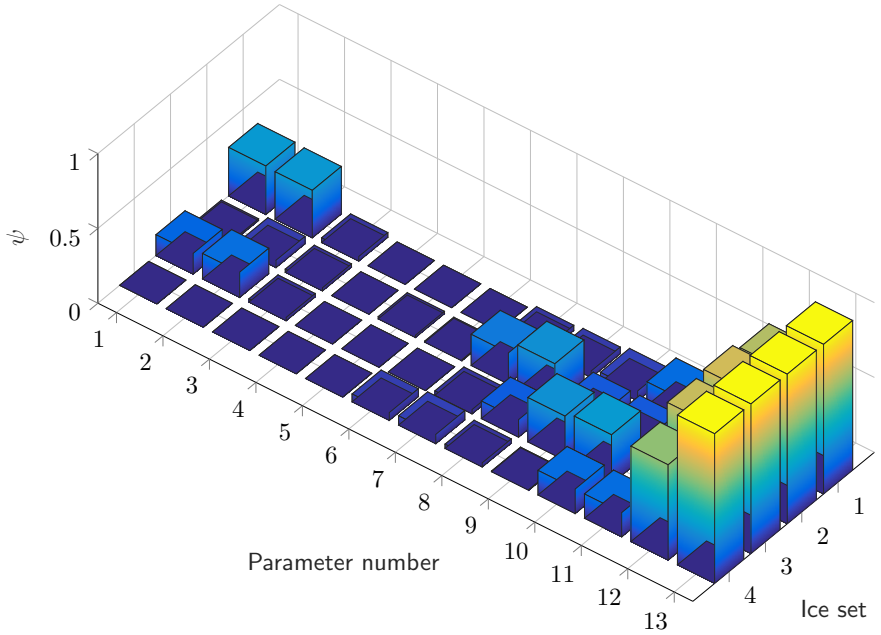


Figure 4.18.: Overview of the vector parameter  $\psi$  for all four ice steps using  $\rho^{\omega+\phi}$ .

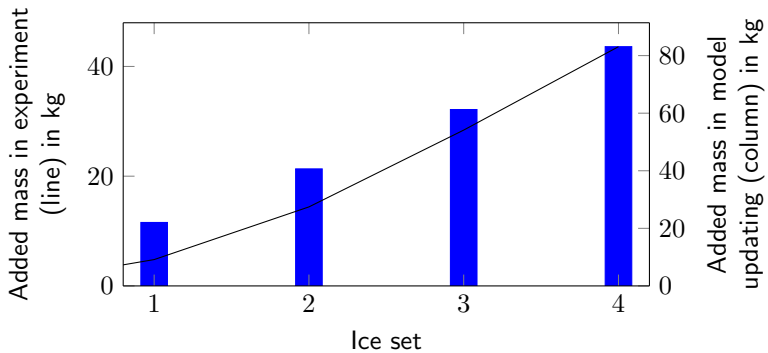


Figure 4.19.: Comparison of added masses during experiment and average additional mass determined using model updating.

## 4. Concept Validation for Parameter Identification

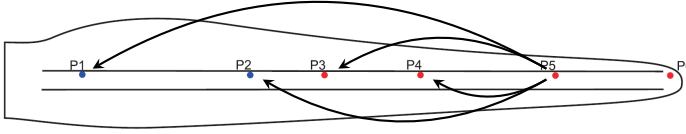


Figure 4.20.: Combination of transmissibility functions starting from measurement point five. To capture all possible combinations,  $\sum_i^{n-1} i$  transmissibility functions are computed, with  $n$  being the number of sensors. Since two channels are measured for each sensor, the number of transmissibility functions is doubled.

4 in 10. Transmissibility functions are formulated using time series that are transferred to the frequency domain using Welch's method, see section 2.2.2. Hence, transient analysis is needed to evaluate these metrics. Especially the damping plays a substantial role in these analyses. Since the damping of this structure is not known precisely, it is modeled using material damping, which is an approach probably being too simple to capture the real damping behavior.

### 4.3. Conclusion

This section investigates the functionality of the algorithm for practical examples. The first example is a laboratory model of a three-story frame structure being excited by random noise. While model updating using modal domain data is successful in linear cases, it is not possible to include nonlinearities to this approach. If  $\rho^s$  is used as objective function, model updating is successful for both linear and nonlinear cases, although the parameter estimation is not as exact as when using  $\rho^{\omega+\phi}$ . If the effect of nonlinearity is getting stronger, even the frequency domain approach is struggling to approximate parameters correctly. This may be caused by inaccurate modeling of the nonlinearity in this model. Surprisingly, updating using  $\rho^{l^2}$  does not perform as good as using  $\rho^s$ . The parameters are not identified as exactly, and the identification does not show good results if nonlinearity is added to the system. Any structural response is the result of loads acting on the structure in combination with the mechanical system. If loads are too big, the influence of the system may be small and cannot be seen in measured time series easily. Both modal and power spectral density approaches focus on the dynamic system itself, leading to changes in the system being recognizable more easily.

The second example adopts the algorithm to the investigation of ice accretion at a real scaled, 34m long rotor blade. Both  $\rho^{\omega+\phi}$  and  $\rho^\tau$  are employed for comparison of model and measurement to test the new metric  $\rho^\tau$  and compare it to a conventional metric. Model updating using modal properties is successful for added masses, locating them at the tip of the blade, exactly where masses are fixed during testing. Though the masses added during the experiment are drastically overestimated, there seems to be a linear relationship between the mass added in experiment and identified by model updating. Hence, the results may be used to quantify ice accretion, being an important tool for wind turbine operators for decisions on shutdowns due to ice. Results presented here are valid for the investigated blade only and small masses. It has to be checked if linear scaling of the masses estimated using model updating is still valid for bigger masses accreting on the blade. An online application of the algorithm is feasible, although each run takes several hours. A possible implementation of an online system could be the real-time ice detection using the approach presented in [163]. If ice is detected, this could be quantified within a few hours using the methodology presented within this chapter. The successful application of the algorithm for parameter identification is presented in this chapter. Since damage localization demands a different interpretation of model updating and its results, the application of model updating to damage localization is demonstrated in the next chapter.



# 5. Concept Validation for Damage Localization

In this chapter, the application of finite element model updating for damage localization is presented using three examples. It starts with the demonstration of the methodology at a scaled model of a tripile-structure, a foundation type used for offshore wind turbines. Since measurement data for different damage severities are available, the sensitivity of the method to different damage severities is investigated using this example. The subsequent section illustrates the application of damage localization to the full-scale rotor blade introduced in chapter 4. Difficulties and possible reasons for the malfunction of model updating algorithms and vibration-based structural health monitoring are illustrated and discussed using this example. The chapter closes with the application of model updating to a model of a prestressed concrete tower, a new manufacturing concept for wind turbine towers aiming to reach higher nacelle heights with reduced costs.

## 5.1. Damage localization at a scaled tripile model

A geometrically scaled model of a tripile structure (see Figure 5.1(a)) is used to investigate the damage localization capabilities of the model updating approach at offshore wind turbine support structures. In this section, the metrics  $\rho^{\omega+\phi}$ ,  $\rho^{l^2}$  and  $\rho^s$  are used as objective functions to quantify the deviation between model and measurement. After an initial updating of the model to the undamaged configuration, the model is updated to locate the damaged area. Results from this section are partially presented in [147], supplemented by the use of  $\rho^s$  and a sensitivity analysis.

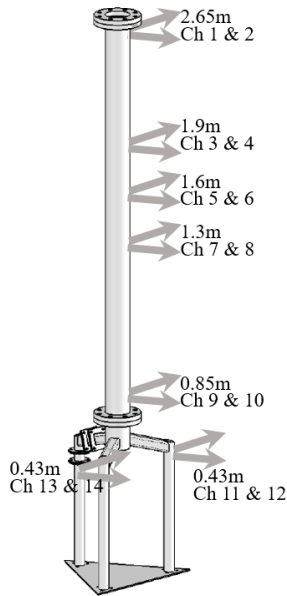
### 5.1.1. Experimental set up and numerical modeling of the tripile

The investigated structure (see Figure 5.1(a)) comprises a tower that is based on a tripile structure. The tripile consists of three legs. In real offshore environments, these piles are driven into the soil [143]. In the considered structure, the piles are represented by tubes welded on a steel plate. These three tubes are connected by square tubes which are called the braces. A head mass is installed on top of the tower to emulate inertial effects of the rotor nacelle assembly. The structure has a total height of  $2.65m$ , the tower has an outer diameter of  $114mm$  and a wall thickness of  $3.2mm$ , whereas the vertical legs have an outer diameter of  $48.3mm$  and a wall thickness of  $3.2mm$ . The braces provide cross-sectional properties of a square tube with a wall thickness of  $3.0mm$  and a lateral length of  $50mm$ . A mass of  $150kg$  is attached to the top to emulate the translational inertia of the rotor-nacelle assembly. One leg is equipped with flanges to enable reversible damage to specific parts of the structure (see Figure 5.1(a)). The structure is excited using an impulse hammer at the height of  $2m$  for excitation of at least both the first and second eigenmode simultaneously, resulting in a free decay of the system. This procedure is widely used practice in analyses of dynamic structures, degenerating the structural response to a stationary system, no forces are acting on the system during the transient decay. With this type of response, it may be compared to an idling wind turbine in calm environmental conditions (e.g., zero velocity wind and no waves) or a bridge after excitation by a wind gust, a train or a truck crossing.

The vibration of the structure is measured using seven triaxial 3g-accelerometers, five attached to the tower, one to an undamaged leg and one to the damaged leg. Vibrations in vertical directions are small. Hence only the horizontal acceleration signals are recorded. Signals are recorded with a sampling frequency of  $600Hz$ . Damage is imposed as a gradually increased saw cut in one of the braces (see Figure 5.1(b) and Table 5.1). Resulting eigenfrequencies of the structure for a cutting depth for damage step 7 are drawn in Table 5.2. The first dominant side-side eigenmode is neglected because it cannot be obtained from the measured signals repeatedly. It is not excited with sufficient energy. The second eigenmode is considered in both dominantly fore-aft and side-side direction. Higher eigenmodes are not considered since they are not excited with enough energy and the limited measurement set up is designed to capture the lower eigenmodes. Especially the third eigenmode has a deflection close to zero at the excitation area. Hence, it is challenging to excite this mode using an impulse at this location. The same is valid for higher eigenmodes. Consequently, the third and higher eigenmodes are omitted. Modal properties of the structure are derived from the measurement



## 5.1. Damage localization at a scaled tripile model



(a) Design drawing of the tripile model with sensor locations



(b) Damage imposed to one of the braces

Figure 5.1.: Overview of sensor locations and saw cut induced to the tripile model.

data using Frequency Domain Decomposition [24].

The corresponding numerical model consists of ten Timoshenko beam elements, where elements one to three denote the vertical piles of the tripile, elements four to six represent the braces and the remaining elements are used to model the tower (see Figure 5.2(a)). Since the welding of the tubes seems to have minor influence regarding clamping conditions (compare Figure 5.2(c)), all three legs are modeled to be connected to the ground by fixed bearings. This rather simple model is found to be sufficient to reproduce the lower eigenmodes identified from measured data. The load is modeled by a short-term force acting on the structure. Prior to the analysis, the magnitude of this load is modified to cause the same initial acceleration as in the measured time series. This model is then updated to match the eigenfrequencies and mode shapes (see Table 5.2 and Figure 5.2(b) and (c)) of the damaged tripile using the adaptive model updating algorithm described in section 2.3.3. Element number four represents the area where the saw cut is applied (see Figure 5.1(b)). Hence, the stiffness of this element should be reduced. Each

## 5. Concept Validation for Damage Localization

Table 5.1.: Overview on investigated damage steps.

Damage step	Cutting depth in mm
1	4.4
2	10.4
3	18.9
4	29.1
5	37.6
6	43.6
7	45.5

Table 5.2.: Comparison of undamaged and damaged (step 7) eigenfrequencies of the tripile model. (FA=Fore-Aft; SS=Side-Side Eigenmode w.r.t. the excitation direction)

	undamaged	damaged	Deviation in %
1 <sup>st</sup>	3.00	2.31	29.8
2 <sup>nd</sup> FA	31.81	31.45	1.14
2 <sup>nd</sup> SS	31.87	31.52	1.11

stiffness parameter modifies both Young's and shear modulus simultaneously, to account for the full stiffness of the element.

### 5.1.2. Damage localization at the tripile

Table 5.3 provides an overview of the results of ten Simulated Quenching runs using  $\rho^{\omega+\phi}$ . The damaged area is covered by element number four. The Simulated Quenching algorithm indicates the correct solution in five runs. In two runs, damage is located in element five, which is another brace, and in one run, damage is located in the other brace (element six). Tower sections have the lowest stiffness value in two runs. In case damage is localized in one of the braces by Simulated Quenching, only the affected legs are considered to be variable in the adaptive Sequential Quadratic Programming runs, according to the adaptive strategy introduced in section 2.3.3. Every other constellation would not be reasonable because adjacent elements belong to another assembly. Hence, the Sequential Quadratic Programming algorithm is started with only two parameters in this case. The resulting objective function values are illustrated in Figure 5.3. In all 'wrong' cases (runs number 2,3,4,5 and 9), the correct element (element number four is the el-

## 5.1. Damage localization at a scaled tripile model

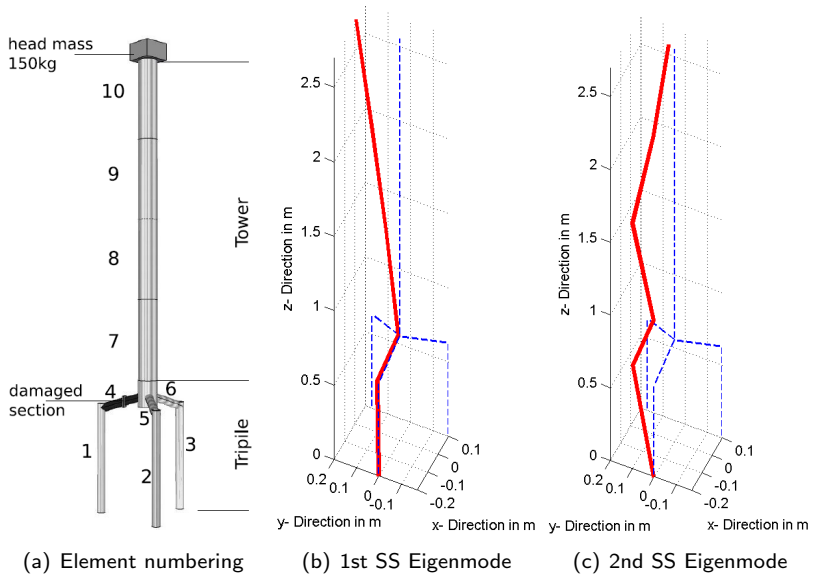


Figure 5.2.: Element numbering of the investigated tripile structure and illustration of two eigenmodes. For graphical reasons, only the damaged leg is plotted here (the deformed mode shapes are drawn in red).

## 5. Concept Validation for Damage Localization

Table 5.3.: Resulting minimal objective function values and corresponding stiffness parameters from ten Simulated Quenching runs using  $\rho^{\omega+\phi}$  at the triple model for damage step 7.

SQ run number	Objective Function Value	element number									
		1	2	3	4	5	6	7	8	9	10
1	0.8334	0.944	0.985	1.001	0.942	0.944	0.972	1.004	0.957	0.968	0.993
2	0.8482	0.937	0.999	0.984	0.946	0.946	0.927	0.970	0.985	0.963	1.006
3	0.8829	0.986	0.984	0.985	0.969	0.968	0.989	0.983	0.967	0.986	1.008
4	0.8295	0.965	1.000	0.988	0.974	0.912	0.989	0.963	1.005	0.979	0.952
5	0.8947	0.978	0.991	0.990	0.985	1.009	0.985	0.986	0.986	0.984	0.973
6	0.8661	0.963	0.991	0.996	0.942	0.999	0.998	1.003	0.967	0.991	0.973
7	0.8884	1.000	0.998	1.003	0.943	0.996	0.944	0.969	1.005	1.002	0.970
8	0.8780	0.958	0.984	0.978	0.931	0.994	1.002	0.987	1.001	0.974	0.959
9	0.8911	0.998	0.949	0.955	0.986	0.939	0.949	0.999	0.972	0.980	0.988
10	0.9006	1.004	1.002	1.004	0.967	0.990	0.970	0.980	0.999	1.007	1.005

Table 5.4.: Resulting minimal objective function values and corresponding stiffness parameters from Sequential Quadratic Programming runs using  $\rho^{\omega+\phi}$  at the triple model for damage step 7, starting adaptively with the results from Table 5.3.

SQP run number	Objective Function Value	element number									
		1	2	3	4	5	6	7	8	9	10
1,6,7,8,10	0.601	1.01	1.0	1.0	0.749	1.0	1.0	1.0	1.0	1.0	1.0
4,9	1.0	1.0	1.0	1.0	1.0	1.0	1.0	1.0	1.0	1.0	1.0
2	1.0	1.0	1.0	1.0	1.0	1.0	1.0	1.0	1.0	1.0	1.0
3	0.7245	1.0	1.0	1.0	1.0	1.0	1.0	0.995	0.953	0.985	1.0
5	0.7513	1.0	1.0	1.0	1.0	1.0	1.0	1.0	1.0	1.01	0.741

ement that modifies the stiffness of the area damaged in the experiment) is also lowered, indicating the sensibility of the objective function to the correct parameter. In other words, parameter 4 must be low to achieve small objective function values.

Based on the results of the Simulated Quenching-method, Sequential Quadratic Programming is initiated adaptively starting with the original stiffness values. In case the lowest stiffness value is found in one of the 'wrong' braces, the algorithm does not converge, whereas it does for the right element, having the lowest objective function value of all solutions (see Figure 5.3). If Sequential Quadratic Programming is started in the tower area (runs number three and five), it converges, but returns a higher final objective function value.

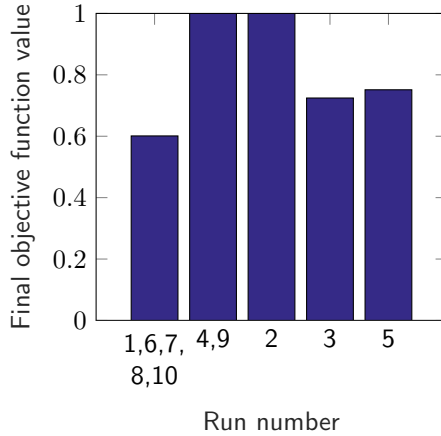


Figure 5.3.: Final objective function values after running ten Simulated Quenching runs and Sequential Quadratic Programming adaptively using modal properties as objective function at the tripile model.

Time series can be used instead of modal properties as an objective function for model updating using  $\rho^{l^2}$ . Figure 5.4 illustrates an exemplary time series of the undamaged model at the tower top node. After the initial transient procedure following the impulse, the highly damped oscillation turns to a sinusoidal oscillation with very low damping. It is assumed that this behavior is caused by the complex damping of the structure due to friction (see [76]) at the flanges at the replaceable section where the saw cut is inserted (see Figure 5.1(b)). The vibrations immediately after the impulse are ignored for damage localization in a first study, whereas they are considered in a second analysis (see Figure 5.4) because skipping the phase immediately after the impulse does not return accurate results for damage localization. The beam model from the preceding section is reformulated for damage localization using time series, two-stage damping is included, as described in [76]. The metric  $\rho^{l^2}$  is employed to compare the time series. Results from Simulated Quenching runs for the first analysis (window 1) are listed in Table 5.5, results of the respective adaptive Sequential Quadratic Programming optimizations are shown in Table 5.6. The minimal value is located in element seven in seven runs, which is the tower base element. It follows that the damage localization returns a wrong damage spot. If Sequential Quadratic Programming is started from these solutions, damage localization remains at that spot and converges to a minimum,

## 5. Concept Validation for Damage Localization

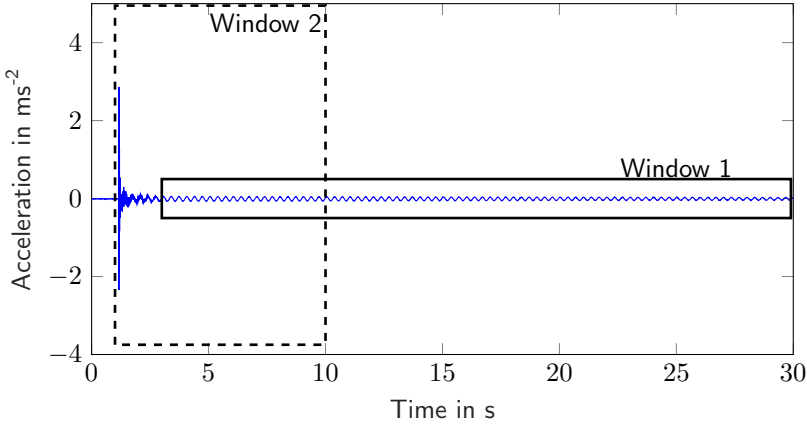


Figure 5.4.: Acceleration time series, measured by the uppermost accelerometer (Channel 1) at the undamaged tripile model under impulse load. In a first study, the transient decay is considered (solid box, Window 1), whereas in a second analysis the impulse loading is included (dashed box, Window 2).

and it confirms the location as a minimum with a lower objective function value than approximated by Simulated Quenching. Obviously, the objective function has another local minimum here. Damage is localized in the damaged brace only in Simulated Quenching run number 1. If Sequential Quadratic Programming is started from here, no convergence is reached, the objective function value remains at the same level.

Results of the second analysis with the impulse phase included and a shorter window (see Figure 5.4, Window 2) are given in Tables 5.7 and 5.8. The Simulated Quenching algorithm locates damage both in the correct brace and one undamaged brace, the objective function cannot be used to distinguish the solutions. The stiffness of element number four is also quite small when the algorithm locates damage in element six, giving strong indication that element four is the correct location. If Sequential Quadratic Programming is started adaptively, results reveal a more distinct behavior (see Table 5.8). If Simulated Quenching located damage in the wrong brace, Sequential Quadratic Programming is not able to reduce the objective function value distinctly, whereas it is reduced below 0.66 for all runs with a correctly located adaptive window (runs 1, 3, 4, and 8), highlighting the importance of the local algorithm. Instead of comparing the time series directly, these may be transferred to frequency domain before comparing them. In this case, the metric  $\rho^s$  is applied. Results of this analysis are drawn in Table 5.9. In this case,

Table 5.5.: Resulting minimal objective function values and corresponding stiffness parameters from eight Simulated Quenching runs using  $\rho^{l_2}$  at the tripile model for damage step 7, including only transient decay (window 1).

SQ run number	Objective Function Value	element number									
		1	2	3	4	5	6	7	8	9	10
1	0.987	0.984	0.983	0.990	0.980	1.000	0.650	0.821	0.885	0.969	0.985
2	0.986	0.879	0.924	0.927	0.990	0.903	0.986	0.687	0.977	0.992	0.991
3	0.979	0.987	0.969	0.983	1.008	0.968	0.985	0.555	0.932	0.990	0.996
4	0.986	0.879	0.984	0.976	0.992	0.879	0.948	0.683	0.995	0.998	0.984
5	0.986	1.001	0.994	0.923	0.941	0.963	0.956	0.611	0.974	0.935	0.982
6	0.987	0.944	0.937	0.975	0.884	0.993	0.970	0.767	0.944	1.006	0.868
7	0.986	0.986	0.945	0.972	0.987	0.879	0.952	0.691	0.904	1.003	0.953
8	0.987	0.871	0.998	0.993	0.927	0.979	0.944	0.771	0.929	0.980	0.925

Table 5.6.: Resulting minimal objective function values and corresponding stiffness parameters from Sequential Quadratic Programming runs using  $\rho^{l_2}$  at the tripile model for damage step 7, including only the transient decay (window 1) and starting adaptively with the results from Table 5.5.

SQP run number	Objective Function Value	element number									
		1	2	3	4	5	6	7	8	9	10
1	0.988	1.000	0.976	1.000	1.000	1.000	0.659	1.000	1.000	1.000	1.000
2	0.490	1.000	1.000	1.000	1.000	1.000	1.000	0.718	1.000	1.000	1.000
3	0.536	1.000	1.000	1.000	1.000	1.000	1.000	0.815	1.000	1.000	1.000
4	0.551	1.000	1.000	1.000	1.000	1.000	1.000	0.688	1.000	1.000	1.000
5	0.518	1.000	1.000	1.000	1.000	1.000	1.000	0.602	1.000	1.000	1.000
6	0.992	1.000	1.000	1.000	1.000	1.000	1.000	0.960	1.000	1.000	1.000
7	0.987	1.000	1.000	1.000	1.000	1.000	1.000	0.441	1.000	1.000	1.000
8	0.987	1.000	1.000	1.000	1.000	1.000	1.000	0.250	1.000	1.000	1.000

## 5. Concept Validation for Damage Localization

Table 5.7.: Resulting minimal objective function values and corresponding stiffness parameters from eight Simulated Quenching runs using  $\rho^{l_2}$  at the tripile model for damage step 7, including transient procedure (window 2).

SQ run number	Objective Function Value	element number									
		1	2	3	4	5	6	7	8	9	10
1	0.752	0.859	0.945	0.951	0.677	0.990	0.989	0.866	1.003	1.004	0.985
2	0.755	1.009	0.983	0.890	0.819	0.982	0.715	0.982	0.979	0.973	0.998
3	0.758	0.834	0.974	0.996	0.759	0.922	0.997	0.985	0.969	0.997	0.878
4	0.757	0.831	0.988	0.905	0.711	0.983	0.992	0.993	0.973	0.992	0.987
5	0.763	1.000	0.919	0.924	0.849	1.006	0.682	0.924	0.998	0.931	0.997
6	0.755	0.998	0.988	0.956	0.832	0.996	0.745	0.982	1.002	0.935	0.922
7	0.793	1.006	0.888	0.963	0.928	0.903	0.746	0.985	1.005	0.884	1.007
8	0.806	0.802	0.991	0.943	0.746	0.988	0.954	0.943	0.981	0.987	0.984

Table 5.8.: Resulting minimal objective function values and corresponding stiffness parameters from Sequential Quadratic Programming runs using  $\rho^{l_2}$  at the tripile model for damage step 7, including transient procedure (window 2) and starting adaptively with the results from Table 5.7.

SQP run number	Objective Function Value	element number									
		1	2	3	4	5	6	7	8	9	10
1	0.621	0.817	1.000	1.000	0.400	1.000	1.000	1.000	1.000	1.000	1.000
2	0.725	1.000	1.000	0.985	1.000	1.000	0.734	1.000	1.000	1.000	1.000
3	0.658	0.744	1.000	1.000	0.212	1.000	1.000	1.000	1.000	1.000	1.000
4	0.631	0.761	1.000	1.000	0.411	1.000	1.000	1.000	1.000	1.000	1.000
5	0.725	1.000	1.000	0.921	1.000	1.000	0.729	1.000	1.000	1.000	1.000
6	0.712	1.000	1.000	0.984	1.000	1.000	0.733	1.000	1.000	1.000	1.000
7	0.746	1.000	1.000	0.888	1.000	1.000	0.748	1.000	1.000	1.000	1.000
8	0.637	0.660	1.000	1.000	0.535	1.000	1.000	1.000	1.000	1.000	1.000



Table 5.9.: Resulting minimal objective function values and corresponding stiffness parameters from Simulated Quenching and adaptive Sequential Quadratic Programming runs using  $\rho^s$  at the tripile model for damage step 7.

SQP run number	Objective Function Value	element number									
		1	2	3	4	5	6	7	8	9	10
1	0.174	0.963	1.000	1.000	0.887	1.000	1.000	1.000	1.000	1.000	1.000
2	0.173	0.985	1.000	1.000	0.883	1.000	1.000	1.000	1.000	1.000	1.000
3	0.183	0.948	1.000	1.000	0.901	1.000	1.000	1.000	1.000	1.000	1.000
4	0.251	1.000	1.000	0.761	1.000	1.000	0.745	1.000	1.000	1.000	1.000
5	0.264	1.000	1.000	0.931	1.000	1.000	0.729	1.000	1.000	1.000	1.000
6	0.176	0.984	1.000	1.000	0.863	1.000	1.000	1.000	1.000	1.000	1.000
7	0.258	1.000	1.000	0.888	1.000	1.000	0.748	1.000	1.000	1.000	1.000
8	0.260	1.000	1.000	0.829	1.000	1.000	0.792	1.000	1.000	1.000	1.000

the wrong and correct results can again be distinguished using the final objective function value. Runs number 1,2,3 and 6 point to the correct element, whereas runs 4,5,7 and 8 are wrong solutions. The parameters of the wrong solutions differ more than the correct ones. All results presented in this section are evaluated for damage step 7 with a cutting depth of  $45.5mm$ . This damage is a cut through the upper flange and the webs and represents a quite severe damage.

Figure 5.5 illustrates results of all damage steps investigated comprehensively. Since the focus is on damage localization here, there is only right or wrong localization. Hence, the interpretation of Figure 5.5 differs from Figure 4.8. The plot reveals that a direct comparison of time series works for damage step 7 only (and only if the right transient data is used using window 2), whereas modal properties provide higher sensitivity to damage. Transformation of the time signals to frequency domain via application of  $\rho^s$  yields best results. A cut depth of  $18.9mm$  is correctly located. Smaller damages cannot be located with any of the metrics used here due to the decreasing effect on the global dynamic behavior which is used to locate damages throughout this thesis. Cuts with a smaller depth reveal no clear identification due to the small changes in the vibrational behavior. In these cases, correct and wrong solutions cannot be distinguished distinctively using the minimum objective function values.

## 5. Concept Validation for Damage Localization

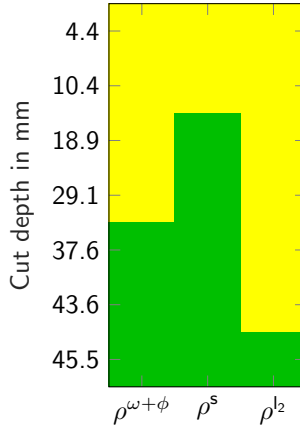


Figure 5.5.: Overview on success of damage localization using different metrics at the tripole structure for different cut depths.

## 5.2. Damage localization at a full scale rotor blade

The rotor blade investigated in section 4.2.3 is driven to fatigue failure in the test facility. A crack occurs at  $6m$  from the blade root at the trailing edge of the airfoil. The damage has a length of  $440mm$  and propagates through both pressure and suction side as well as the bondline. This section aims to demonstrate errors in the application of model updating that may occur when damages are too small to localize them and gives possible reasons. For validation of the localization approach, the damage is modeled in the numerical model firstly and then located. Afterward, the model is updated to reproduce the measurement data of the damaged rotor blade to perform damage localization using both  $\rho^{\omega+\phi}$  and  $\rho^{\tau}$ .

The parameterization is slightly changed in comparison to the model of section 4.2.3. While the aim of that section is to locate changes close to the blade tip, the exact location of structural change is unknown here. Hence, the parameterization is chosen to contain two elements for each parameter, see Figure 5.6.

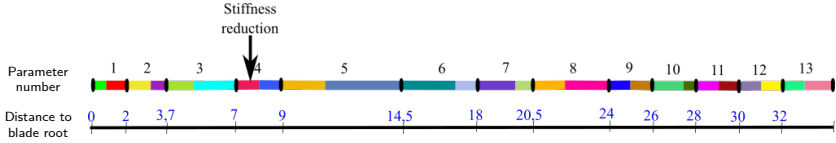


Figure 5.6.: Parameterization of the blade model according to blade construction plans and discretization for damage localization.

### 5.2.1. Damage localization at the rotor blade using artificial data

A stiffness reduction of 0.5% is introduced in the numerical model to evaluate if even small stiffness changes can be located theoretically in the investigated structure. Therefore, the stiffness of element seven is reduced (for the element numbers, refer to Figure 4.14), the structural responses of the numerical model are recorded and used as 'measured' quantities. Afterwards, the initial, undamaged numerical model is updated to reproduce this 'measured' response. A stiffness reduction that small has an only minor influence on the time series or modal properties, but it affects the structural dynamics to a certain degree, which can be captured by the metrics. The optimization problem solved to localize damage is written as

$$\min_{\theta} \rho^{\omega+\phi}(\theta) \quad (5.1a)$$

$$\text{subject to } \theta_i \geq 0.5 \quad \forall i \in [1..n] \quad (5.1b)$$

$$\theta_i \leq 1.01 \quad \forall i \in [1..n] \quad (5.1c)$$

$$\sum_i (1 - \theta_i) \leq 0.5. \quad (5.1d)$$

A small stiffness increase is allowed for numerical reasons. The stiffness decrease is restricted to a maximum of 50%. The last constraint equation ensures that only a single parameter can reach the maximum stiffness decrease. Results of model updating using the two-step optimization algorithm are drawn in Table 5.10. Only run number three locates damage at the correct location, parameter four. All other runs locate damage at a wrong location. Again, the final objective function value is employed to distinguish wrong from right solutions, see Figure 5.7. Problem (5.1) is solved again for localization of the artificial damage using transmissibility functions, using  $\rho^T$  as objective function. Results of this analysis are drawn in Table 5.11. Again, the final objective function value may be used to distinguish wrong from right solutions.

## 5. Concept Validation for Damage Localization

Table 5.10.: Final results after running Simulated Quenching and adaptive Sequential Quadratic Programming to solve problem (5.1) using  $\rho^{\omega+\phi}$  as objective function, stiffness reduction 0.5%.

SQP run number	Objective Function Value	Parameter number												
		1	2	3	4	5	6	7	8	9	10	11	12	13
1	$7.266 \cdot 10^{-08}$	1.00	1.00	1.00	1.00	0.999	1.000	1.000	1.00	1.00	1.00	1.00	1.00	1.00
2	$1.206 \cdot 10^{-07}$	1.00	1.00	1.00	1.00	1.00	1.00	1.00	1.00	1.00	1.00	1.00	0.999	1.000
3	$1.088 \cdot 10^{-09}$	1.00	1.00	1.00	0.996	1.000	1.000	1.00	1.00	1.00	1.00	1.00	1.00	1.00
4	$6.908 \cdot 10^{-08}$	1.009	0.989	1.003	1.00	1.00	1.00	1.00	1.00	1.00	1.00	1.00	1.00	1.00
5	$1.184 \cdot 10^{-07}$	1.00	1.00	1.00	1.00	1.00	1.00	1.00	1.00	1.00	0.999	1.000	1.000	1.00
6	$1.07 \cdot 10^{-07}$	1.00	1.00	1.00	1.00	1.00	1.00	1.00	1.00	1.00	1.00	1.00	0.999	1.000
7	$3.482 \cdot 10^{-07}$	0.997	0.994	1.010	1.00	1.00	1.00	1.00	1.00	1.00	1.00	1.00	1.00	1.00
8	$9.059 \cdot 10^{-06}$	1.00	1.00	1.00	1.00	1.00	1.00	1.00	0.991	0.981	1.010	1.00	1.00	1.00

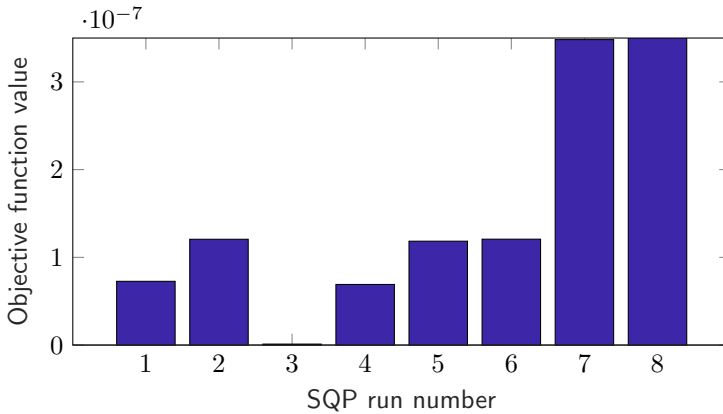


Figure 5.7.: Final objective function values after running eight Simulated Quenching runs and Sequential Quadratic Programming adaptively using  $\rho^{\omega+\phi}$  as objective function at the blade model with an artificial stiffness reduction of 0.5%.

Table 5.11.: Final results after running Simulated Quenching and adaptive Sequential Quadratic Programming to solve problem (5.1) using  $\rho^\tau$  as objective function, stiffness reduction 0.5%.

SQP run number	Objective Function Value	Parameter number												
		1	2	3	4	5	6	7	8	9	10	11	12	13
1	0.0085	1.00	1.00	0.999	0.997	1.000	1.00	1.00	1.00	1.00	1.00	1.00	1.00	1.00
2	0.0678	1.00	1.00	1.00	0.967	1.005	1.007	1.00	1.00	1.00	1.00	1.00	1.00	1.00
3	0.0741	1.00	1.00	1.00	1.00	1.00	1.00	0.999	0.999	1.001	1.00	1.00	1.00	1.00
4	0.0771	1.00	1.00	1.00	1.00	1.00	1.000	0.999	1.000	1.00	1.00	1.00	1.00	1.00
5	0.0773	1.00	1.00	1.00	1.00	1.00	1.000	0.999	1.000	1.00	1.00	1.00	1.00	1.00
6	0.0745	1.00	1.00	1.00	1.00	1.00	1.00	1.00	0.998	1.002	0.999	1.00	1.00	1.00
7	0.0085	1.00	1.00	0.999	0.997	1.000	1.00	1.00	1.00	1.00	1.00	1.00	1.00	1.00
8	0.0779	1.00	1.00	1.00	1.00	1.000	1.000	0.999	1.00	1.00	1.00	1.00	1.00	1.00
9	0.0914	1.00	1.00	1.00	1.00	1.00	1.00	1.00	1.00	1.00	0.999	1.000	1.000	1.00
10	0.1874	0.991	1.010	1.00	1.00	1.00	1.00	1.00	1.00	1.00	1.00	1.00	1.00	1.00

The same analysis is repeated for different damage severities, namely stiffness reductions of 10%,5%,4%,3%,2%,1% and 0.5%. Figure 5.8 is used to determine, if a damage quantification is possible with this approach. The parameters of the damaged section seem to underestimate the real stiffness decrease, although they are close to the real value. Thus, a tendency can be seen in the results, more severe stiffness reductions result in smaller stiffnesses identified by the algorithm. The use of both  $\rho^{\omega+\phi}$  and  $\rho^\tau$  returns similar results in this study. The number of correct solutions varies with ongoing damage severities, no tendency is apparent. There is an outlier at two percent stiffness reduction. This outlier can be assorted by the final objective function value. Hence, it is demonstrated that model-to-model updating performs well to localize damage with both transmissibility functions and modal properties.

### 5.2.2. Damage localization at the rotor blade using experimental data

After the functionality for localization of small stiffness changes in the rotor blade is shown in the previous section, the algorithm is applied to the real damaged rotor blade in this section. An initial model updating to the undamaged configuration yields modal assurance criterion values bigger than 0.992 for all first seven eigenmodes. These are considered in this study because they are identified in all experiments. Eigenfrequencies and mode shapes are averaged from several excitations. The measured and simulated eigenfrequencies differ by a maximum of 5%.

## 5. Concept Validation for Damage Localization

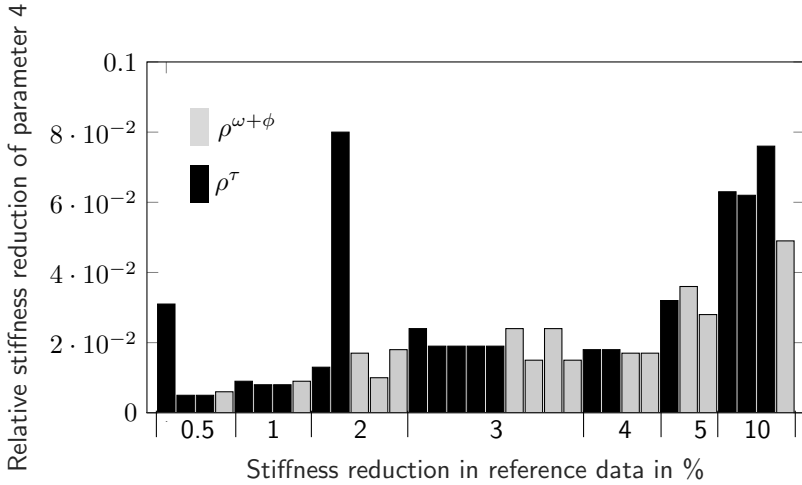


Figure 5.8.: Overview on stiffness parameter 4 for all investigated damage states at the rotor blade. Only the correct solutions are listed here, thus there are different numbers of solutions for each step.

The optimization problem solved to locate the damage accounts to

$$\min_{\theta} \rho^{\omega+\phi}(\theta) \quad (5.2a)$$

$$\text{subject to } \theta_i \geq 0.25 \quad \forall i \in [1..n] \quad (5.2b)$$

$$\theta_i \leq 1.01 \quad \forall i \in [1..n] \quad (5.2c)$$

$$\sum_i (1 - \theta_i) \leq 0.75. \quad (5.2d)$$

The solutions of this problem using the adaptive optimization algorithm are drawn in Table 5.12. The vector parameter  $\psi$  applied to the results of model updating (see Figure 5.9) reveals that damage is most likely located in element 5. The correct location would be in parameter 4, which is not found in a single run of the algorithm. Results are different if  $\rho^{\tau}$  is used as objective function, see Table 5.13. If the vector parameter  $\psi$  is applied to these results (Figure 5.10), a7 localization in element number 1 or 6 is revealed, which are also wrong solutions. Similar results are achieved, if  $\rho^s$  or  $\rho^{l^2}$  are employed as objective functions, the damage is not located correctly.

Table 5.12.: Results of Simulated Quenching and adaptive Sequential Quadratic Programming using  $\rho^{\omega+\phi}$  to locate damage in the rotor blade. Minimum values are highlighted in gray.

SQP run number	Objective Function Value	Parameter number												
		1	2	3	4	5	6	7	8	9	10	11	12	13
1	0.0210	1.00	1.00	1.00	0.998	0.785	0.950	1.00	1.00	1.00	1.00	1.00	1.00	1.00
2	0.0212	1.00	1.00	1.00	0.900	0.781	0.959	1.00	1.00	1.00	1.00	1.00	1.00	1.00
3	0.0222	0.896	0.778	0.946	1.00	1.00	1.00	1.00	1.00	1.00	1.00	1.00	1.00	1.00
4	0.0211	1.00	1.00	1.00	0.964	0.780	0.984	1.00	1.00	1.00	1.00	1.00	1.00	1.00
5	0.0219	0.747	0.898	1.00	1.00	1.00	1.00	1.00	1.00	1.00	1.00	1.00	1.00	1.00
6	0.0211	1.00	1.00	1.00	0.922	0.779	0.979	1.00	1.00	1.00	1.00	1.00	1.00	1.00
7	0.0212	1.00	1.00	1.00	1.00	0.861	0.829	1.010	1.00	1.00	1.00	1.00	1.00	1.00
8	0.0211	1.00	1.00	1.00	0.974	0.813	0.960	1.00	1.00	1.00	1.00	1.00	1.00	1.00
9	0.0211	1.00	1.00	1.00	0.931	0.813	0.983	1.00	1.00	1.00	1.00	1.00	1.00	1.00
10	0.0211	1.00	1.00	1.00	0.971	0.811	0.937	1.00	1.00	1.00	1.00	1.00	1.00	1.00
11	0.0212	1.00	1.00	1.00	0.896	0.822	0.944	1.00	1.00	1.00	1.00	1.00	1.00	1.00
12	0.0210	1.00	1.00	1.00	1.005	0.755	1.001	1.00	1.00	1.00	1.00	1.00	1.00	1.00
13	0.0219	0.759	0.879	1.00	1.00	1.00	1.00	1.00	1.00	1.00	1.00	1.00	1.00	1.00
14	0.0220	0.788	0.984	1.00	1.00	1.00	1.00	1.00	1.00	1.00	1.00	1.00	1.00	1.00
15	0.0222	0.896	0.778	0.946	1.00	1.00	1.00	1.00	1.00	1.00	1.00	1.00	1.00	1.00

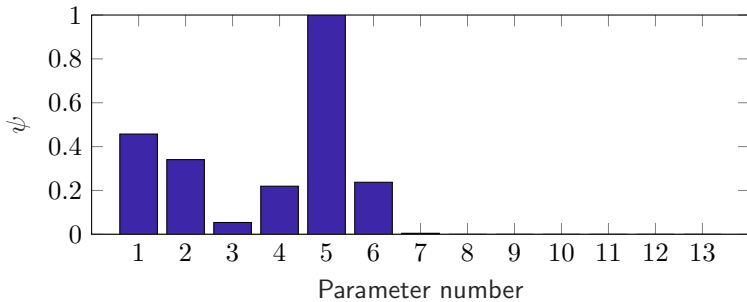


Figure 5.9.: Vector parameter  $\psi$  applied to results of damage localization at the blade using  $\rho^{\omega+\phi}$ .

## 5. Concept Validation for Damage Localization

Table 5.13.: Results of Simulated Quenching and adaptive Sequential Quadratic Programming using  $\rho^r$  to locate damage in the rotor blade. Minimum values are highlighted in gray.

SQP run number	Objective Function Value	Parameter number												
		1	2	3	4	5	6	7	8	9	10	11	12	13
1	14.8480	1.00	1.00	1.00	1.00	0.524	0.676	0.928	1.00	1.00	1.00	1.00	1.00	1.00
2	14.7066	1.00	1.00	1.00	1.00	0.611	0.524	0.701	1.00	1.00	1.00	1.00	1.00	1.00
3	14.9196	1.00	1.00	1.00	1.00	0.851	0.583	0.663	1.00	1.00	1.00	1.00	1.00	1.00
4	14.2878	0.42	0.956	1.007	1.00	1.00	1.00	1.00	1.00	1.00	1.00	1.00	1.00	1.00
5	14.6926	0.573	0.666	1.00	1.00	1.00	1.00	1.00	1.00	1.00	1.00	1.00	1.00	1.00
6	14.4508	1.00	1.00	1.00	1.00	0.939	0.732	0.991	1.00	1.00	1.00	1.00	1.00	1.00
7	14.4848	1.00	1.00	1.00	1.00	0.932	0.743	0.973	1.00	1.00	1.00	1.00	1.00	1.00
8	14.4804	1.00	1.00	1.00	1.00	0.933	0.693	0.994	1.00	1.00	1.00	1.00	1.00	1.00
9	14.9700	0.663	1.010	1.00	1.00	1.00	1.00	1.00	1.00	1.00	1.00	1.00	1.00	1.00
10	14.7138	0.552	0.653	1.00	1.00	1.00	1.00	1.00	1.00	1.00	1.00	1.00	1.00	1.00
11	14.4145	0.485	0.934	1.00	1.00	1.00	1.00	1.00	1.00	1.00	1.00	1.00	1.00	1.00
12	15.2727	1.00	1.00	1.00	1.00	0.987	0.954	0.554	1.00	1.00	1.00	1.00	1.00	1.00

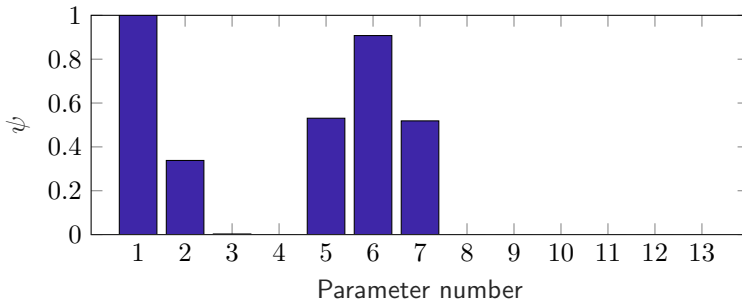


Figure 5.10.: Measure  $\psi$  applied to results of damage localization at the blade using  $\rho^r$ .



## 5.3. Damage localization at a scaled prestressed concrete tower

During the last decade, hybrid towers emerged as an alternative to conventional steel wind turbine towers. Recent development led to the construction of hybrid towers made partially from precast and prestressed concrete segments that are assembled on site. A conventional steel tower is then installed on top of the prestressed concrete construction [103]. This method enables higher hub heights. The lower part of the tower is made from premanufactured concrete tube segments that are stacked without adhesive materials between them, solely being fixed by the friction between the segments caused by prestressing forces [19]. Since the dynamic behavior of these structures is not known in detail, structural health monitoring is a useful supplement to ensure long-term service of these structures. This section aims to validate the damage localization approach at a scaled model of a prestressed concrete tower being installed in the Test Center for Support Structures Hanover.

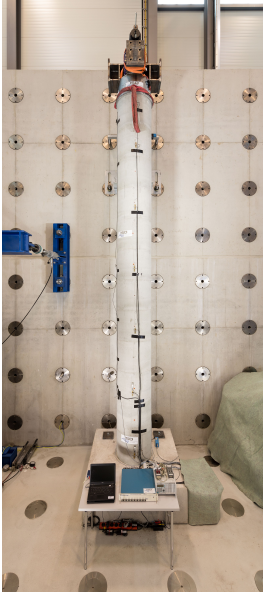
### 5.3.1. Experimental set up and numerical modeling of the tower

The investigated structure is an externally prestressed concrete tower (see Figure 5.11(a)), based on a concrete foundation. A head mass of  $470\text{kg}$ , a subassembly needed to transfer the prestressing force from the prestressing rod to the uppermost concrete segment, is attached on top of the tower. The model itself consists of twelve tubular concrete segments with a height of  $0.5\text{m}$  each (see Figure 5.11(b)), an outer diameter of  $0.6\text{m}$  and a wall thickness of  $0.05\text{m}$ . The segments are numbered in ascending order, starting from the bottom. The mass of all concrete segments and the head mass is given in Table 5.14. According to the technical approval, the threaded rod has a cross-sectional area of  $1735\text{mm}^2$ . Specimens of the concrete used for the segments are tested according to DIN EN 12390-13. The tests reveal the compressive strength to  $75.1\frac{\text{N}}{\text{mm}^2}$ , a density of  $2291\frac{\text{kg}}{\text{m}^3}$  and Young's modulus to  $33170\frac{\text{N}}{\text{mm}^2}$ . The compressive strength is close to a C70/85 concrete, whereas Young's modulus is close to a C30/37.

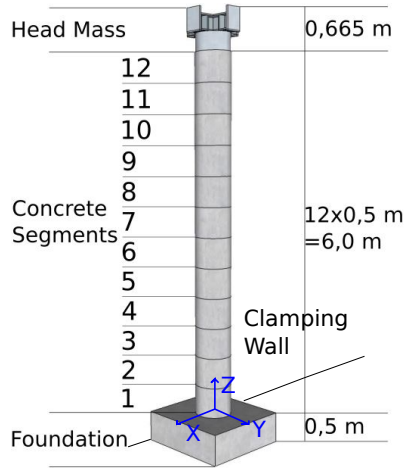
Accelerometers are installed on all concrete segments with an uneven number as well as the top segment to track dynamic responses of the tower. Besides, two accelerometers are attached to the tower at segment 7 and segment 12 contorted by  $90^\circ$  to account for torsional vibrations.

The structure is excited using three different excitation types, impulse excitation with a hammer, free decay with bigger amplitudes and swept sine excitation using

## 5. Concept Validation for Damage Localization



(a) Experimental structure installed in the test facility



(b) Schematic overview on experimental tower structure

Figure 5.11.: Overview on the experimental prestressed concrete tower structure.

Table 5.14.: Mass distribution of the tower.

Segment Number	Mass [kg]
1	- <sup>1</sup>
2	100.5
3	102.6
4	102.0
5	101.8
6	106.5
7	104.0
8	104.8
9	103.7
10	104.0
11	106.0
12	142.0
Head Mass	470.0

<sup>1</sup> The mass of this segment is irrelevant because it is clamped to the foundation.

### 5.3. Damage localization at a scaled prestressed concrete tower

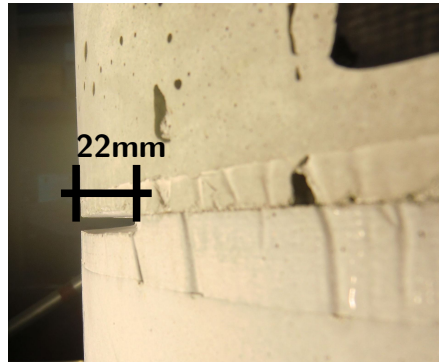


Figure 5.12.: Damage degree 1 applied to the experimental structure between segments 2 and 3, a 22mm deep cut.

an electrodynamic shaker. Only the hammer excitation is considered here because each periodic excitation is running several hours. Simulation of these time series would cause too long computational times. The free decay experiments are not considered due to the small number of these tests being performed, making a simulation of the contact nonlinearities being activated in these tests difficult. Hence, the impulse tests are used for model updating in this analysis.

The impulse excitation is applied using hammer strokes on the head mass and centric on segments 11, 8 and 5 in y-direction and on the head mass and segment 8 in x-direction. Furthermore, a torsional impulse is applied by strokes on the side of the outer plate of the head mass (compare Figure 5.11(a)). Every test is repeated 10 times to account for statistical variance and is also repeated for all configurations of the experimental structure, which is varied first in the parameter of the prestressing force and second in the extent of the damage applied to the structure (see Table 5.16). During the first configuration, the prestressing force is set to 23 % of the compressive strength of the concrete. Afterwards, it is reduced to 19 %, 15 % and finally 11 % of the compressive strength of the concrete. Then the force is increased to 20 % of the compressive strength of the concrete and damage is applied to the structure. Damage is imposed by gradually increasing parts being removed from the cross-sectional area in the x-y-plane of the tower in four steps (step 1, see Figure 5.12) between segments 2 and 3. The maximum degree of damage results in a reduction of one third of the geometrical moment of inertia. The depth of the straight cuts into the tower and the resulting percentage of the remaining geometrical moment of inertia are listed in Table 5.15. A typ-

## 5. Concept Validation for Damage Localization

Table 5.15.: Damage degrees applied to the experimental structure.

Damage degree	Depth of the cut $h$	Remaining geometrical moment of inertia $I^1$
	mm	%
1	22	91.7
2	33	83.2
3	42	75.3
4	51	66.2

<sup>1</sup> This can be determined using the formula given in Appendix A.2.

Table 5.16.: Configurations investigated at the experimental structure.

Configuration No.	Description	Parameter varied
1	23% $f_{ck}$ , No damage	Prestressing force
2	19% $f_{ck}$ , No damage	
3	15% $f_{ck}$ , No damage	
4	11% $f_{ck}$ , No damage	
5	20% $f_{ck}$ , No damage	Damage
6	20% $f_{ck}$ , damage degree 1	
7	20% $f_{ck}$ , damage degree 2	
8	20% $f_{ck}$ , damage degree 3	
9	20% $f_{ck}$ , damage degree 4	

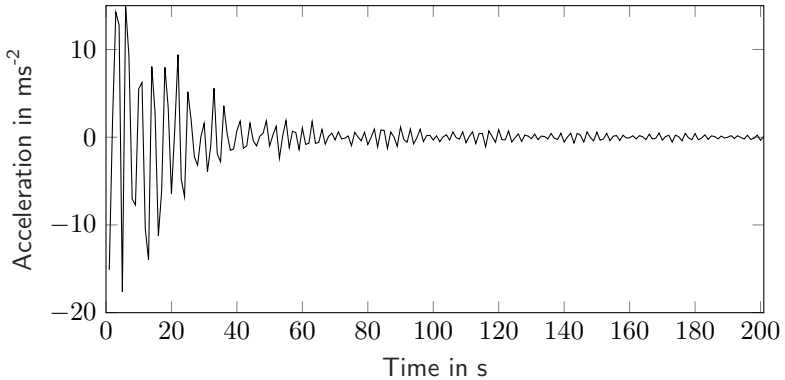


Figure 5.13.: Acceleration time series of a test conducted at the tower with a prestressing force of  $11\%f_{ck}$ , no damage, measured at segment 9.

ical response of the conducted experiment is illustrated in Figure 5.13, revealing a decent signal to noise ratio. Modal analysis using stochastic subspace identification reveals decreasing eigenfrequencies, if the prestressing force is reduced or if the structure is damaged, whereas it remains stable within the configuration. The first eigenfrequencies identified for configurations 5 and 6 from the time series are given in Figure 5.14, revealing a drop of the eigenfrequency of 2.2%. This is similar to higher eigenfrequencies. Another noteworthy result is a drop of the eigenfrequency during tests conducted in configuration 1 (see Figure 5.15). This change is attributed to the screws that ensure clamping of the baseplate. These loosen during a free decay experiment conducted between impulse tests, possibly changing the clamping conditions.

The simulation model is built using three different element types. Timoshenko beam elements are employed for the concrete segments of the tower, taking shear deformation effects into account. Even though shell and volume elements are more precise than beam elements, beams are chosen due to computational costs. The material properties of these elements are listed in Table 5.17. The element densities are adjusted according to measured masses of the segments (see Table 5.14) as given in Table 5.18. The head mass is simulated using a mass element without consideration of rotational inertia. The clamping of the base plate is modeled by rotational spring-damper elements at two axes.



### 5.3. Damage localization at a scaled prestressed concrete tower

Table 5.18.: Locations of elements in simulation model of the tower and their density.

Element No.	z-Coordinate in m		Element Type	Density kgm <sup>-3</sup>	Material Parameter
	Start	End			
1	0	0.25	Timoshenko Beam	2291	1
2	0.25	0.5	Timoshenko Beam	2291	1
3	0.5	1.25	Timoshenko Beam	2337	2
4	1.25	1.5	Timoshenko Beam	2386	3
5	1.5	2	Timoshenko Beam	2372	4
6	2	2.25	Timoshenko Beam	2367	5
7	2.25	2.5	Timoshenko Beam	2367	5
8	2.5	3	Timoshenko Beam	2477	6
9	3	3.25	Timoshenko Beam	2419	7
10	3.25	3.5	Timoshenko Beam	2419	7
11	3.5	3.75	Timoshenko Beam	2437	8
12	3.75	4	Timoshenko Beam	2437	8
13	4	4.25	Timoshenko Beam	2412	9
14	4.25	4.5	Timoshenko Beam	2412	9
15	4.5	5	Timoshenko Beam	2477	10
16	5	5.25	Timoshenko Beam	2465	11
17	5.25	5.5	Timoshenko Beam	2465	11
18	5.5	5.75	Timoshenko Beam	3302	12
19	5.75	6	Timoshenko Beam	3302	12
20	6		Mass		
21	0		Spring-Damper		
22	0		Spring-Damper		

Table 5.17.: Material properties of the concrete in the simulation model

Property	Value	
Young's modulus	$E$	$2.32 \cdot 10^{10} \text{ Nm}^{-2}$
Shear modulus	$G$	$9.67 \cdot 10^9 \text{ Nm}^{-2}$
Rayleigh Damping Coefficient	$\alpha$	0.0437
	$\beta$	$3.3070 \cdot 10^{-4}$

Damping is considered using Rayleigh damping (see equation (2.2)). The values  $\alpha$  and  $\beta$  are given in Table 5.17. A force of  $1.3 \cdot 10^6 \text{ N}$  is used to model the prestressing force. Since the impulse force is not measured during the experiment, it is approximated according to the maximum acceleration after the impulse, individually for each time series.

#### 5.3.2. Damage localization at the tower

Since the application of  $\rho^{l^2}$  does not deliver satisfying results in the tripile and the three-story frame presented so far, another, new time-domain based comparison

## 5. Concept Validation for Damage Localization

method shall be employed within this section. Namely, this is the Mahalanobis norm which is used to formulate the metric  $\rho^\mu$  (see equation (2.35)). Hence, time domain metrics are compared in this section solely.

### Configuration 1: Localization of failure at basement clamping

A failure at the clamping occurs during the experiments. In real applications of the method, the location of this failure would be unknown. Therefore, this modification of the structural behavior is located in this section. The numerical model is parameterized using 13 parameters. Parameters two to thirteen represent the stiffnesses of the tower elements whereas parameter one is used to modify the stiffness of rotational springs connecting the tower to the ground. The optimization problem solved to locate the investigated damage is

$$\min_{\theta} \rho^{l2}(\theta) \quad (5.3a)$$

$$\text{subject to } \theta_i \geq 0.9 \forall i \in [2\dots 13] \quad (5.3b)$$

$$\theta_1 \geq 0.05 \quad (5.3c)$$

$$\theta_i \leq 1.01 \forall i \in [2\dots 13] \quad (5.3d)$$

$$\sum_i (1 - \theta_i) \leq 0.95. \quad (5.3e)$$

The stiffness of the rotational springs connecting the tower to the ground is expected to change more distinctively in the investigated case. Therefore, the restriction of parameter one is chosen to be relatively free (see eqn. (5.3c)), whereas the maximum stiffness decrease of the beam elements is restricted to 10% (see eqn. (5.3b)). A small increase is allowed for numerical reasons (eqn. (5.3d)) as before. Equation (5.3e) is employed again to ensure only one parameter being reduced, though its influence is expected to be small here, because it is adjusted to the high expected stiffness decrease of the rotational springs (eqn. (5.3c)).

Results from ten runs to solve problem (5.3) are listed in Table 5.19. While parameter one is expected to be reduced, it is raised by a medium of 13% in all runs. The stiffness parameters of the beam elements remain close to the initial value, although the stiffness of the beam element at the base (parameter 2) is reduced in all solutions. This may be interpreted as the damage being in this area. Obviously, there is an optimum here that is different from the expected one, with parameter one being reduced. On the other hand, the normalized objective function values remain close to the initial value.

If problem (5.3) is solved again applying  $\rho^\mu$ , results are different (see Table 5.20).



### 5.3. Damage localization at a scaled prestressed concrete tower

Table 5.19.: Results of Simulated Quenching and Sequential Quadratic Programming using  $\rho^{l^2}$  to locate clamping failure in the tower (config. 1).

SQP run number	Objective Function Value	Parameter number												
		1	2	3	4	5	6	7	8	9	10	11	12	13
1	0.993	1.122	0.98	0.959	0.994	1.01	1.01	1.01	1.01	1.01	1.01	0.948	0.98	0.98
2	0.993	1.137	0.972	0.964	0.991	1.01	1.01	1.01	1.01	1.01	1.01	0.954	0.972	0.972
3	0.993	1.134	0.972	0.965	0.991	1.01	1.01	1.01	1.01	1.01	1.01	0.955	0.972	0.972
4	0.993	1.134	0.972	0.965	0.991	1.01	1.01	1.01	1.01	1.01	1.01	0.955	0.972	0.972
5	0.993	1.121	0.98	0.959	0.995	1.01	1.01	1.01	1.01	1.01	1.01	0.949	0.98	0.98
6	0.993	1.135	0.972	0.965	0.992	1.01	1.01	1.01	1.01	1.01	1.01	0.955	0.972	0.972
7	0.993	1.136	0.972	0.964	0.991	1.01	1.01	1.01	1.01	1.01	1.01	0.955	0.972	0.972
8	0.993	1.136	0.972	0.964	0.991	1.01	1.01	1.01	1.01	1.01	1.01	0.955	0.972	0.972
9	0.993	1.122	0.98	0.959	0.994	1.01	1.01	1.01	1.01	1.01	1.01	0.948	0.98	0.98
10	0.993	1.135	0.972	0.964	0.99	1.01	1.01	1.01	1.01	1.01	1.01	0.955	0.972	0.972
$\mathcal{M}$	0.993	1.131	0.975	0.963	0.992	1.01	1.01	1.01	1.01	1.01	1.01	0.953	0.975	0.975
$\sigma$	0	0.006	0.004	0.003	0.002	0	0	0	0	0	0	0.003	0.004	0.004

Table 5.20.: Results of Simulated Quenching and Sequential Quadratic Programming using  $\rho^{\mu}$  to locate clamping failure in the tower (config. 1).

SQP run number	Objective Function Value	Parameter number												
		1	2	3	4	5	6	7	8	9	10	11	12	13
1	0.766	0.98	1.053	1.025	0.961	0.997	0.979	1.034	1.095	1.085	1.052	0.991	0.986	0.964
2	0.687	0.165	0.95	1.013	1.005	1.057	1.054	0.951	0.937	0.978	1.051	0.944	1.038	0.923
3	0.769	1.052	0.938	0.988	0.999	1.02	0.986	1.032	0.967	1.068	1.099	1.085	1.067	0.931
4	0.762	0.807	0.903	0.966	0.969	0.987	0.952	1.014	1.014	1.069	1.013	1.05	1.019	0.91
5	0.763	0.828	0.977	0.947	1.072	0.956	1.035	1.041	1.087	1.064	0.933	0.951	1.056	1.014
6	0.647	0.097	1.024	1.022	1.039	1.013	0.921	1.028	1.088	0.987	1.067	1.079	1.034	0.936
7	0.749	0.557	0.932	0.998	1.095	1.005	1.043	1.086	1.062	0.97	1.083	0.96	1.058	1.049
8	0.74	0.483	0.904	1.036	0.966	0.958	0.961	1.007	1.072	1.084	1.061	1.047	1.067	1.053
9	0.765	1.003	0.946	1.001	0.912	0.981	1.014	1.036	1.037	1.09	1.048	1.07	1.085	1.021
10	0.767	0.997	1.014	1.014	0.958	0.91	1.055	1.085	1.077	0.987	1.014	1.087	0.968	0.969
$\mathcal{M}$	0.742	0.697	0.964	1.001	0.998	0.989	1	1.031	1.044	1.038	1.042	1.027	1.038	0.977
$\sigma$	0.039	0.336	0.049	0.026	0.054	0.039	0.045	0.037	0.052	0.048	0.044	0.056	0.035	0.051

## 5. Concept Validation for Damage Localization

In this case, the algorithm detects several local optima. All these solutions have in common, that the final objective function is small, if parameter one is small (see especially runs 2 and 6 in Table 5.20). The standard deviation of parameter 1 is quite high (0.336), making possible quantifications questionable.

### Configuration 6: Localization of small saw cut

Since the basement screws are fixed in subsequent experiments, the rotational springs connecting the tower to the ground are removed from the parameter set. Hence, parameters one to twelve denote the stiffnesses of the elements used to model the tower in Tables 5.21 and 5.22. The smallest damage applied to the structure is to be located here (configuration 6, damage degree 1). This configuration is characterized by a saw cut with a cutting depth of  $22mm$ , resulting in a stiffness decrease of 8.3% (determined using Appendix A.2). The correct solutions provide slightly smaller objective function values, and the stiffness decrease is underestimated. In the experiment, the damage is applied in the section modified by parameter 2. Hence, this value should be reduced to locate damage in the correct spot.

If  $\rho^{l^2}$  is applied for damage localization (Table 5.21), localization is successful in three runs (solutions 3,7 and 8). Again, objective function values may be used to distinguish wrong from right solutions, although the difference between correct and wrong solutions is marginal in this case. The correct stiffness change of 8.3% is underestimated in all three correct solutions. If  $\rho^{\mu}$  is employed for damage localization (Table 5.22), six of ten solutions locate the damage in the correct area (runs 2,3,4,5,7,10). The difference between correct and wrong solutions can be seen in the objective function values, which are around 0.9, whereas the wrong solutions provide associated objective function values close to 1. An exception is solution 9, where the initial adaptive window is set to parameters 3, 4 and 5, making it impossible to point to the correct solution. However, it points towards the neighbored parameter. A move of the adaptive window as described earlier in section 3.3 helps to find the correct solution. This intermediate solution has a final objective function value of 0.95, which is in the middle between the correct and the wrong solutions. The value of parameter 2 is between 0.908 and 0.931 which is fairly close to the real stiffness decrease of 8.3% in all correct solutions. A local optimum seems to be achieved if parameter 12 is reduced (runs 1,6 and 8). Hence, the localization of the saw cut is possible using the presented approach, but only if  $\rho^{\mu}$  is employed as objective function.

### 5.3. Damage localization at a scaled prestressed concrete tower

Table 5.21.: Results of Simulated Quenching and adaptive Sequential Quadratic Programming using  $\rho^{l^2}$  to locate damage in the tower (configuration 6).

SQP run number	Objective Function Value	Parameter number											
		1	2	3	4	5	6	7	8	9	10	11	12
1	0.998	0.975	1.01	1.0	1.0	1.0	1.0	1.0	1.0	1.0	1.0	1.0	1.0
2	0.998	0.983	1.01	1.0	1.0	1.0	1.0	1.0	1.0	1.0	1.0	1.0	1.0
3	0.991	1.01	0.951	1.01	1.0	1.0	1.0	1.0	1.0	1.0	1.0	1.0	1.0
4	0.997	1.01	1.01	1.01	1.0	1.0	1.0	1.0	1.0	1.0	1.0	1.0	1.0
5	0.998	1.01	1.01	1.01	1.0	1.0	1.0	1.0	1.0	1.0	1.0	1.0	1.0
6	0.998	1.01	1.01	1.01	1.0	1.0	1.0	1.0	1.0	1.0	1.0	1.0	1.0
7	0.992	1.01	0.981	1.01	1.0	1.0	1.0	1.0	1.0	1.0	1.0	1.0	1.0
8	0.993	1.01	0.987	1.01	1.0	1.0	1.0	1.0	1.0	1.0	1.0	1.0	1.0
9	0.998	1.001	1.01	1.0	1.0	1.0	1.0	1.0	1.0	1.0	1.0	1.0	1.0
10	0.998	0.998	1.01	1.0	1.0	1.0	1.0	1.0	1.0	1.0	1.0	1.0	1.0
$\mathcal{M}$	0.996	1.002	0.999	1.006	1.0	1.0	1.0	1.0	1.0	1.0	1.0	1.0	1.0
$\sigma$	0.003	0.013	0.020	0.005	0.0	0.0	0.0	0.0	0.0	0.0	0.0	0.0	0.0

Table 5.22.: Results of Simulated Quenching and adaptive Sequential Quadratic Programming using  $\rho^\mu$  to locate damage in the tower (configuration 6).

SQP run number	Objective Function Value	Parameter number											
		1	2	3	4	5	6	7	8	9	10	11	12
1	0.991	1.0	1.0	1.0	1.0	1.0	1.0	1.0	1.0	1.0	1.0	1.01	0.931
2	0.899	0.981	0.910	1.0	1.0	1.0	1.0	1.0	1.0	1.0	1.0	1.0	1.0
3	0.903	0.976	0.920	1.0	1.0	1.0	1.0	1.0	1.0	1.0	1.0	1.0	1.0
4	0.874	0.961	0.911	0.926	1.0	1.0	1.0	1.0	1.0	1.0	1.0	1.0	1.0
5	0.906	0.983	0.904	1.0	1.0	1.0	1.0	1.0	1.0	1.0	1.0	1.0	1.0
6	0.991	1.0	1.0	1.0	1.0	1.0	1.0	1.0	1.0	1.0	1.0	1.01	0.942
7	0.921	1.0	0.931	0.977	1.01	1.0	1.0	1.0	1.0	1.0	1.0	1.0	1.0
8	0.991	1.0	1.0	1.0	1.0	1.0	1.0	1.0	1.0	1.0	1.0	1.01	0.918
9	0.951	1.0	1.0	0.906	1.01	1.01	1.0	1.0	1.0	1.0	1.0	1.0	1.0
10	0.900	0.982	0.908	1.0	1.0	1.0	1.0	1.0	1.0	1.0	1.0	1.0	1.0
$\mathcal{M}$	0.925	0.988	0.948	0.981	1.002	1.001	1.0	1.0	1.0	1.0	1.0	1.003	0.985
$\sigma$	0.040	0.014	0.045	0.035	0.004	0.003	0	0	0	0	0	0.005	0.027

### 5.4. Conclusion

A saw cut is inserted into a brace of a scaled tripile structure to prove the functionality of the algorithm using real measured data. In case modal properties are employed as the objective function, the Simulated Quenching algorithm approximates correct solutions in 50% of the examples. If the damage is located in one of the undamaged braces by Simulated Quenching, Sequential Quadratic Programming does not converge, and it is obvious, that damage can only be present in one of the other braces. The objective function seems to have another local optimum in the upper section of the tower, but the respective objective function values are 25% bigger than those of the correct damage location. Furthermore, the fact that 50% of all solutions locate damage in one single brace is a strong indication of the damage to be in this area. In practice, this would imply to instruct a maintenance crew to look for damages in the brace first. If no damage is found here, the maintenance team should move on to the upper section of the tower and check for damages there. The final objective function values are bigger than in the numerical example, which presumably has two reasons: The initial model is not a perfect representation of the undamaged system, and the damage is not modeled correctly, raising the uncertainty (see section 1.1 and compare section 4.2.2). The validity of the simplified modeling approach for damage is presented in section 3.2. If time series are employed as an objective function for damage localization with a window that excludes the impulse phase, the algorithm locates damage in the wrong spot, the tower base element instead of the brace, which is the real damaged area. It is assumed that the system mainly vibrates in the first eigenmode, whereas the transient procedure immediately after the impulse load is skipped. Including the impulse phase in the time series considered in the objective function has a concise effect on the performance of the algorithm. With the complete transient procedure included in the evaluation of the objective function, the algorithm locates damage in the correct location in 50 percent of all optimization runs, allowing the use of the final objective function value to distinguish right from wrong solutions. This analysis underlines the importance of choosing the right data basis for model updating. A sensitivity analysis reveals that damages can be located at every cut depth above  $18.9mm$ . In this example,  $\rho^8$  returns best results whereas  $\rho^{l_2}$  performs worst, only the most severe damage can be located reliably using this metric.

Although the functionality in the rotor blade is proven using simulated data, the damage cannot be localized using this approach if applied to measurement data. Several reasons come into account for the malfunction of the damage localization algorithm in the rotor blade. The first and most important is the fact that damage occurs at the airfoil of the rotor blade and hence not at the load carrying

frame. This damage affects the global dynamic behavior of the blade only subordnately. Though being caused by mechanical loading, the effect of this damage on the global structural behavior is negligible, the damage is too small regarding decreased stiffness to be located. Comparison of measured eigenvectors before and after damage results in an average modal assurance criterion value of 0.99989, the sum of the deviations of the first seven eigenfrequencies is only 8.05%, meaning that each frequency differs by an average of 1.15%. These numbers quantify the diminutiveness of the occurred damage regarding the global structural behavior. Another reason may be the sensor set up (see Table 4.9). Damage occurs  $6m$  from the blade root, whereas the next sensor is installed at  $12m$ . This may affect the ability to determine structural changes only starting from the region of the sensor towards the blade tip. If  $\rho^{\omega+\phi}$  is used, and the damage is located in the area of this sensor. The results of using  $\rho^\tau$  also reveal a tendency towards this area being the damaged section. In the use of transmissibility functions presented here, only ten out of thirty functions are affected by the damage. The remaining contain relationships between sensors that do not cover the damaged area. Hence, the algorithm may fail because the effect of damage may be obliterated between all functions used.

Prestressed concrete towers are a new and economic construction for onshore wind turbines, enabling higher hub heights and more freedom in the design of new towers. The algorithm is applied to two different damage scenarios at a  $6m$  high scaled prestressed concrete tower for testing its damage localization capabilities in these structures. The two investigated damages include modified clamping conditions, and a  $22mm$  deep saw cut induced to one of the segments. The metrics  $\rho^{l_2}$  and  $\rho^\mu$ , used for quantification of the difference between measured data and numerical results, are compared concerning their performance for damage localization. These employ the Euclidean and Mahalanobis distance and are hence both time domain methods. Both damages can be located with  $\rho^\mu$ , but  $\rho^{l_2}$  is not effective in the location of the changing clamping conditions. This failure may indicate a too simple numerical model. In reality, the modified clamping causes a tilting foundation block, whereas it is modeled with rotational springs here, ignoring the contact nonlinearity between foundation block and ground. This may be an explanation why the modified clamping, which is much bigger damage, cannot be located thoroughly. Even with  $\rho^\mu$ , this damage is located in a few cases, but the parameter values modifying the rotational stiffness scatter heavily. The saw cut, which is much smaller damage regarding altering the global structural dynamics is successfully located with both metrics, and this damage does not cause nonlinear structural behavior. If  $\rho^\mu$  is employed, the parameter values are close to the real stiffness decrease.



# 6. Summary, Conclusion and Outlook

## 6.1. Summary

One of the major drawbacks of the growing complexity of sophisticated computational models for structural systems is their need for more parameters that may be unknown. In many cases, these parameters are hardly measurable which leads to numerical models that are heavily influenced by engineering assumptions and therefore simulation results that do not represent measured data recorded on the investigated structures. Model updating is an inverse strategy used for adaption of these parameters to contribute to better approximations of numerical models to measured data. In this thesis, the major challenges and tasks are addressed, and a new algorithm for model updating is presented to contribute to the research field of computational modeling of structural systems and model updating.

A general scheme for model updating is introduced, and the mathematical formulation of the model updating problem as a constrained optimization problem is given. The optimization problems are demonstrated to provide several local minima, both from a theoretical perspective as well as using practical examples. This section illustrates the need for global optimization algorithms in model updating. Constraints ensure the numerical model to remain within meaningful ranges. The proposed two-step method is a numerically efficient implementation of this scheme, employing Simulated Quenching to approximate the global solution and Sequential Quadratic Programming to find the exact solution locally. Various examples are employed to demonstrate the functionality of the proposed algorithm. These examples include both theoretical studies aiming to verify the general performance and practical examples used to confirm the efficiency using real measured data. The successful application of the algorithm for parameter identification is demonstrated using two examples, and the utilization of the algorithm for damage localization is explained. However, it is shown that damages must be big enough to be located successfully. In some examples, an outlook towards damage quantification is given, but damage quantification is beyond the scope of this thesis.

### 6.2. Conclusion

Different metrics are employed to compare simulation results and measured data. Metrics based on eigenfrequencies in combination with mode shapes, time domain, and frequency domain are implemented and compared concerning their performance for parameter identification and damage localization.

The first example comprises a simulated cantilever beam that is partially modeled by shell elements. Several shell elements are deleted to simulate a more realistic damage representation than the usual beam representation used in model updating. The same structure is simulated using beam elements. This beam model is then updated to responses of the damaged shell model. This investigation proves the applicability of beam elements for damage localization, even for small damages. Results are compared using a metric formulated based on power spectral densities, which is capable of efficiently reducing measurement noise. A second example applies the algorithm to a more complex representation of a virtual wind turbine, with complex loads acting on the structure and simulated damage. Damage is successfully located and can even be quantified using the presented approach based on a direct comparison of time series.

Furthermore, the framework is applied to a lab-scaled frame structure excited by a shaker, using real measured data. Acceleration signals are measured on each floor of the structure. The frame is modified using added masses, reduced stiffnesses and a supplementary nonlinearity with varying impact on the dynamic behavior. Comparing eigenfrequencies and mode shapes delivers best results in this analysis. As long as the nonlinearity is not activated, all parameters are identified successfully. Even their quantity is nearly matched. Modal properties are not used in case the nonlinearity is activated. Instead, time series are compared directly or using a metric in the frequency domain. The metric in the frequency domain delivers best results. However, the success of parameter identification decreases as the effect of the nonlinearity increases, prompting the need for more accurate modeling of the nonlinearity.

A metric based on transmissibility functions is applied to ice quantification at a 34.2m long wind turbine rotor blade and compared to the classical metric based on eigenfrequencies and mode shapes. Additional masses are applied to the tip of a rotor blade during an experiment in a real-scaled blade installed in a test rig to emulate icing, which usually starts at the blade tip. Successful localization of ice masses is demonstrated with modal properties only. The added ice masses are overestimated by this approach nearly linearly by factor two to three. A correction factor may be introduced that adjusts the identified additional mass to the real ice mass accreted on the blade. Although working fine in numerical analyses, model



updating using the metric based on transmissibility functions as presented in this thesis seems to be inefficient if measurement data are employed.

The application of model updating to damage localization is another interpretation of model updating and its results. The same algorithms and methods may be reused for this utilization. After an initial updating to undamaged measurement data and a damage event, the element stiffnesses of beam elements are set to be variable. The model is updated to the new measurement data recorded on a damaged structure. The application to a lab-scaled tripile structure, excited by impulse hammer strokes, reveals the importance of using the correct set of measurement data. Updating based on time series is not successful if the initial, complex vibrations after the excitation are not considered in model updating, whereas this is the case if these vibrations are included in the evaluation of the metric. The structure is damaged by gradually increasing damages. A sensitivity analysis confirms the observation that a transfer of time series to the frequency domain is beneficial because model updating is more sensitive using this approach. Saw cuts up to a depth of  $18.9\text{mm}$  can be localized using this technique, whereas only the most severe damage is localized using a direct comparison of time series. Modal properties perform on a medium level. A cut depth of  $37.6\text{mm}$  is successfully localized.

In a second experiment, the  $34.2\text{m}$  long wind turbine rotor blade is damaged. Fatigue damage occurs at  $6\text{m}$  from the blade root in the airfoil on both suction and pressure side. The damage cannot be localized because it is restricted to the airfoil. The airfoil has a minor influence on the global structural dynamic behavior, which is dominantly affected by the webs and girders of the rotor blade. Hence, the effect of this damage on the global structural behavior of the blade is limited and can hence not be located using the approach presented in this thesis.

Due to the limited success of the direct comparison of measured data and simulated results based on time series in the previous examples, a new time series comparison method is introduced and tested on a scaled model of a prestressed concrete tower. This metric is based on the Mahalanobis distance, and it is successfully applied to localize both artificially induced damage and a malfunction at the basement clamping that arose during the experiments. Because the clamping causes a nonlinearity, success is limited. The 'classical' metric employing  $\rho^{1/2}$  fails in locating this damage. Both metrics are successful in locating an artificial saw cut that reduces the bending stiffness locally by 8.3%.

Different metrics are used throughout this text to compare numerical results and measured data in both frequency and time domain. For linear cases, the classical approach using eigenfrequencies and mode shapes performs adequately, whereas a direct comparison of time series does not yield as good results. If nonlinearities exist, a transformation to the frequency domain seems beneficial. Alternatively,

## 6. Summary, Conclusion and Outlook

the Mahalanobis distance may be employed for comparison of transient signals in the time domain. A conclusion would be to use modal properties in case a linear behavior of the model is expected and switch to frequency domain or employ the Mahalanobis-distance, if nonlinearities are awaited. If none of these approaches yields expected results, it seems to be a good advice to check if all physical processes that influence the dynamics of the investigated structure are considered adequately in the numerical model.

Since the algorithm takes long time periods to identify structural changes, it is not feasible to apply it to real-time evaluations in structures being in service. However, an online application in structures is still imaginable, being started if other approaches, for instance, [70] and [163], detect damages. Then, damage localization may be started. Parameter identification should be repeated on a regular basis to account for changing conditions.

### 6.3. Outlook

Except for the structures excited by hammer strokes, loads acting on the structures are known in all examples examined throughout this thesis, either from free decay processes or measured shaker loads. Even if the structures are excited by a hammer, the load can be assumed known to some extent since the exact time and location are known. This assumption is often not the case in real environments, where complex load scenarios have a significant influence on the structural response measured by sensors on the structure. A way to tackle this is the use of Kalman filtering to approximate the loads and then update the models. The loads may be an additional factor during the updating process. Furthermore, environmental and operational conditions that heavily influence the structural dynamics of structures, especially in wind turbines, must be taken into account. A possible way to handle these would be to cluster measurement data to certain combinations of environmental and operational conditions and update individual models for each of these clusters.

Robust optimization methods may be beneficial to account for different uncertainty levels of the parameters. On the other hand, these have the drawback that more information on the parameters is needed to implement this approach. A combination of metrics from different domains may have a positive influence on the model updating results since more information would be considered by this approach. Although updating results from different metrics should be similar, Pareto optimization may help to compromise between results from different domains. Although damage localization at the rotor blade is not successful due to the limited influence on the global dynamic behavior, there are condition parameters that

successfully detect this damage [163], based on residues from stochastic subspace identification or autoregressive models. These residues may also be employed to quantify differences between numerical results and measured data, especially in the time domain. Furthermore, a state-space representation is built during stochastic subspace identification. This model may replace a 'conventional' finite element model that is updated to newly incoming measurement data.

To the best knowledge of the author, there is no reference data set for model updating that may be employed to test different updating approaches methods. For model updating, both construction and measurement data are needed. Access to these data is often restricted due to confidentiality reasons by operators and manufacturers of structural systems. Hence, creating a fully described reference data set for model updating would be beneficial for the research community because this would enable researchers to test new methods on this data set, making results comparable to previous results gained with different methods.

Although many examples in the text derive from applications in wind turbine structures, this is not the main focus of the thesis. All methods presented are intended to apply to all kinds of structural systems such as bridges, skyscrapers, and all other vibratory systems. Furthermore, the approach presented here could be transferred to other applications than structural dynamics. In fact, every numerical model that is validated using measurement data could be calibrated with the approach presented in this thesis.



# A. Calculation of stiffness reductions in circular cross sections

## A.1. Straight elimination of cross sectional area

The geometrical moment of inertia of a circular cross section is

$$I_{damage} = \frac{\pi}{4} \cdot (R^4 - r^4), \quad (\text{A.1})$$

with  $R$  and  $r$  denoting the outer and the inner radius of the tower, see Figure A.1. Two different states have to be considered, if the difference of moments of inertia after a straight cut shall be determined. The first state is a cut depth being smaller than the wall thickness. The geometrical moment of inertia of the removed area based on the center of mass of the removed area,  $I_{circleSegment}$  is calculated using

$$I_{circleSegment} = R^4 \cdot \left( \frac{4\alpha - \sin(4\alpha)}{16} - \frac{8 \sin^6(\alpha)}{9 \cdot (2\alpha - \sin(2\alpha))} \right). \quad (\text{A.2})$$

$\alpha$  denotes the angle between center line and outermost point of the cut, compare Figure A.1. Adding Steiner's theorem, the full influence of the reduction of the cross-section area yields

$$\Delta I = I_{circleSegment} + \left( \frac{4}{3} \cdot \frac{R \cdot \sin^3(\alpha)}{2\alpha - \sin(2\alpha)} \right)^2 \cdot \frac{R^2}{2} (2\alpha - \sin(2\alpha)). \quad (\text{A.3})$$

## A. Calculation of stiffness reductions in circular cross sections

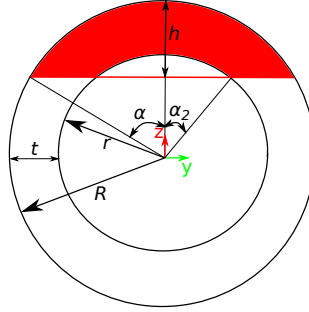


Figure A.1.: Geometrical properties of circle cross section in case of a straight cut. Removed area is marked in red.

Equation A.3 is valid, if the depth of the cut is smaller than the wall thickness  $t$  of the tower. If the depth is bigger than  $t$ ,  $\Delta I$  is obtained using

$$\begin{aligned} \Delta I = & I_{circleSegment} + \left( \frac{4}{3} \cdot \frac{R \cdot \sin^3(\alpha)}{2\alpha - \sin(2\alpha)} \right)^2 \cdot \frac{R^2}{2} (2\alpha - \sin(2\alpha)) \\ & - r^4 \cdot \left( \frac{4\alpha_2 - \sin(4\alpha_2)}{16} - \frac{8 \sin^6(\alpha_2)}{9 \cdot (2\alpha_2 - \sin(2\alpha_2))} \right) - \left( \frac{4}{3} \cdot \frac{r \cdot \sin^3(\alpha_2)}{2\alpha_2 - \sin(2\alpha_2)} + z_s \right)^2 \\ & \cdot \frac{r^2}{2} (2\alpha_2 - \sin(2\alpha_2)), \end{aligned} \quad (A.4)$$

where  $z_s$  denotes the deflection of the center of mass, which is determined using

$$z_s = \frac{2(R^3 - r^3) \sin(\Pi - \alpha)}{3(R^2 - r^2)(\Pi - \alpha)}. \quad (A.5)$$

The angles  $\alpha$  and  $\alpha_2$  are defined as

$$\alpha = \arccos \left( 1 - \frac{h}{R} \right) \quad (A.6a)$$

$$\alpha_2 = \arccos \left( 1 - \frac{h-t}{R-t} \right), \quad (A.6b)$$

with  $h$  denoting the depth of the cut.

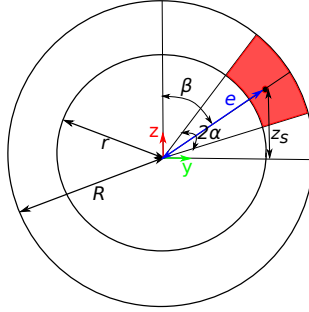


Figure A.2.: Geometrical properties of circle cross section in case of a angular elimination of area. Removed area is marked in red.

## A.2. Angular elimination of cross sectional area

The geometrical moment of inertia of a removed circle segment described by an angle  $\alpha$  (see Figure A.2) referred to the center of mass of this area is determined using

$$I_{yLocal} = \frac{(R^4 - r^4)(2\alpha + \sin(2\alpha))}{8} - e^2\alpha(R^2 - r^2), \quad (A.7)$$

with  $R$  and  $r$  denoting the outer and the inner radius and  $e$  denoting the distance from the center of the circle to the center of mass of the removed area (Fig. A.2). This distance is computed using

$$e = \frac{2(R^3 - r^3)\sin(\alpha)}{3(R^2 - r^2)\alpha}. \quad (A.8)$$

To consider a displacement of the removed area from the  $z$  axis by the angle  $\beta$ , the local coordinate system of the circle segment is transformed to the global one

$$I_{yGlobal} = \frac{1}{2}(I_{yLocal} + I_{zLocal}) + \frac{1}{2}(I_{yLocal} - I_{zLocal})\cos(2\beta) + I_{xyLocal} \cdot \sin(2\beta), \quad (A.9)$$

with

$$I_{zLocal} = \frac{(R^4 - r^4)(2\alpha - \sin(2\alpha))}{8} \quad (A.10)$$

## A. Calculation of stiffness reductions in circular cross sections

and  $I_{xyLocal} = 0$  due to symmetry. Furthermore, Steiner's theorem is added. Hence, the influence of the reduction of the cross-section area yields

$$I_{circleSegment} = I_{yGlobal} + z_s^2 \cdot A. \quad (\text{A.11})$$

$z_s$  denotes the distance from the y axis to the center of mass of the removed circle segment. It is calculated using

$$z_s = e \cdot \sin\left(\frac{\Pi}{4} - \beta\right). \quad (\text{A.12})$$

$A$  denotes the removed area which is determined by

$$A = (R^2 - r^2) \alpha. \quad (\text{A.13})$$



# Bibliography

- [1] ADAMS, R. ; CAWLEY, P. ; PYE, C. ; STONE, B. : A Vibration Technique for Non-Destructively Assessing the Integrity of Structures. In: *Journal of Mechanical Engineering Science* 20 (1978), Nr. 2, S. 93–100
- [2] AHMADIAN, H. ; MOTTERSHEAD, J. ; FRISWELL, M. : Regularisation methods for finite element model updating. In: *Mechanical Systems and Signal Processing* 12 (1998), Nr. 1, S. 47–64
- [3] ALLEMANG, R. : The modal assurance criterion—twenty years of use and abuse. In: *Sound and Vibration* 37 (2003), Nr. 8, S. 14–23
- [4] ANDRIEU, C. ; FREITAS, N. D. ; DOUCET, A. ; JORDAN, M. : An introduction to MCMC for machine learning. In: *Machine learning* 50 (2003), Nr. 1-2, S. 5–43
- [5] ANTONIADOU, I. ; DERVILIS, N. ; PAPTHEOU, E. ; MAGUIRE, A. ; WORDEN, K. : Aspects of structural health and condition monitoring of offshore wind turbines. In: *Phil. Trans. R. Soc. A* 373 (2015), Nr. 2035, S. 20140075
- [6] ARORA, J. : *Introduction to Optimum Design*. third edition. Elsevier, 2012
- [7] ASTROZA, R. ; EBRAHIMIAN, H. ; LI, Y. ; CONTE, J. : Bayesian nonlinear structural FE model and seismic input identification for damage assessment of civil structures. In: *Mechanical Systems and Signal Processing* 93 (2017), S. 661–687
- [8] AVITABILE, P. ; PECHINSKY, F. ; O'CALLAHAN, J. : Study of Vector Correlation using Various Techniques for Model Reduction. In: *IMAC X*, , Kissemmee, USA, 1992, S. 572–583
- [9] BAKIR, P. ; REYNDERS, E. ; ROECK, G. D. : An improved finite element model updating method by the global optimization technique ‘Coupled Local Minimizers’. In: *Computers and Structures* 86 (2008), Nr. 11-12, S. 1339–1352
- [10] BALAGEAS, D. ; FRITZEN, C. ; GÜEMES, A. : *Structural Health Monitoring*. ISTE Ltd, 2006
- [11] BALMÈS, E. : Review and evaluation of shape expansion methods. In: *International Modal Analysis Conference*, 2000, S. 555–561
- [12] BARUCH, M. : Optimization Procedure to Correct Stiffness and Flexibility Matrices Using Vibration Tests. In: *AIAA Journal* 16 (1978), Nr. 11, S. 1208–1210
- [13] BARUCH, M. : Optimal correction of mass and stiffness matrices using measured modes. In: *AIAA journal* 20 (1982), Nr. 11, S. 1623–1626
- [14] BAYES, T. : An Essay towards solving a problem in the doctrine of chances. In: *Philosophical Transactions of the Royal Society* (1763), S. 370–418

## Bibliography

- [15] BEASLEY, D. ; BULL, D. ; MARTIN, R. : A sequential niche technique for multimodal function optimization. In: *Evolutionary computation* 1 (1993), Nr. 2, S. 101–125
- [16] BECK, J. ; KATAFYGIOTIS, L. : Updating models and their uncertainties. I: Bayesian statistical framework. In: *Journal of Engineering Mechanics* 124 (1998), Nr. 4, S. 455–461
- [17] BEHMANESH, I. ; MOAVENI, B. ; LOMBAERT, G. ; PAPADIMITRIOU, C. : Hierarchical Bayesian model updating for structural identification. In: *Mechanical Systems and Signal Processing* 64 (2015), S. 360–376
- [18] BOGGS, P. ; TOLLE, J. : Sequential Quadratic Programming. In: *Acta Numerica* 4 (1995), S. 1–51
- [19] BÖGL, S. ; KNITL, J. ; HIERL, M. : *Tower of a wind power plant and method for producing a tower of a wind power plant*. Dez. 22 2011. – US Patent 9,091,095
- [20] BOULKAIBET, I. ; MTHEMBU, L. ; NETO, F. D. L. ; MARWALA, T. : Finite element model updating using fish school search and volitive particle swarm optimization. In: *Integrated Computer-Aided Engineering* 22 (2015), Nr. 4, S. 361–376
- [21] BOX, G. ; JENKINS, G. ; REINSEL, G. ; LJUNG, G. : *Time series analysis: forecasting and control*. John Wiley & Sons, 2015
- [22] BRINCKER, R. ; ANDERSEN, P. : ARMA Models in Modal Space. In: *IMAC XVII, Kissemmee, USA* (1999)
- [23] BRINCKER, R. ; ANDERSEN, P. : Understanding stochastic subspace identification. In: *Proceedings of the 24th IMAC, St. Louis, Missouri* (2006), S. 279–311
- [24] BRINCKER, R. ; ZHANG, L. ; ANDERSEN, P. : Modal identification of output-only systems using frequency domain decomposition. In: *Smart materials and structures* 10 (2001), Nr. 3, S. 441
- [25] BROWNJOHN, J. ; XIA, P. ; HAO, H. ; XIA, Y. : Civil structure condition assessment by FE model updating:: methodology and case studies. In: *Finite elements in analysis and design* 37 (2001), Nr. 10, S. 761–775
- [26] BROYDEN, C. : The convergence of a class of double-rank minimization algorithms 1. general considerations. In: *IMA Journal of Applied Mathematics* 6 (1970), Nr. 1, S. 76–90
- [27] BYRD, R. ; SCHNABEL, R. ; SHULTZ, G. : A trust region algorithm for nonlinearly constrained optimization. In: *SIAM Journal on Numerical Analysis* 24 (1987), Nr. 5, S. 1152–1170
- [28] CARDEN, E. ; FANNING, P. : Vibration Based Condition Monitoring: A Review. In: *Structural Health Monitoring* 3 (2004), Nr. 4, S. 355–377
- [29] CHEN, H. : Application of regularization methods to damage detection in large scale plane frame structures using incomplete noisy modal data. In: *Engineering Structures* 30 (2008), Nr. 11, S. 3219–3227
- [30] CHEUNG, S. ; BECK, J. : Bayesian model updating using hybrid Monte Carlo simulation with application to structural dynamic models with many uncertain parameters. In: *Journal of engineering mechanics* 135 (2009), Nr. 4, S. 243–255

- [31] CIANG, C. ; LEE, J. ; BANG, H. : Structural health monitoring for a wind turbine system: a review of damage detection methods. In: *Measurement Science and Technology* 19 (2008), Nr. 12
- [32] COBB, R. ; LIEBST, B. : Structural Damage Identification Using Assigned Partial Eigenstructure. In: *AIAA Journal* 35 (1997), Nr. 1, S. 152–158
- [33] COLLINS, J. ; YOUNG, J. ; KIEFLING, L. : Methods and application of system identification in shock and vibration. In: *System identification of vibrating structures: mathematical models from test data*, 1972, S. 45–71
- [34] DEVRIENDT, C. : *On the use of transmissibility functions in operational modal analysis*, Vrije Universiteit Brussel, Diss., 2010
- [35] DEVRIENDT, C. ; PRESEZNIAK, F. ; SITTER, G. D. ; VANBRABANT, K. ; TROYER, T. D. ; VANLANDUIT, S. ; GUILLAUME, P. : Structural health monitoring in changing operational conditions using transmissibility measurements. In: *Shock and Vibration* 17 (2010), Nr. 4-5, S. 651–675
- [36] DOEBLING, S. ; FARRAR, C. ; PRIME, M. ; SHEVITZ, D. : Damage identification and health monitoring of structural and mechanical systems from changes in their vibration characteristics: a literature review. (1996)
- [37] DUBOIS, J. ; MUSKULUS, M. ; SCHAUMANN, P. : Advanced representation of tubular joints in jacket models for offshore wind turbine simulation. In: *Energy Procedia* 35 (2013), S. 234–243
- [38] EGLESE, R. : Simulated annealing: a tool for operational research. In: *European journal of operational research* 46 (1990), Nr. 3, S. 271–281
- [39] EWINS, D. : Model Validation: Correlation for Updating. In: *Sadhana Academy Proceedings in Engineering Sciences* 25 (2000), Nr. 3, S. 221–234
- [40] EWINS, D. : *Modal Testing: Theory, Practice and Application*. Research Studies Press, 2000
- [41] FANG, S. ; PERERA, R. ; ROECK, G. D.: Damage identification of a reinforced concrete frame by finite element model updating using damage parameterization. In: *Journal of Sound and Vibration* 313 (2008), Nr. 3, S. 544–559
- [42] FARRAR, C. ; WORDEN, K. : An introduction to structural health monitoring. In: *Philosophical Transactions of the Royal Society* 365 (2007), S. 303–315
- [43] FARRAR, C. ; WORDEN, K. : *Structural health monitoring: a machine learning perspective*. John Wiley & Sons, 2012
- [44] FENG, D. ; FENG, M. : Model updating of railway bridge using in situ dynamic displacement measurement under trainloads. In: *Journal of Bridge Engineering* 20 (2015), Nr. 12, S. 04015019
- [45] FIGUEIREDO, E. ; PARK, G. ; FIGUEIRAS, J. ; FARRAR, C. ; WORDEN, K. : Structural health monitoring algorithm comparisons using standard data sets. In: *Los Alamos National Laboratory: LA-14393* 6 (2009)

## Bibliography

- [46] FINNILA, A. ; GOMEZ, M. ; SEBENIK, C. ; STENSON, C. ; DOLL, J. : Quantum annealing: A new method for minimizing multidimensional functions. In: *Chemical Physics Letters* 219 (1994), Nr. 5-6, S. 343–348
- [47] FLETCHER, R. : A new approach to variable metric algorithms. In: *The computer journal* 13 (1970), Nr. 3, S. 317–322
- [48] FLETCHER, R. : *Practical methods of optimization*. John Wiley & Sons, 2013
- [49] FOTI, D. ; DIAFERIO, M. ; GIANNOCCARO, N. ; MONGELLI, M. : Ambient vibration testing, dynamic identification and model updating of a historic tower. In: *NDT & e International* 47 (2012), S. 88–95
- [50] FOTI, D. ; GATTULLI, V. ; POTENZA, F. : Output-Only Identification and Model Updating by Dynamic Testing in Unfavorable Conditions of a Seismically Damaged Building. In: *Computer-Aided Civil and Infrastructure Engineering* 29 (2014), Nr. 9, S. 659–675
- [51] FRISWELL, M. : The Adjustment of Structural Parameters using a Minimum Variance Estimator. In: *Mechanical Systems and Signal Processing* 3 (1989), Nr. 2, S. 143–155
- [52] FRISWELL, M. : Calculation of second and higher order eigenvector derivatives. In: *Journal of Guidance, Control, and Dynamics* 18 (1995), Nr. 4, S. 919–921
- [53] FRISWELL, M. ; INMAN, D. ; PILKEY, D. : Direct updating of damping and stiffness matrices. In: *AIAA journal* 36 (1998), Nr. 3, S. 491–493
- [54] FRISWELL, M. ; MOTTERSHEAD, J. : Best practice in finite element model updating. In: *International Forum on Aeroelasticity and Structural Dynamics*, 1995, S. 2:51–1 – 57–11
- [55] FRISWELL, M. ; MOTTERSHEAD, J. : *Finite Element Model Updating in Structural Dynamics*. Kluwer Academic Publishers, 1995
- [56] FRISWELL, M. ; MOTTERSHEAD, J. ; AHMADIAN, H. : Combining subset selection and parameter constraints in model updating. In: *Journal of Vibration and Acoustics* 120 (1998), Nr. 4, S. 854–859
- [57] FRITZEN, C. : Vibration-based structural health monitoring concepts and applications. In: *Key Engineering Materials* 293 (2005), S. 3–20
- [58] FU, Y. ; LU, Z. ; LIU, J. : Damage identification in plates using finite element model updating in time domain. In: *Journal of sound and vibration* 332 (2013), Nr. 26, S. 7018–7032
- [59] GARCIA-PALENCIA, A. ; SANTINI-BELL, E. ; SIPPLE, J. ; SANAYEI, M. : Structural model updating of an in-service bridge using dynamic data. In: *Structural Control and Health Monitoring* 22 (2015), Nr. 10, S. 1265–1281
- [60] GASCH, R. ; KNOTHE, K. : *Strukturdynamik*. Bd. 1- Diskrete Systeme. Springer-Verlag, 1987
- [61] GEBHARDT, C. ; ROCCIA, B. : Non-linear aeroelasticity: An approach to compute the response of three-blade large-scale horizontal-axis wind turbines. In: *Renewable Energy* 66 (2014), S. 495–514

- [62] GILL, P. ; MURRAY, W. ; SAUNDERS, M. : SNOPT: An SQP Algorithm for Large-Scale Constrained Optimization. In: *SIAM review* 47 (2005), Nr. 1, S. 99–131
- [63] GOLDFARB, D. : A family of variable-metric methods derived by variational means. In: *Mathematics of computation* 24 (1970), Nr. 109, S. 23–26
- [64] GRANVILLE, V. ; KŘIVÁNEK, M. ; RASSON, J. : Simulated annealing: A proof of convergence. In: *Pattern Analysis and Machine Intelligence, IEEE Transactions on* 16 (1994), Nr. 6, S. 652–656
- [65] GUDMUNDSON, P. : The dynamic behaviour of slender structures with cross-sectional cracks. In: *Journal of the Mechanics and Physics of Solids* 31 (1983), Nr. 4, S. 329–345
- [66] HAAKE, G. : *Systemidentifikation mit Autoregressiven Modellen und Validierung numerischer Strukturmodelle bei Offshore- Windenergieanlagen*. Mitteilungen des Instituts fuer Statik und Dynamik der Leibniz Universitaet Hannover, 2010
- [67] HÄCKELL, M. : *A Holistic Evaluation Concept for Long-Term Structural Health Monitoring*, Leibniz Universität Hannover, Germany, Dissertation, 2015
- [68] HÄCKELL, M. ; ROLFES, R. : Long-term Monitoring of Modal Parameters for SHM at a 5 MW Offshore Wind Turbine. In: *Proceedings of the 9th International Workshop on Structural Health Monitoring*. Stanford, California, USA : Proceedings, 2013, S. 1310–1317
- [69] HÄCKELL, M. ; ROLFES, R. : Monitoring a 5 MW offshore wind energy converter - Condition parameters and triangulation based extraction of modal parameters. In: *Mechanical Systems and Signal Processing* 40 (2013), S. 322–343
- [70] HÄCKELL, M. ; ROLFES, R. ; KANE, M. ; LYNCH, J. : Three-Tier Modular Structural Health Monitoring Framework Using Environmental and Operational Condition Clustering for Data Normalization: Validation on an Operational Wind Turbine System. In: *Proceedings of the IEEE* 104 (2016), Nr. 8, S. 1632–1646
- [71] HÄFELE, J. ; HÜBLER, C. ; GEBHARDT, C. ; ROLFES, R. : An improved two-step soil-structure interaction modeling method for dynamical analyses of offshore wind turbines. In: *Applied Ocean Research* 55 (2016), S. 141–150
- [72] HALLING, M. ; MUHAMMAD, I. ; WOMACK, K. : Dynamic field testing for condition assessment of bridge bents. In: *Journal of Structural Engineering* 127 (2001), Nr. 2, S. 161–167
- [73] HAO, H. ; XIA, Y. : Vibration-based damage detection of structures by genetic algorithm. In: *Journal of computing in civil engineering* 16 (2002), Nr. 3, S. 222–229
- [74] HARTMANN, D. ; SMARSLY, K. ; LAW, K. : Coupling sensor-based structural health monitoring with finite element model updating for probabilistic lifetime estimation of wind energy converter structures. In: *Proceedings of the 8th international workshop on structural health monitoring*, 2011, S. 13–15
- [75] JACOBSEN, N. ; ANDERSEN, P. ; BRINCKER, R. : Using enhanced frequency domain decomposition as a robust technique to harmonic excitation in operational

- modal analysis. In: *Proceedings of ISMA2006: international conference on noise & vibration engineering*, 2006, S. 18–20
- [76] JAHJOU, M. ; NACKENHORST, U. : A modified harmony search approach on structural identification and damage detection of wind turbine supporting structures. In: *Journal of Vibroengineering* 18 (2016), Nr. 1, S. 103–118
- [77] JAISHI, B. ; REN, W. : Structural Finite Element Model Updating Using Ambient Vibration Test Results. In: *Journal of Structural Engineering* 131 (2005), Nr. 4, S. 617–628
- [78] JANG, J. ; YEO, I. ; SHIN, S. ; CHANG, S. : Experimental investigation of system-identification-based damage assessment on structures. In: *Journal of Structural Engineering* 128 (2002), Nr. 5, S. 673–682
- [79] JANG, S. ; LI, J. ; JR, B. S.: Corrosion estimation of a historic truss bridge using model updating. In: *Journal of Bridge Engineering* 18 (2012), Nr. 7, S. 678–689
- [80] JONKMAN, J. : The new modularization framework for the FAST wind turbine CAE tool. In: *51st AIAA Aerospace Sciences Meeting including the New Horizons Forum and Aerospace Exposition* The American Institute of Aeronautics and Astronautics, 2013, 2013, S. 1–26
- [81] JONKMAN, J. ; BUTTERFIELD, S. ; MUSIAL, W. ; SCOTT, G. : Definition of a 5-MW reference wind turbine for offshore system development. In: *National Renewable Energy Laboratory, Golden, CO, Technical Report No. NREL/TP-500-38060* (2009)
- [82] JUANG, J. ; PAPPAS, R. : An eigensystem realization algorithm for modal parameter identification and model reduction. In: *Journal of Guidance, Control and Dynamics* 8 (1985), Nr. 5, S. 620–627
- [83] KAMMER, D. : Correlation Considerations-Part 2 Model Reduction Using Modal, Serep, and Hybrid. In: *Proceedings-SPIE International Society For Optical Engineering* Bd. 1, 1998, S. 177–184
- [84] KENNEDY, J. : Particle Swarm Optimization. In: *Encyclopedia of Machine Learning*. Springer, 2010, S. 760–766
- [85] KENNEDY, M. ; O'HAGAN, A. : Bayesian calibration of computer models. In: *Journal of the Royal Statistical Society: Series B (Statistical Methodology)* 63 (2001), Nr. 3, S. 425–464
- [86] KHAN, Z. ; PRASAD, B. ; SINGH, T. : Machining condition optimization by genetic algorithms and simulated annealing. In: *Computers Operations Research* 24 (1997), Nr. 7, S. 647–657
- [87] KHODAPARAST, H. ; MOTTERSHEAD, J. ; BADCOCK, K. : Interval model updating with irreducible uncertainty using Kriging predictor. In: *Mechanical Systems and Signal Processing* 25 (2010), S. 1204–1226
- [88] KIM, J. ; RYU, Y. ; CHO, H. ; STUBBS, N. : Damage identification in beam-type structures: frequency-based method vs mode-shape-based method. In: *Engineering Structures* 25 (2003), Nr. 1, S. 57–67

- [89] KIRKPATRICK, S. ; GELATT, C. ; VECCHI, M. : Optimization by simulated annealing. In: *science* 220 (1983), Nr. 4598, S. 671–680
- [90] KOH, C. ; SEE, L. ; BALENDRA, T. : Damage detection of buildings: numerical and experimental studies. In: *Journal of Structural Engineering* 121 (1995), Nr. 8, S. 1155–1160
- [91] KUHN, H. ; TUCKER, A. : Nonlinear programming. In: *Proc. of the second Berkeley Symposium on Mathematical Statistics and Probability*, Univ. of California Press, 1951, S. 481–492
- [92] KURT, M. ; MOORE, K. ; ERITEN, M. ; MCFARLAND, D. ; BERGMAN, L. ; VAKAKIS, A. : Nonlinear model updating applied to the IMAC XXXII Round Robin benchmark system. In: *Mechanical Systems and Signal Processing* 88 (2017), S. 111–122
- [93] LEWIS, J. : Fast normalized cross-correlation. In: *Vision interface* Bd. 10, 1995, S. 120–123
- [94] LI, J. ; LAW, S. ; DING, Y. : Substructure damage identification based on response reconstruction in frequency domain and model updating. In: *Engineering Structures* 41 (2012), S. 270–284
- [95] LINDEMANN, S. : *Model Updating an einem biegeelastischen Rotor*. Kassel University Press GmbH, 2008
- [96] LINK, M. : Updating of analytical models—review of numerical procedures and application aspects. In: *Structural Dynamics Forum SD2000*, 1999, S. 1–31
- [97] LIU, X. : *System Identification of a Wind Energy Converter using Wavelet-based Damage Detection and Robust Model Updating Strategy*, Ruhr Universitaet Bochum, Dissertation, 2013
- [98] LJUNG, L. : *System Identification*. Springer, 1998
- [99] LUCZAK, M. ; MANZATO, S. ; PEETERS, B. ; BRANNER, K. ; BERRING, P. ; KAHSIN, M. : Updating finite element model of a wind turbine blade section using experimental modal analysis results. In: *Shock and Vibration* 2014 (2014)
- [100] MARES, C. ; MOTTERSHEAD, J. ; FRISWELL, M. : Stochastic model updating: part 1—theory and simulated example. In: *Mechanical Systems and Signal Processing* 20 (2006), Nr. 7, S. 1674–1695
- [101] MARWALA, T. : Fault identification using neural networks and vibration data. In: *Doctor of Philosophy, University of Cambridge* (2001)
- [102] MARWALA, T. : *Finite-element-model updating using computational intelligence techniques: applications to structural dynamics*. Springer, 2010
- [103] MAX BÖGL WIND AG: *Hybridturm System Max Bögl*. 2016
- [104] MERUANE, V. ; HEYLEN, W. : An hybrid real genetic algorithm to detect structural damage using modal properties. In: *Mechanical Systems and Signal Processing* 25 (2011), Nr. 5, S. 1559–1573
- [105] MESSAC, A. : *Optimization in Practice with Matlab for Engineering Students and Professionals*. Cambridge University Press, 2015

## Bibliography

- [106] METROPOLIS, N. ; ULAM, S. : The Monte Carlo Method. In: *Journal of the American Statistical Association* 44 (1949), Nr. 247, S. 335–341
- [107] MITCHELL, M. : *An Introduction to Genetic Algorithms*. Massachusetts Institute of Technology, 1998
- [108] MOELLER, P. ; FRIBERG, O. : Updating large finite element models in structural dynamics. In: *AIAA journal* 36 (1998), Nr. 10, S. 1861–1868
- [109] MOJTAHEDI, A. ; LOTFOLLAHI, Y. ; HASSANZADEH, Y. ; ETTEFAGH, M. ; AMINFAR, M. ; AGHDAM, A. : Developing a robust SHM method for offshore jacket platform using model updating and fuzzy logic system. In: *Applied Ocean Research* 33 (2011), Nr. 4, S. 398–411
- [110] MORASSI, A. ; ROVERE, N. : Localizing a notch in a steel frame from frequency measurements. In: *Journal of Engineering Mechanics* 123 (1997), Nr. 5, S. 422–432
- [111] MOTTERSHEAD, J. ; FRISWELL, M. : Model Updating in Structural Dynamics: A Survey. In: *Journal of Sound and Vibration* 167 (1993), Nr. 2, S. 347–375
- [112] MOTTERSHEAD, J. ; LINK, M. ; FRISWELL, M. : The sensitivity method in finite element model updating: a tutorial. In: *Mechanical systems and signal processing* 25 (2011), Nr. 7, S. 2275–2296
- [113] MOTTERSHEAD, J. ; MARES, C. ; JAMES, S. ; FRISWELL, M. : Stochastic Model Updating: Part 2 - Application to a set of physical structures. In: *Mechanical Systems and Signal Processing* 20 (2006), S. 2171–2185
- [114] MÜLLER-GRONBACH, T. ; NOVAK, E. ; RITTER, K. : *Monte Carlo-Algorithmen*. Springer-Verlag, 2012
- [115] MUSTAFA, S. ; DEBNATH, N. ; DUTTA, A. : Bayesian probabilistic approach for model updating and damage detection for a large truss bridge. In: *International Journal of Steel Structures* 15 (2015), Nr. 2, S. 473–485
- [116] MUTO, M. ; BECK, J. : Bayesian Updating and Model Class Selection for Hysteretic Structural Models Using Stochastic Simulation. In: *Journal of Vibration and Control* 14 (2008), Nr. 1-2, S. 7–34
- [117] NAEIM, F. ; KELLY, J. : *Design of seismic isolated structures: from theory to practice*. John Wiley & Sons, 1999
- [118] NATKE, H. : Vergleich von Algorithmen für die Anpassung des Rechenmodells einer schwingungsfähigen elastomechanischen Struktur an Versuchswerte. In: *ZAMM-Journal of Applied Mathematics and Mechanics/Zeitschrift für Angewandte Mathematik und Mechanik* 59 (1979), Nr. 6, S. 257–268
- [119] NATKE, H. : Updating computational models in the frequency domain based on measured data: a survey. In: *Probabilistic Engineering Mechanics* 3 (1988), Nr. 1, S. 28–35
- [120] NATKE, H. : Error localization within spatially finite-dimensional mathematical models. In: *Computational Mechanics* 8 (1991), Nr. 3, S. 153–160
- [121] NATKE, H. : *Einführung in Theorie und Praxis der Zeitreihen- und Modalanalyse*. 3. Vieweg, 1992



- [122] NATKE, H. : On regularization methods within system identification. In: *Inverse problems in engineering mechanics*. Springer, 1993, S. 3–20
- [123] NATKE, H. ; LALLEMENT, G. ; COTTIN, N. ; PRELLS, U. : Properties of various residuals within updating of mathematical models. In: *Inverse Problems in Engineering I* (1995), Nr. 4, S. 329–348
- [124] NEGRO, V. ; LÓPEZ-GUTIÉRREZ, J. ; ESTEBAN, M. ; MATUTANO, C. : Uncertainties in the design of support structures and foundations for offshore wind turbines. In: *Renewable energy* 63 (2014), S. 125–132
- [125] NELSON, R. : Simplified calculation of eigenvector derivatives. In: *AIAA Journal* 14 (1976), Nr. 9, S. 1201–1205
- [126] NOCEDAL, J. ; WRIGHT, S. : *Numerical Optimization*. Springer, 2006
- [127] NOZARI, A. ; BEHMANESH, I. ; YOUSEFIANMOGHADAM, S. ; MOAVENI, B. ; STAVRIDIS, A. : Effects of variability in ambient vibration data on model updating and damage identification of a 10-story building. In: *Engineering Structures* 151 (2017), S. 540–553
- [128] O'BRIEN, T. : Stiffness change as a nondestructive damage measurement. In: *Mechanics of nondestructive testing*. Springer, 1980, S. 101–121
- [129] OVERSCHEE, P. V. ; MOOR, B. D.: *Subspace Identification for Linear Systems: Theory, Implementation, Applications*. Kluwer Academic Publishers, 1996
- [130] PANDEY, A. ; BISWAS, M. ; SAMMAN, M. : Damage detection from changes in curvature mode shapes. In: *Journal of sound and vibration* 145 (1991), Nr. 2, S. 321–332
- [131] PAPADIMITRIOU, C. ; BECK, J. L. ; AU, S.-K. : Entropy-based optimal sensor location for structural model updating. In: *Journal of Vibration and Control* 6 (2000), Nr. 5, S. 781–800
- [132] PARK, G. ; MUNTGES, D. ; INMAN, D. : Self-Monitoring and Self-Healing Jointed Structures. In: *Key Engineering Materials* 204-205 (2001), S. 75–84
- [133] PATELLI, E. ; GOVERS, Y. ; BROGGI, M. ; GOMES, H. ; LINK, M. ; MOTTERSHEAD, J. : Sensitivity or Bayesian model updating: a comparison of techniques using the DLR AIRMOD test data. In: *Archiv of Applied Mechanics* 87 (2017), Nr. 5, S. 905–925
- [134] PAULTRE, P. : *Dynamics of structures*. John Wiley & Sons, 2013
- [135] PEETERS, B. ; ROECK, G. D.: Stochastic system identification for operational modal analysis: a review. In: *Journal of Dynamic Systems, Measurement, and Control* 123 (2001), Nr. 4, S. 659–667
- [136] PERERA, R. ; TORRES, R. : Structural damage detection via modal data with genetic algorithms. In: *Journal of Structural Engineering* 132 (2006), Nr. 9, S. 1491–1501
- [137] RATH, T. ; MANMATHA, R. : Word image matching using dynamic time warping. In: *Computer Vision and Pattern Recognition, 2003. Proceedings. 2003 IEEE Computer Society Conference on* Bd. 2 IEEE, 2003, S. II–II

## Bibliography

- [138] ROHDE, S. ; IFJU, P. ; SANKAR, B. : Experimental Quantification of Bend-Twist Coupling in Composite Shafts. In: *Advancement of Optical Methods in Experimental Mechanics, Volume 3*. Springer, 2016, S. 63–70
- [139] ROLFES, R. ; SCHAUMANN, P. : *Ganzheitliches Dimensionierungskonzept fuer OWEA- Tragstrukturen anhand von Messungen im Offshore- Testfeld alpha ventus: Abschlussbericht GIGAWIND alpha ventus*. Shaker, 2013
- [140] ROSS, S. : *Stochastic Processes*. John Wiley and Sons, 1996
- [141] RUTENBAR, R. : Simulated annealing algorithms: an overview. In: *Circuits and Devices Magazine, IEEE* 5 (1989), Nr. 1, S. 19–26
- [142] RYTTER, A. : *Vibration based Inspection of Civil Engineering Structures*. Aalborg Universitetsforlag, 1994
- [143] SALEEM, Z. : Alternatives and modifications of Monopile foundation or its installation technique for noise mitigation. In: *Report by Delft University of Technology for Stichting De Noordzee (the North Sea Foundation)* (2011)
- [144] SCHLIPF, D. ; SCHULER, S. ; GRAU, P. ; ALLGOEWER, F. ; KUEHN, M. : Look-ahead cyclic pitch control using lidar. In: *Torque 2010: the science of making torque from wind*, 2010, S. 1–4
- [145] SCHMIDT, B. ; ERNST, B. ; WILMS., M. ; HILDEBRANDT, A. ; HANSEN, M. : Messdatenbasierte Empfehlungen von Wind-und Wellenparametern für die Auslegung von Offshore-Windenergieanlagen. In: *Bautechnik* 91 (2014), Nr. 8, S. 533–542
- [146] SCHRÖDER, K. ; GEBHARDT, C. ; ROLFES, R. : Damage Localization at Wind Turbine Support Structures Using Sequential Quadratic Programming for Model Updating. In: *8th European Workshop On Structural Health Monitoring, Bilbao*, 2016, S. 1–10
- [147] SCHRÖDER, K. ; GEBHARDT, C. ; ROLFES, R. : A two-step approach to damage localization at supporting structures of offshore wind turbines. In: *Structural Health Monitoring* (2017)
- [148] SCHRÖDER, K. ; ROLFES, R. : Application of a Finite Element Model Updating Approach to Damage Localization at Offshore Wind Energy Converters. In: *International Workshop on Structural Health Monitoring (IWHSM)*, 2015, S. 1–8
- [149] SCHRÖDER, K. ; SCHOLLE, N. ; ROLFES, R. ; LOHAUS, L. : An Approach for Local-Global Structural Health Monitoring for Offshore Wind Energy Converters. In: *International Wind Engineering Conference*, 2014, S. 1–8
- [150] SEIFERT, H. : Betrieb von Windenergieanlagen unter Vereisungsbedingungen–Ergebnisse und Empfehlungen aus einem EU–Forschungsprojekt; AUF· WIND 99 St. In: *Pöltten, October* (1999), S. 21–22
- [151] SHABBIR, F. ; OMENZETTER, P. : Particle swarm optimization with sequential niche technique for dynamic finite element model updating. In: *Computer-Aided Civil and Infrastructure Engineering* 30 (2015), Nr. 5, S. 359–375

- [152] SHADAN, F. ; KHOSHNOUDIAN, F. ; ESFANDIARI, A. : A frequency response-based structural damage identification using model updating method. In: *Structural Control and Health Monitoring* 23 (2016), Nr. 2, S. 286–302
- [153] SHANNO, D. : Conditioning of quasi-Newton methods for function minimization. In: *Mathematics of computation* 24 (1970), Nr. 111, S. 647–656
- [154] SIMOEN, E. ; PAPADIMITRIOU, C. ; LOMBAERT, G. : On prediction error correlation in Bayesian model updating. In: *Journal of Sound and Vibration* 332 (2013), Nr. 18, S. 4136–4152
- [155] SIMOEN, E. ; ROECK, G. D. ; LOMBAERT, G. : Dealing with uncertainty in model updating for damage assessment: A review. In: *Mechanical Systems and Signal Processing* 56-57 (2014), S. 123–149
- [156] SIPPLE, J. ; SANAYEI, M. : Finite element model updating using frequency response functions and numerical sensitivities. In: *Structural Control and Health Monitoring* 21 (2014), Nr. 5, S. 784–802
- [157] SONG, H. ; DAMIANI, R. ; ROBERTSON, A. ; JONKMAN, J. : A new structural-dynamics module for offshore multimember substructures within the wind turbine computer-aided engineering tool fast. In: *The Twenty-third International Offshore and Polar Engineering Conference* International Society of Offshore and Polar Engineers, 2013, S. 1–12
- [158] STEENACKERS, G. ; DEVRIENDT, C. ; GUILLAUME, P. : On the use of transmissibility measurements for finite element model updating. In: *Journal of sound and vibration* 303 (2007), Nr. 3, S. 707–722
- [159] TACIROGLU, E. ; GHAHARI, S. ; ABAZARSA, F. : Efficient model updating of a multi-story frame and its foundation stiffness from earthquake records using a timoshenko beam model. In: *Soil Dynamics and Earthquake Engineering* 92 (2017), S. 25–35
- [160] TEUGHELS, A. ; MAECK, J. ; ROECK, G. D.: Damage assessment by FE model updating using damage functions. In: *Computers and Structures* 80 (2002), Nr. 25, S. 1869–1879
- [161] TEUGHELS, A. ; ROECK, G. D.: Structural damage identification of the highway bridge Z24 by FE model updating. In: *Journal of Sound and Vibration* 278 (2004), Nr. 3, S. 589–610
- [162] TEUGHELS, A. ; ROECK, G. D. ; SUYKENS, J. : Global optimization by coupled local minimizers and its application to FE model updating. In: *Computers & structures* 81 (2003), Nr. 24, S. 2337–2351
- [163] TSIAPOKI, S. ; HÄCKELL, M. ; GRIESSMANN, T. ; ROLFES, R. : Damage and ice detection on wind turbine rotor blades using a three-tier modular structural health monitoring framework. In: *Structural Health Monitoring* (2017), S. 1–24
- [164] VASAN, A. ; RAJU, K. : Comparative analysis of simulated annealing, simulated quenching and genetic algorithms for optimal reservoir operation. In: *Applied Soft Computing* 9 (2009), Nr. 1, S. 274–281

## Bibliography

- [165] VELAZQUEZ, A. ; SWARTZ, R. : Operational model updating of low-order horizontal axis wind turbine models for structural health monitoring applications. In: *Journal of Intelligent Material Systems and Structures* 26 (2015), Nr. 13, S. 1739–1752
- [166] WAECHTER, M. ; HEISSELMANN, H. ; HOELLING, M. ; MORALES, A. ; MILAN, P. ; MUECKE, T. ; PEINKE, J. ; REINKE, N. ; RINN, P. : The turbulent nature of the atmospheric boundary layer and its impact on the wind energy conversion process. In: *Journal of Turbulence* 13 (2012)
- [167] WAHAB, M. ; ROECK, G. D. ; PEETERS, B. : Parameterization of Damage in Reinforced Concrete Structures Using Model Updating. In: *Journal of Sound and Vibration* 228 (1999), Nr. 4, S. 717–730
- [168] WEI, W. : *Time series analysis*. Addison-Wesley publ Reading, 1994
- [169] WEISE, T. : Global optimization algorithms-theory and application. In: *Self-Published*, (2009)
- [170] WELCH, P. : The use of fast Fourier transform for the estimation of power spectra: a method based on time averaging over short, modified periodograms. In: *IEEE Transactions on audio and electroacoustics* 15 (1967), Nr. 2, S. 70–73
- [171] WORDEN, K. ; DULIEU-BARTON, J. : An Overview of Intelligent Fault Detection in Systems and Structures. In: *Structural Health Monitoring* 3 (2004), Nr. 1, S. 85–98
- [172] WORDEN, K. ; FARRAR, C. ; MANSON, G. ; PARK, G. : The fundamental axioms of structural health monitoring. In: *Proceedings of the Royal Society A: Mathematical, Physical and Engineering Science* 463 (2007), Nr. 2082, S. 1639–1664
- [173] YU, D. ; REN, W. : EMD-based stochastic subspace identification of structures from operational vibration measurements. In: *Engineering Structures* 27 (2005), Nr. 12, S. 1741–1751
- [174] YUEN, M. : A numerical study of the eigenparameters of a damaged cantilever. In: *Journal of Sound and Vibration* 103 (1985), Nr. 3, S. 301–310
- [175] ZIMMERMAN, A. ; LYNCH, J. : A Parallel Simulated Annealing Architecture for Model Updating in Wireless Sensor Networks. In: *IEEE Sensors Journal* 9 (2009), Nr. 11, S. 1503–1510